1985

A numerical approach for determining the variable ascent velocity of a granitoid diapir

Keith I. Mahon
University at Albany, State University of New York

A NUMERICAL APPROACH FOR DETERMINING THE VARIABLE ASCENT VELOCITY OF A GRANITOID DIAPIR

A thesis presented to the Faculty
of the State University of New York
at Albany
in partial fulfillment of the requirements
for the degree of
Master of Science

Department of Geological Sciences

Keith I. Mahon

1985

A NUMERICAL APPROACH FOR DETERMINING THE VARIABLE ASCENT VELOCITY OF A GRANITOID DIAPIR

Abstract of

a thesis presented to the Faculty

of the State University of New York

at Albany

in partial fulfillment of the requirements

for the degree of

Master of Science

Department of Geological Sciences

Keith I. Mahon

1985

ABSTRACT

A mathematical model for granitoid diapirism has been developed that accounts for the time dependent thermal and rheological conditions encountered by the intruding body. This model is derived by the simultaneous solution of the partial differential equations of energy, continuity, and momentum utilizing scaling analysis. The underlying assumption is that deformation of the surrounding country rock is confined to a relatively thin layer with a temperature dependent Newtonian viscosity. When the country rock is modeled as a power-law fluid, the effective viscosity is dependent upon temperature and shear strain rate.

This model allows for realistic temperature gradients within the crust and variable shear strain rates. This is made possible through use of a numerical approximation referred to as the "snapshot" approach. This method allows the pluton to ascend in finite time increments while the boundary conditions remain fixed. Following each snapshot, the ascent velocity is calculated and new boundary and initial conditions are set for the next increment of time.

Several model runs have been performed using a FORTRAN program. The results exhibit time dependent variations in the ascent velocity due to corresponding changes in the overall rheology, and thickness, of the deformation layer. One of the conclusions from this study is that larger plutons ascend at slower rates, but emplace higher in the crust due to the additional energy available relative to smaller plutons.

State University of New York at Albany

College of Sciences and Mathematics

Department of Geological Sciences

The thesis for the master's degree submitted by

Keith I. Mahon

under the title

A Numerical Approach for Determining the Variable Ascent Velocity of a Granitoid Diapir

has been read by the undersigned. It is hereby recommended for acceptance by the Faculty with credit to the amount of six semester hours.

Dr. Stephen DeLong Stephen F. DeLong July 31, 1985

Dr. Donald Drew Donald A. Drew July 31, 1985

Dr. T. Mark Harrison (Chairman) T. Mark Harrison July 31, 1985

Dr. E. Bruce Watson E. Bruce Watson 7/31/85

Recommendation accepted by the Dean of Graduate Studies for the Graduate Academic Council.

_____

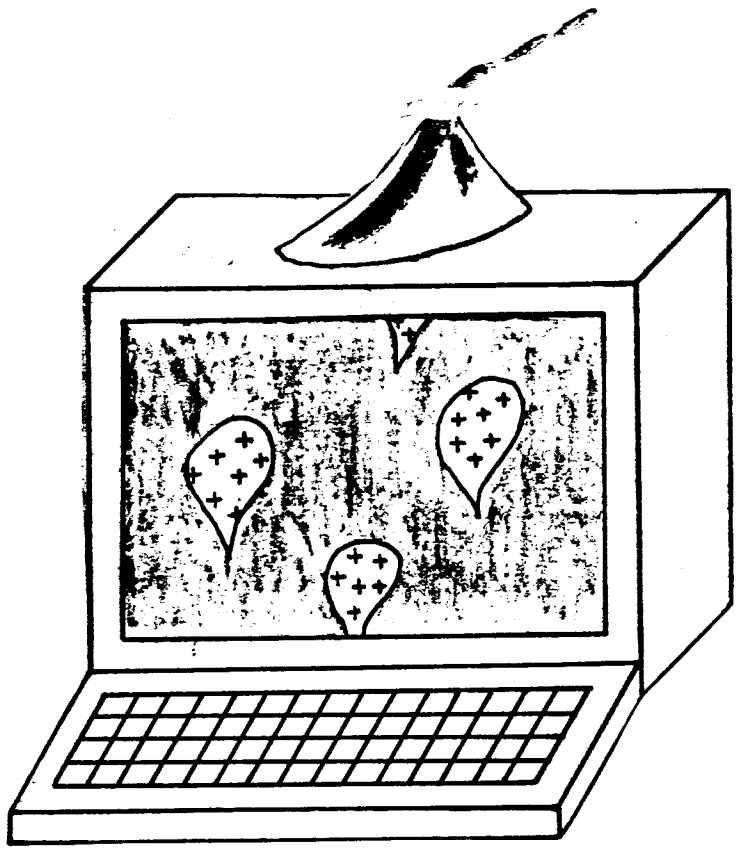

"Geology is not a fundamental science. Rather, it involves the application of principles from the basic sciences, such as physics, chemistry, and mathematics to the study of the EARTH."

Mark Twain ?

TABLE OF CONTENTS

Page

LIST OF FIGURES

LIST OF TABLES

ACKNOWLEDGMENTS

I am grateful to Dr. Mark Harrison for his guidance throughout my graduate studies at SUNYA and for insuring that financial assistance was always available.

I would also like to thank Drs. John Delano, Steve DeLong, Greg Harper, Bill Kidd, Winthrop Means, George Putman, and Bruce Watson for their knowledge, help and time during the preparation of this work.

A very special thanks to Dr. Donald Drew for invaluable assistance in deriving the equations presented in this work.

I wish to thank Suzanne Baldwin, Dave Bonner, Bruce Idleman, Mark Jessell, Daniel Loureiro, Dave Pace, Bill Shaw, and Steve Tanski for their help throughout my graduate stay at SUNYA.

I am very appreciative of the help I received in the final preparation of this work from Suzanne Baldwin, Mark Jessell, and Diana Paton.

To Mom, Dad, Jacalyn, Keith, Michael, Dorcas, Casey, Caity, and Meghan thanks for being a great family.

Finally, a very special thanks to Iris who quietly sacrificed for my educational goals.

CHAPTER I
INTRODUCTION

1.1 Objective

Despite their abundance and clear field evidence of forceful emplacement (Grout, 1932; Pitcher, 1978), little is known about the time scales and mechanisms of granitoid intrusions within the earth's crust. Previous mathematical models of magmatic ascent have rarely taken into account the temporal variations of the boundary conditions encountered (Berner et al., 1972; Ahern et al., 1981; Anderson, 1981; Marsh, 1982; Morris, 1982; Bateman, 1984).

Bateman (1984) points out that when attempting to correlate what is viewed in the field with the mechanisms that take place over much of the ascent, one must keep in mind that the field evidence is a direct result of the ascent mechanisms in progress during final emplacement. What happened prior to this may have little to do with the more permissive emplacement mechanisms in progress during the last tens or hundreds of meters of ascent. In general, for a pluton to ascend from the base of the crust to a point of final emplacement in the upper crust, a forceful and energy conservative mechanism must be at work for a large portion of the ascent.

These facts, and the substantial lack of work done on crustal diapirs, justifies the development of a model to

profile the ascent velocity of a granitoid diapir within the framework of the rheological and thermal conditions of the crust.

1.2 Crustal Magmatic Ascent

Igneous bodies vary widely in composition and distribution within the crust. Granitoid plutons are inferred to have circular shapes in cross section (Pitcher, 1978), which may indicate the ascent of an ellipsoidal bulb of magma. Although it is generally agreed that granitoids rise from depth to their region of final emplacement due to a density instability, the mechanism of this process is still a subject of conjecture (Turcotte, 1982; Bateman, 1984).

The major focus in what became known as the "granite controversy" earlier in this century (Bowen, 1948; Read, 1948; Buddington, 1959) was the "room problem". That is, what happened to the rock that the granite replaces? When the surrounding country rock is modeled as a completely rigid solid, six mechanisms could account for emplacment of granites within the crust.

The first mechanism is simply in situ granitization, or solid state transformation (Read, 1948), of the region now occupied by the granite. This would require enormous diffusion rates that are not possible at shallow- and mid-crustal temperatures without the presence of a significant heat source (e.g., magma).

The herculean task of uplifting overlying strata during ascent, resulting in doming at the surface, has been considered as a second possible emplacement mechanism. This may be viable at near-surface depths, but due to the limited buoyancy of the granite body it could not occur at the greater depths that granitoid bodies are known to intrude (Marsh, 1982).

The third mechanism is stoping, where blocks of thermally spalled roof rock fall through the magma as it rises. This may be a common final emplacement mechanism, but due to the clutter of crustal blocks within the magma body (Marsh, 1982) this could not occur for more than a few hundred meters, regardless of the body's size.

Zone melting, or zone refining, is another mechanism that may account for granitoid ascent through a rigid crust. This mechanism can be described as the melting of rock at the top of the pluton coinciding with solidification at the bottom. The result would be a felsic magma isotopically equilibrated with the country rock ... a circumstance not often documented. This argument against zone melting as a mechanism for granitoid intrusion, involves the initial Sr^{87}/Sr^{86} in I-type granites. Geochemical evidence suggests that these granites have a source sufficiently deep, yielding a felsic magma from the partial fusion of mantle and lower crust. The initial strontium isotopic ratio for I-type granites is approximately 0.704#0.706. This ratio is below

that of average crust (Ø.71) and above the values common in mantle rocks (Ø.7Ø3-Ø.7Ø4). S-type granites derived solely from a crustal source generally have initial ratios greater than Ø.7Ø6. During zone melting the low initial Sr^{87}/Sr^{86}, often observed between host rock and pluton, will be lost (Chappell and White, 1974; Faure, 1977).

Ahern et al. (1981) showed that zone melting may be a viable mechanism for granitoid emplacement when the initial magma has sufficient height and energy to cause melting temperatures to vary from top to bottom (magma melting temperatures increase with depth in most natural rock systems). The distance such a 'body' could travel would be limited by the height of the initial magma chamber and any heat transfer within the magma, short of rapid convection. The resulting ascent distances are generally less than the initial height, and the final size of the granitoid pluton is a fraction of the initial volume (Ahern et al., 1981).

Another mechanism that may take place in the crust when it is modeled as a rigid solid is ring-dike intrusion (Hughes, 1982), which is related to the stoping mechanism mentioned earlier. Generally, dikes will intrude along structural weaknesses within the the country rock. As a result of stoping, a magma will inject into the evacuated area above a block of country rock. When this occurs on a large scale the final emplacement may be called a ring-dike complex or cauldron subsidence intrusion, depending on the

field relationship between the granitic dikes and the stoped country rock. In comparison to diapirs, the magma body comprising the ring-dike complex will have a much larger surface area to volume ratio. This would result in relatively rapid cooling to the solidus temperature, inhibiting further ascent. Assuming that heat is simply transferred by conduction within the host rock, the energy loss difference between a dike and a spherical diapir of the same volume can be examined mathematically with the conductive heat flow solutions of Carslaw and Jaeger (1959) for a plane sheet and a sphere.

The final mechanism considered is similar to the brittle deformation associated with a ring-dike intrusion. When the upper crust is brittlely deformed via extension, magma and fluid in the region will take advantage of the structural weakness by filling the cracks formed. This is the case when the overlying slab in a convergent tectonic area undergoes large scale brittle deformation as a result of the subducting slab generating extensive, and compressive, stresses within it (Windley, 1977).

The six mechanisms mentioned can be broken down into two regions of occurrence ... the upper crust (epizone) and the lower crust (katazone). The mechanisms that are possible in the katazone are zone melting and granitization. Doming (uplift), stoping, ring-dyke intrusion, and emplacement during regional extension are possible mechanisms at work in

the epizone during final emplacement of a magma body. In actuality, regional extension may be important at all crustal levels.

In 1932, Grout suggested that magma may rise "by rock flowage in the roof and walls" (from Marsh, 1982). This idea suggests a more forceful intrusion mechanism than the ones described above. It also implies that on a geological time scale the adjacent country rock can be described as a viscous fluid that flows around the pluton. If a mobile pluton forcibly intrudes its surroundings, and approaches ellipsoidal geometry, then it behaves diapirically.

Numerous models of diapiric ascent have been performed experimentally and derived mathematically. The most fundamental mathematical description of igneous diapirism is Stokes' law. In 1851, Stokes developed a relationship for the motion of a solid sphere through a viscous fluid. The terminal velocity that this object could achieve is

[1.1] $$U_\infty = \tfrac{2}{9} \Delta\rho \vec{g} R^2/\mu$$

where $\Delta\rho$ is the density difference between the ball and its surroundings, $\vec{g}$ is the acceleration due to gravity, R is the sphere's radius, and μ is the viscosity of the fluid at any point. Equation 1.1 can be used to approximate the ascent of a diapir anywhere in the lithosphere, but the results are generally too slow (Anderson, 1981; Marsh, 1982). The reason for this is two-fold.

Firstly, the boundary condition at the sphere's surface

for a solid moving through a fluid is called the no-slip condition. In other words, a fluid molecule on the surface of the sphere remains stationary relative to the sphere itself. In the case of a magma body rising through an extremely viscous medium, the no-slip condition is replaced by the stress-free boundary condition. The stress-free boundary condition allows the fluid molecule to flow freely by the diapir's surface. This will result in a higher estimation of the ascent velocity (see Chapter IV).

Secondly, Stokes' equation is based on the assumption of an isoviscous surrounding medium (see Figure 1.1). Because the diapir is very hot, relative to the country rock, heat will be transferred from the diapir to the surroundings. This will result in a temperature gradient in the adjacent country rock. Because all rocks have temperature-dependent viscosities, the viscosity distribution in the country rock is far from isoviscous, especially in the region near the diapir - country rock interface.

Experimental work on diapirism has also been performed. Many of the earlier works simply dealt with isoviscous flow. Ramberg (1963) used centrifuge models of putty in putty to show the deformation in both the low density diapir and in the denser surroundings. Berner et al. (1972) used a finite element method to predict the results found from centrifuge models.

Whitehead and Luther (1975) performed an experimental

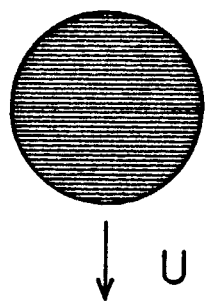

$$U = 2\Delta\rho g R^2/9\mu$$

A ball falling through an isoviscous medium.

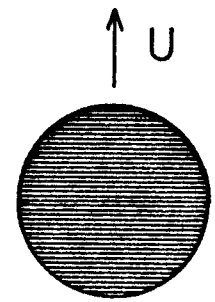

$$U = ?$$

A hot diapir rising through rock with variable viscosity.

FIGURE 1.1

study on the effects of low Reynolds flow on the shape of viscous bodies intruding a fluid of differing viscosity and higher density. The results show that long vertical intrusions will form when the surrounding medium has a lower viscosity than the intrusion. When the surrounding medium's viscosity is higher, spherical pockets of the intruding fluid will rise. This occurs because the intruding body attempts to minimize the viscous stresses, exerted on its surface, by lessening its surface area.

In a second set of experiments, Whitehead and Luther injected fluid through a spout into a fluid of higher viscosity and density. A spherical pocket of the less viscous fluid formed and began to rise when it obtained a diameter large enough "to buoyantly rise more rapidly than the rate of growth of the radius". As the 'diapir' rose, the spout continued to inject fluid into the expanding pocket through a link, or feeder, between itself and the source. This link remained even when the spout was shut off and restarted after a short period of time.

The second set of experiments performed by Whitehead and Luther dealt with a viscosity ratio of 6000/1. In nature, the feeder connected to an actual diapir would contain a hot magma of relatively low viscosity surrounded by country rock with a viscosity several orders of magnitude higher. Due to the large stresses exerted by the adjacent country rock on this link, it may not be capable of sustaining the transport

of fresh magma to the diapir for a large portion of the ascent.

Ribe (1983) performed a series of experiments to examine the temperature-dependent viscosity encountered by a hot sphere as it descends through a viscous fluid. Due to temperature-dependent viscosity found in virtually all geologic materials, the results of this study are important. Ribe points out that his experiments are not perfect models of igneous diapirism. The main reason for this is that by using a solid ball the no-slip condition at the sphere's surface is applied, rather than the more realistic condition of an essentially stress-free surface. Ribe's results exhibit a contrast in ascent (descent) velocity and heat transfer mechanism, by the use of Peclet and Nusselt numbers, for different viscosity contrasts in the adjacent fluid.

In order to get an idea of how igneous diapirs rise at reasonable rates, geologists have been applying mathematical models to the problem. Anderson (1981) modeled igneous diapirs in the upper mantle. He suggested that the mantle viscosities, estimated from glacial rebound studies, are too high. Anderson reasons that Stokes' law estimates of ascent velocities are too slow for the accepted viscosities. Marsh and Morris (1981) commented that Anderson did not take into account the heat transfer from the hot diapir, which contributes to softening the adjacent country rock.

The most complete analytical models concerning diapiric

ascent to date are the work by Marsh (1982) and Morris (1982). These models apply to the steady state intrusion of a spherical pluton at a constant temperature, intruded below island arcs. Both confine most of the deformation within a thin layer of variable viscosity country rock, located near the diapir's surface. Marsh points out that in Stokes' flow the deformation of the surroundings can be out as far as 9-10 body radii. In their work, the viscosity of the country rock varies with distance from the pluton due to the exponential drop off in temperature. This allows the country rock in contact with the diapir to deform more easily relative to the deformation when it is considered isoviscous.

Although the work by Marsh and Morris is related to transport of andesitic diapirs beneath island arcs, many of the concepts used may be applied to granitoid diapirism within the crust. This is especially true of the relatively thin deformation layer surrounding the magma body. A major drawback of their models when applied to granitoid diapirism is the idea that the body will travel further, and up to 25 times faster, if it is preceded by a diapir of greater size within a few thousand years. This does not take into account the existence of a buoyant plume of rock processed through the deforming layer of the earlier body, nor does it take into account the minimal density contrast encountered when the younger diapir intrudes the older one. Granted, ascent is made easier by higher ambient temperatures, but a

sufficient density instability is a prerequsite for any amount of rise.

Some investigators concerned with the rise of granitoid diapirs have reservations as to whether they are capable of sufficient ascent when isolated from their source regions (Pitcher, 1978; Bateman, 1984). Rather, the diapirs are considered to be balloon like bodies as they rise, enabling them to have sufficient energy to deform, or melt, the surrounding country rock. A ballooning diapir is fed magma pulses through a link from its source. This could be an important mechanism in the early ascent and agglomeration of a granitoid body, but unless the feeder is two-way (i.e., feeder and extractor) it would be quite difficult to get large volumes of magma into the body without reinvoking the room problem. When the body's volume remains relatively constant, the adjacent country rock is shouldered aside, but for a growing body much of the rock replaced must replace the volume of melt leaving the source. This would be exceedingly difficult if the body is more than a few kilometers away from this region.

1.3 Overview of this Study

This particular work deals with an isolated diapir rising through the crust, beginning at a post agglomeration stage and ending short of its region of final emplacement. The surrounding country rock is modeled as a viscous fluid

with temperature- and, in the case of a power-law fluid, shear strain rate-dependent viscosity. The ambient temperature of the country rock is defined by the geothermal gradient. The pluton's ascent will vary with time due to changes in the effective viscosity in the country rock adjacent to the diapir, as a result of changing ambient and diapir temperatures.

In the pages that follow, the governing equations of heat transfer and fluid flow are algebraically manipulated to derive a solution for the particular conditions encountered at any instant during diapiric ascent. To lessen the potential mathematical complexities that would occur if the equations were solved for more general conditions, a few assumptions are used in the derivation. Some of these assumptions are used to scale the governing equations in a manner similar to that of Morris (1982). The dimensionless equations that result from this analysis will be much simpler to use in deriving a solution.

The most important assumption used, prior to scaling, is that the width of the deformation layer is thin relative to the diapir's radius. When this is false, the solutions found are invalid.

The governing equations will be dependent on spatial and temporal coordinates. Since this would yield four independent variables (r,θ,ϕ,t), some generalizations are made. Firstly, any variation in the azimuthal angle ϕ, is

considered negligible. Secondly, time dependence will be considered by a difference method that is referred to as the "snapshot approach". This is described in detail in Chapter II. Suffice to say that the snapshot approach assumes a quasi-equilibrium state for deformation of the adjacent country rock during short periods of ascent.

As a hot diapir rises from depth, it will lose energy to the cooler surroundings via heat conduction and forced convection. Earlier investigators have used analytical methods to help solve the complexities encountered by forced convection within the adjacent country rock (Marsh and Kantha, 1978; Marsh, 1982; Morris, 1982). This study utilizes the snapshot approach and the assumption that deformation, hence forced convection, is confined to a thin layer. From this the "cyclic method", also described in Chapter II, will point to one of several intervals within the deformation layer to take up the deformation at a particular instant. Regions where deformation is much greater will be called upon more frequently by the cyclic method than in regions in which deformation is not as pronounced.

The temperature within the diapir is considered to vary with time due to the loss of energy to the cooler surroundings and the heat gained by latent heat of crystallization and other heat generating processes. The variation of temperature across the diapir is considered negligible throughout ascent. The buoyant stresses

encountered within the fluid diapir itself will result in a natural convective process that takes place on a much shorter time scale than the flow of country rock adjacent to the diapir's surface. The lack of a significant temperature gradient across the magma body may not be a good approximation when the diapir approaches its solidus temperature, but the mechanism of softening the adjacent country rock, allowing for ascent, will be greatly slowed by the time the diapir's average temperature approaches its solidus.

The final generalization to be considered is the shape of the diapir. Pitcher (1978) notes that in outcrop many granitoid plutons have circular sections. This may justify modeling a diapir as a sphere, but both Pitcher (1978) and Bateman (1984) believe that diapirs are ballooning bodies with feeders connected to their source regions. This yields an inverted tear drop shape at best. Arguments for prolate and oblate ellipsoids may also be justified. Marsh (1982) points out that the shape of the body has little effect on the actual drag on it in low Reynolds number ($Re = \rho U_\infty R/\mu$) flow. Therefore, this study will only consider a simple spherical shape for the diapir.

CHAPTER II

DERIVATION OF THE DIAPIR MODEL

2.Ø Introduction

In this chapter, a model for the time dependent ascent velocity of a hot granitic diapir is developed. Many variables and parameters are introduced, which are defined within the text.

In the first section, 2.1, an analytical solution for the ascent velocity of an igneous diapir is derived by solving the governing equations together with the assumption that deformation of the surrounding country rock is confined to a very narrow layer of variable viscosity. The simplified result is obtained with the aid of scaling analysis.

In section 2.2, an in-depth description of the methods used to solve the energy balance for the entire system is covered. Basically, this concerns the conduction of heat away from the diapir - country rock interface and the forced convection of energy and material within the deformation layer.

Section 2.3 merges the solutions from the first two sections into a coherent model of time dependent ascent velocity, utilizing the snapshot approach. The program "Socrates" (see Appendix A), which is the FORTRAN source code of the model, is summarized and discussed.

2.1 Steady State Ascent Velocity Derivation

During the ascent of an igneous body, numerous physical processes are taking place simultaneously. For a slow moving granitic diapir rising through cooler continental crust, the rate limiting processes are heat transfer from the hot diapir and 'fluid flow' of the deforming country rock. Other processes, such as convective heat transfer within the diapir, are also taking place, but only affect the ascent velocity by varying the boundary conditions of the governing equations.

2.1.1 Snapshot Approach

As a granitic diapir rises, it will lose thermal energy to the country rock and encounter lower ambient crustal temperatures. These, and other variations in the conditions during ascent, result in a time-dependent terminal velocity. To help overcome many mathematical complexities, I have introduced the "snapshot" approach to solve this problem.

Since igneous diapirs rise for a period of 10^4 to 10^5 years before solidifying, the ascent velocity during a considerably shorter period, for example 10 years, will remain relatively constant. In other words, over a ten year period the ascent velocity could be approximated by a steady state solution of the governing equations. This short period is referred to as a "snapshot" of a particular instant during

ascent. By applying the snapshot approach to the time-dependent energy equation for the entire system (see section 2.2), an accurate variation in the ascent velocity can be obtained.

2.1.2 The Deformation Layer

When thermal energy is transferred from the hot diapir to the country rock, the drag exerted by the country rock upon the surface of the body is lessened. This concept is important in the derivation because, unlike Stokes' result for isoviscous flow, the result given here is dependent on the variation of the country rock's viscosity with temperature (shear strain rate will also be important if the country rock is modeled as a power-law fluid). Chapter III contains graphs of log viscosity versus inverse temperature for the two country rocks modeled in this study (see Figures 3.1 and 3.2). The first country rock, CR1, is simply a Newtonian fluid, while CR2 is a power-law fluid modeled as a pseudo-Newtonian fluid with a temperature- and shear strain rate-dependent effective viscosity.

By lessening the drag on a stagnant diapir, the buoyant force may overcome confining forces, enabling the diapir to rise. Eventually, the diapir will cool to a point where the mechanism of softening the surrounding country rock ceases to allow the body to move. If the diapir is still partially molten, another mechanism of ascent may be initiated (e.g.,

stoping or dike intrusion).

When the diapir has sufficient energy to effectively soften the country rock and allow it to flow around the pluton, it will rise at a rate determined by: the variation in viscosity near the diapir, the actual country rock viscosity, and other mechanical considerations. Because temperature drops off exponentially with distance from the diapir, and viscosity is exponentially dependent on temperature, there exists a narrow region near the diapir where viscosity increases very rapidly. Most of the surrounding country rock's deformation is occuring in this region, henceforth referred to as the deformation layer.

Morris (1982) defined the width of a similar deformation layer by an increase in viscosity of e (2.72) from the diapir - country rock interface. This concept is used in this study, but for now the factor increase is considered an arbitrary value, F. This factor is referred to as the deformation factor.

The deformation layer is very similar mathematically to the laminar boundary layer in fluids of lower viscosity, and like the boundary layer its thickness, d, is small compared to the radius of the diapir, R. This similarity is a necessary condition in order to find an analytical solution for the ascent velocity. When it is violated, that is, when the deformation layer's width exceeds a critical fraction of the diapir's radius, the equations derived cease to be valid.

In actuality, when a pluton is surrounded by material with a strong temperature-dependent viscosity this would not occur unless the diapir's temperature approaches the country rock's ambient temperature, the case when the diapir's available energy has been significantly depleted.

2.1.3 The Governing Equations

The problem will be modeled in spherical coordinates, since most diapirs approach spherical symmetry, due in part to the viscosity contrast between the magma and the country rock. Trailing tails will be neglected geometrically, but may be important if capable of maintaining an energy, or material, transport link between the source and the diapir.

The center of the diapir will be the point of origin throughout ascent. The entire model will be considered in two spatial coordinates, with r being the radial distance from the origin and θ the polar angle ($\theta = 0$ directly above the diapir). Any dependence on the azimuthal angle, ϕ, is neglected.

The first portion of this derivation is concerned with the flow of deforming country rock within the deformation layer. The country rock's viscosity is quite sensitive to variations in temperature, therefore the energy equation for this region must be solved simultaneously with the momentum and continuity equations.

The Continuity Equation

The continuity equation is a statement of the conservation of mass. In vector form for an incompressible fluid,

$$\operatorname{div} \vec{V} = 0$$

where $\vec{v}$ is the velocity vector (u_r, v_θ). In spherical coordinates, neglecting any ϕ component or dependence,

$$\frac{1}{r^2}\frac{\partial}{\partial r}(r^2 u) + \frac{1}{r\sin\theta}\frac{\partial(v\sin\theta)}{\partial\theta} = 0$$

where u is the r-component of velocity vector and v is the θ-component. By differentiating, this equation becomes

[2.1] $$\partial u/\partial r + 2u/r + 1/r\,\partial v/\partial\theta + v/r\cot\theta = 0 .$$

The Momentum Equation

The momentum equation, or equation of motion, can best be represented by the Navier-Stokes equation with variable viscosity. In vector form,

$$\rho\left(\frac{\partial \vec{V}}{\partial t} + \nabla\left(\frac{V^2}{2}\right) - \vec{V}\times(\nabla\times\vec{V})\right) = -\nabla P + \mu\nabla^2\vec{V} + 2(\nabla\mu)\cdot\nabla\vec{V} + (\nabla\mu)\times(\nabla\times\vec{V})$$

where ρ is the country rock's density, t is time, μ is the absolute viscosity, and P is the "modified pressure" (Batchelor,1967). The modified pressure results from motion of the deforming rock within the deformation layer. Using Batchelor's notation,

$$P = p - p_o - \rho\vec{g}\cdot\vec{x}$$

where p is the total pressure and $p_o+\rho g\cdot x$ is the pressure that would result if the fluid were at rest. The importance

of the pressure term will resurface later in this section when forces acting on the rising diapir are discussed.

Breaking the vector form of the momentum equation down into spherical coordinates results in an r- and θ-component.

r-component:

$$\rho\left(\partial u/\partial t + u\,\partial u/\partial r + \frac{v}{r}\,\partial u/\partial\theta - v^2/r\right)$$
$$= -\partial P/\partial r + \left(1/r^2\,\partial/\partial r\left(r^2 2\mu\,\partial u/\partial r\right)\right.$$
$$+ \frac{1}{r\sin\theta}\,\partial/\partial\theta\left(\mu\sin\theta\left(r\,\partial/\partial r\left(v/r\right) + 1/r\,\partial u/\partial\theta\right)\right)$$
$$\left. - 2\mu/r^2\left(\partial v/\partial\theta + 2u + v\cot\theta\right)\right)$$

θ-component:

$$\rho\left(\partial v/\partial t + u\,\partial v/\partial r + \frac{v}{r}\,\partial v/\partial\theta + uv/r\right)$$
$$= -1/r\,\partial P/\partial\theta + \left(1/r^2\,\partial/\partial r\left(r^2\mu\left(r\,\partial/\partial r\left(v/r\right) + 1/r\,\partial u/\partial\theta\right)\right)\right.$$
$$+ \frac{1}{r\sin\theta}\,\partial/\partial\theta\left(\sin\theta\,(2\mu)\left(1/r\,\partial v/\partial\theta + u/r\right)\right)$$
$$\left. + \mu/r\left(r\,\partial/\partial r\left(v/r\right) + 1/r\,\partial u/\partial\theta\right) - \frac{\cot\theta}{r^2}\,(2\mu)\left(u + v\cot\theta\right)\right)$$

As mentioned before, a strong temperature dependent rheology of the country rock is assumed (see Chapter III). To emphasize this, spatial variations of viscosity will be changed to temperature variations via the chain rule.

$$\partial\mu/\partial r = \partial\mu/\partial T\;\partial T/\partial r \qquad \text{and} \qquad \partial\mu/\partial\theta = \partial\mu/\partial T\;\partial T/\partial\theta$$

After differentiation and rearrangement, the components of the momentum equation become,

r-component:

[2.2a]
$$\rho\left(\partial u/\partial t + u\,\partial u/\partial r + \frac{v}{r}\,\partial u/\partial\theta - v^2/r\right)$$
$$= -\partial P/\partial r + \mu\left(4/r\,\partial u/\partial r + 2\,\partial^2 u/\partial r^2 + \frac{1}{r}\,\partial v/\partial r\cot\theta + \frac{1}{r}\,\partial/\partial\theta\left(\partial v/\partial r\right)\right.$$
$$+ 1/r^2\,\partial u/\partial\theta\cot\theta + 1/r^2\,\partial^2 u/\partial\theta^2 - 3/r^2\,\partial v/\partial\theta - 4u/r^2 - 3v/r^2\cot\theta\Big)$$
$$\left. + \partial\mu/\partial T\left(\partial T/\partial r\left(2\,\partial u/\partial r\right) + \partial T/\partial\theta\left(\frac{1}{r}\,\partial v/\partial r - v/r^2 + 1/r^2\,\partial u/\partial\theta\right)\right)\right.$$

θ-component:

[2.2b] $$\rho\left(\partial v/\partial t + u\,\partial v/\partial r + v/r\,\partial v/\partial\theta + uv/r\right)$$
$$= -1/r\,\partial p/\partial\theta\,\mu\left(2/r\,\partial v/\partial r + \partial^2 v/\partial r^2 + 1/r\,\partial/\partial r\left(\partial u/\partial\theta\right)\right.$$
$$+ 2/r^2\,\partial v/\partial\theta\cot\theta + 2/r^2\,\partial^2 v/\partial\theta^2 - \frac{2v}{r^2} + \frac{4}{r^2}\partial u/\partial\theta + \frac{2v}{r^2}\cot^2\theta\Big)$$
$$+ \partial\mu/\partial T\left(\partial T/\partial r\left(\partial v/\partial r - v/r + 1/r\,\partial u/\partial\theta\right) + \partial T/\partial\theta\left(\frac{2}{r^2}\,\partial v/\partial\theta + 2u/r^2\right)\right).$$

The Energy Equation

The energy equation is a statement of the principle of conservation of energy. In vector form, for an incompressible fluid,

$$\partial Q/\partial t + \Phi + K\nabla^2 T = \rho C_v\, DT/Dt$$

where $\partial Q/\partial t$ is the internal heat generation with time, Φ is the viscous dissipation function, K is the thermal conductivity, T is the absolute temperature, C_v is the specific heat at constant volume, and DT/Dt is the substantial, or material, derivative of absolute temperature. The heat generation term can be neglected within the deformation layer because little or no phase changes are occurring in this region and other sources are negligible. The viscous dissipation function reflects the frictional heating occurring due to the motion of the deforming country rock within this layer. This is a direct result of the conversion of potential energy to kinetic energy as the diapir rises to a region of lower potential energy. Although this particular dissipation takes place within the deformation layer, the time scale is too long to consider

this a source of appreciable heat (see section 2.2).

After dropping the terms for viscous dissipation and heat generation, the energy equation for the deformation layer, in spherical coordinates, becomes

[2.3] $$\chi\left(\frac{\partial^2 T}{\partial r^2}+\frac{2}{r}\frac{\partial T}{\partial r}+\frac{1}{r^2}\frac{\partial^2 T}{\partial \theta^2}+\frac{\cot\theta}{r^2}\frac{\partial T}{\partial \theta}\right)=\frac{\partial T}{\partial t}+u\frac{\partial T}{\partial r}+\frac{v}{r}\frac{\partial T}{\partial \theta}$$

where χ is the thermal diffusivity.

Viscosity-Temperature Relationship

The final general equation for consideration is the viscosity-temperature relationship, which is of the form,

[2.4] $$\mu(T)=\mu_o \exp(\gamma(T_o-T))$$

where μ_o is the viscosity at temperature T_o and γ reflects the magnitude of the variation of viscosity with temperature. This relationship is a good approximation for the experimental results analyzed in Chapter III.

Boundary Conditions

Temperature, viscosity, velocity, and pressure are all interrelated in equations 2.1, 2.2, and 2.3. Therefore, in order to find a solution, these partial differential equations must be solved simultaneously. The boundary conditions that must be satisfied are,

at $r = R$ (Diapir-country rock interfce)

$u=0$ (No-slip condition for the r-component of V)

$\partial\sigma_r/\partial r=0$ (Stress-free surface condition)

$T=T_o$ (Temperature of the diapir)

$\mu = \mu_o$ (Viscosity of the country rock at T_o)

at $r = \infty$ (Undisturbed country rock)

$u = U_\infty \cos\theta$ (Radial component of ascent velocity)

$V = U_\infty \sin\theta$ (Tangential component of ascent velocity)

$T = T_\infty$ (Temperature of the country rock)

$\mu = \mu_\infty$ (Viscosity of the country rock at T_∞).

2.1.4 Scaling Analysis

In their present form, the equations and necessary boundary conditions can only be solved by a very time consuming numerical approach, yielding large computational errors. To make the solution tractable some generalizations must be made concerning the magnitude of individual terms found in these equations. This is done through an objective evaluation utilizing scaling analysis.

First, each independent and dependent variable within the governing equation must be made dimensionless by multiplying by an appropriately chosen scale that utilizes one's intuitive understanding of a particular region during diapiric ascent. A dimensionless parameter that will be frequently used in these scales is ϵ, where

$$\epsilon = d/R$$

and is generally much less than unity. Therefore, terms preceded by ϵ are usually of negligible value when compared to terms without an ϵ, all else being equal. If the value of ϵ becomes 'significant', solutions found using this

parameter are in question.

Table 2.1 lists the dimensionless variables, denoted by primes, and the scales used to equate them back to the actual variables. Note that pressure and time have scales of unknown size. In the temporal case, the scale τ is quite large. Therefore, terms with τ in the denominator are usually considered negligible when compared to other terms. This is analogous to the snapshot approach where a quasi-equilibrium state exists within the deformation layer during individual intervals. The pressure scale P, is a quantity that will be found when all terms of negligible value, within the momentum equations, have been dropped. The pressure terms will not be dropped because pressure is the driving mechanism of fluid flow within the deformation layer.

In order to conserve mass, average fluid flow velocity within the deformation layer must be faster than the corresponding ascent velocity. Therefore, a scale for the velocity components within the deformation layer must be chosen appropriately. The scale U_o, found in Table 2.1, corresponds to a tangential velocity that may be found at some point in this region. It is defined relative to the actual ascent velocity as

$$U_\infty = \epsilon U_o .$$

The next step in scaling analysis is to substitute the dimensionless variables, and scales, for the actual variables in the governing equations. These substitutions are found in

	Dimensionless Variables	Scales
θ-comp. of velocity	$V' = V/U_o$	$V = V'U_o$
r-comp. of velocity	$u' = u/\epsilon U_o$	$u = u'\epsilon U_o$
Absolute viscosity	$\mu' = \mu/\mu_o$	$\mu = \mu'\mu$
Thermal diffusivity	$\alpha' = \alpha/\alpha_o \; (=1)$	$\alpha = \alpha'\alpha_o$
Temperature	$T' = \frac{T - T_\infty}{T_o - T_\infty}$	$T = T'(T_o - T_\infty) + T_\infty$
Modified pressure	$P' = P/\rho$	$P = P'\rho$
Radial distance	$r' = (r - R)/d$	$r = r'd + R$ $= R(r'\epsilon + 1)$
Time	$t' = t/\tau$	$t = t'\tau$

TABLE 2.1

the right column of Table 2.1.

Equation 2.1 becomes

$$\left(U_o\epsilon/d\right)\partial u'/\partial r' + \left(U_o\epsilon/R\right)\frac{2u'}{1+\epsilon r'} + \left(U_o/R\right)\frac{1}{1+\epsilon r'}\,\partial v'/\partial\theta + \left(U_o/R\right)\frac{v'\cot\theta}{1+\epsilon r'} = 0 .$$

A few points should be made before dropping negligible terms. First, $\frac{U_o\epsilon}{d} = \frac{U_o}{R}$ because $\epsilon = d/R$. Secondly, $1+\epsilon r'$ is approximately 1, since r' is between Ø and 1 within the deformation layer and ϵ is much less than 1. Applying this last approximation and dividing by U_o/R, the continuity equation becomes

$$\partial u'/\partial r' + \epsilon 2u' + \partial v'/\partial\theta + v'\cot\theta = 0 .$$

The second term is preceded by an ϵ, which means it is substantially smaller than the other terms and can be dropped from consideration. The resulting continuity equation is

[2.5] $$\partial u'/\partial r' + \partial v'/\partial\theta + v'\cot\theta = 0 .$$

Placing both the r-component and the θ-component of the momentum equation into dimensionless form with scales,

r-component:

$$\begin{aligned}
&(\rho U_o)\left((1/\tau)\partial u'/\partial t' + \left(U_o\epsilon^2/d\right)u'\,\partial u'/\partial r' + \left(U_o\epsilon/R\right)\frac{v'}{1+\epsilon r'}\,\partial u'/\partial\theta - \left(U_o/R\right)\frac{v'^2}{1+\epsilon r'}\right)\\
&\quad = -\left(P/d\right)\partial P'/\partial r' + (\mu_o U_o)\mu'\Big(\left(\epsilon/Rd\right)\frac{4}{1+\epsilon r'}\,\partial u'/\partial r' + \left(\epsilon/d^2\right)2\,\partial^2 u'/\partial r'^2 + \left(1/Rd\right)\frac{\cot\theta}{1+\epsilon r'}\,\partial v'/\partial r' + \left(1/Rd\right)\frac{1}{1+\epsilon r'}\,\partial/\partial\theta\left(\partial r'/\partial r'\right)\\
&\qquad + \left(\epsilon/R^2\right)\frac{\cot\theta}{(1+\epsilon r')^2}\,\partial u'/\partial\theta + \left(\epsilon/R^2\right)\frac{1}{(1+\epsilon r')^2}\,\partial^2 u'/\partial\theta^2 - \left(1/R^2\right)\frac{3}{(1+\epsilon r')^2}\,\partial v'/\partial\theta - \left(\epsilon/R^2\right)\frac{4u'}{(1+\epsilon r')^2} - \left(1/R^2\right)\frac{3v'}{(1+\epsilon r')^2}\cot\theta\\
&\qquad + (\mu_o U_o)\,\partial u'/\partial T'\Big(\left(\epsilon/d^2\right)\partial T'/\partial r'\,\partial u'/\partial r' + \left(1/Rd\right)\frac{1}{1+\epsilon r'}\,\partial T'/\partial\theta\,\partial v'/\partial r' - \left(1/R^2\right)\frac{v'}{(1+\epsilon r')^2}\,\partial T'/\partial\theta + \left(\epsilon/R^2\right)\frac{1}{(1+\epsilon r')^2}\,\partial T'/\partial\tau\,\partial u'/\partial\theta\Big)
\end{aligned}$$

θ-component:

$$\begin{aligned}
&(\rho U_o)\left((1/\tau)\partial v'/\partial t' + \left(U_o\epsilon/d\right)u'\,\partial v'/\partial r' + \left(U_o/R\right)\frac{v'}{1+\epsilon r'}\,\partial v'/\partial\theta + \left(U_o\epsilon/R\right)\frac{u'v'}{1+\epsilon r'}\right)\\
&\quad = -\left(P/R\right)\frac{1}{1+\epsilon r'}\,\partial P'/\partial\theta + (\mu_o U_o)\mu'\Big(\left(1/dR\right)\frac{2}{1+\epsilon r'}\,\partial v'/\partial r' + \left(1/d^2\right)\partial^2 v'/\partial r'^2 + \left(\epsilon/Rd\right)\frac{1}{1+\epsilon r'}\,\partial/\partial r'\left(\partial u'/\partial\theta\right) + \left(1/R^2\right)\frac{2\cot\theta}{(1+\epsilon r')^2}\,\partial v'/\partial\theta\\
&\qquad + \left(1/R^2\right)\frac{2}{(1+\epsilon r')^2}\,\partial^2 v'/\partial\theta^2 - \left(1/R^2\right)\frac{2v'}{(1+\epsilon r')^2} + \left(\epsilon/R^2\right)\frac{4}{(1+\epsilon r')^2}\,\partial u'/\partial\theta + \left(1/R^2\right)\frac{2v'\cot\theta}{(1+\epsilon r')^2} + (\mu_o U_o)\,\partial\mu'/\partial T'\Big(\left(1/d^2\right)\partial T'/\partial r'\,\partial v'/\partial r'\\
&\qquad - \left(1/Rd\right)\partial T'/\partial r'\,\frac{v'}{1+\epsilon r'} + \left(\epsilon/Rd\right)\frac{1}{1+\epsilon r'}\,\partial T'/\partial r'\,\partial u'/\partial\theta + \left(1/R^2\right)\frac{2}{(1+\epsilon r')^2}\,\partial T'/\partial\theta\,\partial v'/\partial\theta + \left(\epsilon/R^2\right)\frac{2u'}{(1+\epsilon r')^2}\Big) .
\end{aligned}$$

Even at the highest temperatures experienced within the deformation layer, the absolute viscosity will remain quite large. In turn, the maximum velocity will be relatively slow. This is characteristic of low Reynolds' number flow ($Re = \rho U_\infty R/\mu$). Taking this into account, and the fact that the diapir's radius is much greater than the deformation layer's thickness, only a few terms will dominate the two components of the momentum equation. Namely,

$$(\rho/d)\,\partial P'/\partial r'$$

$$(\rho/R)\,\partial P'/\partial \theta$$

$$\left(\frac{\mu_o U_o}{d^2}\right)\mu'\,\partial^2 v'/\partial r'^2$$

and $$\left(\frac{\mu_o U_o}{d^2}\right)\partial\mu'/\partial T'\cdot\partial T'/\partial r'\cdot\partial v'/\partial r' .$$

Letting $\rho = \frac{\mu_o U_o R}{d^2}$ generates the following,

r-component:

[2.6a] $$\partial P'/\partial r' = 0$$

θ-component:

[2.6b] $$\partial P'/\partial \theta = \mu'\,\partial^2 v'/\partial r'^2 + \partial\mu'/\partial T'\cdot\partial T'/\partial r'\cdot\partial v'/\partial r'$$
$$= \partial/\partial r'\left(\mu'\,\partial v'/\partial r'\right) .$$

The final partial differential equation to be analyzed within the deformation layer is the energy equation. In dimensionless form with scales,

$$\left(\mathcal{H}_o(T_o - T_\infty)\right)\mathcal{K}'\left(\left(\tfrac{1}{d^2}\right)\partial^2 T'/\partial r'^2 + \left(\tfrac{1}{Rd}\right)\frac{2}{1+\epsilon r'}\cdot\partial T'/\partial r' + \left(\tfrac{1}{R^2}\right)\frac{1}{(1+\epsilon r')^2}\,\partial^2 T'/\partial s^2 + \left(\frac{1}{R^2}\right)\frac{\cot\theta}{(1+r'\epsilon)^2}\,\partial T'/\partial\theta\right)$$
$$= (T_o - T_\infty)\left(\left(\tfrac{1}{\tau}\right)\partial T'/\partial t' + \left(\frac{U_o\epsilon}{d}\right)u'\,\partial T'/\partial r' + \left(\frac{U_o}{R}\right)\frac{v'}{1+\epsilon r'}\cdot\partial T'/\partial\theta\right) .$$

In the momentum equation it was obvious that the time derivative would be negligible compared to the dominant terms. In this case it is not as apparent. The snapshot

approach rids most doubt by defining the situation as steady state for short periods of time, hence the time derivative is dropped from consideration. This results in the first term being the only dominant term in the above equation. This assertion simplifies the equation to

[2.7] $\partial^2 T'/\partial r'^2 = 0$.

The viscosity-temperature relationship in equation 2.4 must be placed in dimensionless form because it is directly involved in finding a solution for the partial differential equations. In order to be consistent, the coefficient γ, which has units T^{-1}, will be defined as

$$\gamma = \gamma'/(T_o - T_\infty) .$$

The resulting viscosity-temperature equation is

[2.8] $\mu' = \exp(\gamma'(1-T'))$.

Table 2.2 gives the entire set of equations and boundary conditions in dimensionless form. Note that the outer boundary conditions are defined at the outer edge of the deformation layer, unlike the boundary contions in dimensioned form, which are defined at infinity. Also, the dimensionless viscosity at the outer edge of the deformation layer represents the increase in viscosity from the diapir - country rock interface to this boundary.

2.1.5 Solving the Differential Equations

The next step in the derivation process is to find solutions for the dimensionless components of velocity,

Scaled Governing Equations

Viscosity-Temperature	$\mu' = \exp(\gamma'(1-T'))$
Continuity	$\partial u'/\partial r' + \partial v'/\partial \theta + v'\cot\theta = 0$
r-comp. of Momentum	$\partial P'/\partial r' = 0$
θ-comp. of Momentum	$\partial P'/\partial \theta = \partial/\partial r'(\mu' \partial v'/\partial r')$
Energy	$\partial^2 T'/\partial r'^2 = 0$

Dimensionless Boundary Conditions

at $r' = 0$:	at $r' = 1$:
$u' = 0$	$u' = -\cos\theta$
$\partial v'/\partial r' = 0$	$v' = 0$
$T' = 0$	$T' = T_F'$
$\mu' = 1$	$\mu' = F$

TABLE 2.2

pressure, and temperature. The following is a step by step derivation of the equations found in Table 2.2.

Step 1: The energy equation is

$$\partial^2 T'/\partial r'^2 .$$

Integrating twice,

$$T' = C_1(\theta) r' + C_2(\theta) .$$

Applying the boundary conditions T' = 1 at r' = ∅ and T' = T'_F at r' = 1, yields

[2.9] $$T' = r' (T_F' - 1) + 1 .$$

Step 2: The r-component of the momentum equation is

$$\partial P'/\partial r' = 0 .$$

Integrating,

$$P' = C_3(\theta) .$$

Step 3: The θ-component of the momentum equation is

$$\partial P'/\partial \theta = \partial/\partial r' \cdot (\mu' \partial v'/\partial r') .$$

Integrating,

$$r'/\mu' \cdot \partial P'/\partial \theta + \frac{1}{\mu'} \cdot C_4(\theta) = \partial v'/\partial r' .$$

Applying the boundary condition $\partial v'/\partial r' = \emptyset$ at r' = ∅, yields

$$C_4(\theta) = 0 .$$

Therefore,

$$r'/\mu' \cdot \partial P'/\partial \theta = \partial v'/\partial r' .$$

Integrating,

$$v' = \partial P'/\partial \theta \int \frac{r'}{\mu'} dr' .$$

Evaluating the integral yields

$$v' = \partial P'/\partial\theta \left(\exp(r'\chi)(r'/\chi - 1/\chi^2) + C_5(\theta)\right.$$

where $\chi = \gamma'(T_F' - 1)$.

Applying the boundary condition v' = 0 at r' = 1, yields

$$C_5(\theta) = -\exp(\chi)(1/\chi - 1/\chi^2) .$$

Therefore,

[2.10] $$v' = \partial P'/\partial\theta \left(\exp(r'\chi)(r'/\chi - 1/\chi^2) + \exp(\chi)(1/\chi^2 - 1/\chi)\right).$$

Step 4: The continuity equation is

$$\partial u'/\partial r' + \partial v'/\partial\theta + v'\cot\theta = 0 .$$

Substituting and rearranging,

$$\partial u'/\partial r' = \left(\partial^2 P'/\partial\theta^2 + \partial P'/\partial\theta \cot\theta\right)\left(\exp(r'\chi)(1/\chi^2 - r'/\chi) + \exp(\chi)(1/\chi - 1/\chi^2)\right).$$

Integrating,

$$u' = \left(\partial^2 P'/\partial\theta^2 + \partial P'/\partial\theta \cot\theta\right)\left(\int \frac{\exp(r'\chi)}{\chi^2} dr' - \int \frac{\exp(r'\chi)}{\chi} r' dr' + \int \exp(\chi)(1/\chi - 1/\chi^2) dr'\right).$$

Evaluating the integrals and substituting back,

$$u' = \left(\partial^2 P'/\partial\theta^2 + \partial P'/\partial\theta \cot\theta\right)\left(\exp(r'\chi)\left(\frac{-2}{\chi^3} - \frac{r'}{\chi^2}\right) + r'\exp(\chi)(1/\chi - 1/\chi^2) + C_6(\theta)\right).$$

Applying the boundary condition at r' = 0, u' = 0, yields

$$C_6(\theta) = -2/\chi^3 .$$

Therefore,

[2.11] $$u' = \left(\partial^2 P'/\partial\theta^2 + \partial P'/\partial\theta \cot\theta\right)\left(\exp(r'\chi)(2/\chi^3 - r'/\chi^2) + r'\exp(\chi)(1/\chi - 1/\chi^2) - 2/\chi^3\right).$$

Step 5: To find a solution for P', apply the boundary condition at r' = 1, u' = - cosθ, to equation 2.11,

$$\cos\theta = \left(\partial P'/\partial\theta \cot\theta + \partial^2 P'/\partial\theta^2\right) Z$$

where $Z = \exp(\chi)(2/\chi^2 - 2/\chi^3 - 1/\chi) + 2/\chi^3$.

Rearranging,

$$\partial\rho'/\partial\theta \cot\theta + \partial^2\rho'/\partial\theta^2 = \frac{\cos\theta}{z} .$$

Let $\gamma = \partial\rho'/\partial\theta$ and $d\gamma/d\theta = \partial^2\rho'/\partial\theta^2$.

Therefore,

$$\gamma \cot\theta + d\gamma/d\theta = \frac{\cos\theta}{z} .$$

Multiplying both sides by ξ,

$$\xi\left(\gamma\cot\theta + d\gamma/d\theta\right) = \xi\left(\frac{\cos\theta}{z}\right)$$

where

$$\frac{d}{d\theta}(\xi\gamma) = \xi\, d\gamma/d\theta + \gamma\, d\xi/d\theta$$

and

$$d\xi/d\theta = \xi\cot\theta .$$

Rearranging,

$$d\xi/\xi = \cot\theta\, d\theta .$$

Integrating,

$$\ln\xi = \ln\sin\theta .$$

Therefore,

$$\xi = \sin\theta .$$

Substituting $\sin\theta$ for ξ, yields

$$\sin\theta\left(\gamma\cot\theta + d\gamma/d\theta\right) = \sin\theta\cos\theta/z .$$

Rearranging,

$$\left(\gamma\cos\theta - \sin\theta\cos\theta/z\right)d\theta + \sin\theta\, d\gamma = 0.$$

The above equation is an "exact equation". Following the instructions for solving exact equations from Rainville and Bedient (1981):

Let $M = \gamma\cos\theta - \sin\theta\cos\theta/z$

and $N = \sin\theta$.

To satisfy the assertion that the equation is exact, the

following partial derivatives must be equal.

$$\partial M/\partial y = \cos\theta$$
$$\partial N/\partial \theta = \cos\theta$$

From this it is apparent that a solution B exists, which is equal to a constant.

$$dB = M\,d\theta + N\,dy$$
$$= 0$$

where $M = \partial B/\partial \theta$

and $N = \partial B/\partial y$.

To determine B, use $N = \partial B/\partial y = \sin\theta$.

$$dB = \sin\theta\, dy$$
$$B = y\sin\theta + T(\theta).$$

To determine T(θ), use $M = \partial B/\partial \theta$

$$\partial B/\partial \theta = y\cos\theta - \sin\theta\cos\theta/2$$
$$= T'(\theta) + y\cos\theta.$$

Rearranging,

$$T'(\theta) = -\sin\theta\cos\theta/2.$$

Integrating,

$$T(\theta) = -1/2 \int \sin\theta\cos\theta\, d\theta$$
$$= -1/2\ \sin^2\theta/2.$$

Therefore,

$$B = y\sin\theta - \sin^2\theta/2z.$$

Plugging back in $y = \partial P'/\partial \theta$, yields

$$B = \partial P'/\partial \theta \sin\theta - \sin^2\theta/2z.$$

Rearranging,

$$\partial P'/\partial \theta = B/\sin\theta + \sin\theta/2z.$$

Integrating,

$$P' = B\int \csc\theta\, d\theta + \tfrac{1}{2}z\int \sin\theta\, d\theta + C_\eta(r')$$

$$= B \ln(\tan\theta/2) - \frac{\cos\theta}{2z} + C_\eta(r').$$

Since P' is constant in r' (Step 2),

$$P' = B \ln(\tan\theta/2) - \cos\theta/2z + C_\eta .$$

When $\theta = \pi/2$,

$$\ln(\tan\theta) = 0$$

and $$\cos\theta = 0.$$

Therefore,

$$C_\eta = P'(\pi/2)$$

$$= P'_E .$$

At $\theta=0$, $\ln(\tan\theta)$ goes to negative infinity. Since this is not a singular point, $B = 0$. Therefore,

[2.12] $$P' = \frac{-\cos\theta}{2z} + P'_E .$$

Table 2.3 lists the solutions for the dimensionless partial differential equations derived in steps 1-5.

2.1.6 Forces on the Diapir

In order to find a relationship for the actual ascent velocity, the forces acting on the diapir must be considered. The total force acting on the body is the sum of the surface integral of normal pressure and tangential shear stress acting on it, and the diapir's weight. Mathematically,

[2.13] $$F_{Tot} = F_n + F_t + W$$

where $$F_n = -\int p\vec{n}\, dA$$

$$F_t = \int \tau_{r\theta}|_{r=R}\, dA$$

$$W = \int \rho_D \vec{g}\, dV$$

Solutions for the Dimensionless Partial Differential Equations

$u' = \exp\left(\gamma'\left(1-T'\right)\right)$
$T' = r'\left(T_F'-1\right)+1$
$v' = \frac{\partial p'}{\partial \theta}\left(\exp\left(r'\chi\right)\left(\frac{r'}{\chi}-\frac{1}{\chi^2}\right)+\exp\left(\chi\right)\left(\frac{1}{\chi^2}-\frac{1}{\chi}\right)\right)$
$u' = -\left(\frac{\partial p'}{\partial \theta}\cot\theta+\frac{\partial^2 p'}{\partial \theta^2}\right)\left(\exp\left(r'\chi\right)\left(\frac{2}{\chi^3}-\frac{r'}{\chi^2}\right)+r'\exp\left(\chi\right)\left(\frac{1}{\chi}-\frac{1}{\chi^2}\right)-\frac{3}{\chi^3}\right)$
$p' = -\cos\theta/2\, z + p_E'$
where $\chi = \gamma'\left(T_F'-1\right) = -\ln\left(F\right)$ $z = \exp\left(\chi\right)\left(\frac{2}{\chi^2}-\frac{2}{\chi^3}-\frac{1}{\chi}\right)+\frac{2}{\chi^3}$

TABLE 2.3

$$p = p_o + \rho \vec{g} \cdot \vec{x} + P$$

$\tau_{r\theta}|_{r=R} = 0$ (from the stress-free surface condition)

and ρ_D is the density of the diapir.

The total and Batchelor's modified pressures, p and P, are discussed in subsection 2.1.3. When the solutions for the governing equations were derived, only the modified pressure, P, was considered. When the density remains constant during individual snapshots, the use of the modified pressure is convenient, as shown in the following integration. Substituting for p in the pressure integral above and using the divergence theorem, yields

$$F_n = -\left(\int \nabla(p_o + \rho \vec{g} \cdot \vec{x})\, dV + \int P \vec{n}\, dA\right)$$

$$= -\rho \vec{g} V - \int P \vec{n}\, dA .$$

In spherical coordinates, over the diapir's surface, yields

$$F_n = -4/3\, \pi R^3 \rho \vec{g} - 2\pi \int_0^{\pi} (P \cos\theta) R^2 \sin\theta\, d\theta .$$

From Table 2.3, the dimensionless modified pressure within the deformation layer, is

$$P' = -\cos\theta / 2z + P_E'$$

where

$$P' = P/\rho$$

and

$$\rho = \mu_o U_o R / d^2 .$$

Therefore, the modified pressure, with proper scale, is

$$P = \mu_o U_o R / d^2 \left(P_E' - \frac{\cos\theta}{2z}\right).$$

Substituting back into the integral and evaluating, yields

$$= -2\pi \int_0^{\pi} (P\cos\theta) R^2 \sin\theta \, d\theta$$

$$= -2\pi \mu_0 U_0 R^3/d^2 \left(P_E' \int_0^{\pi} \cos\theta \sin\theta \, d\theta - \tfrac{1}{2} z \int_0^{\pi} \cos^2\theta \sin\theta \, d\theta \right)$$

$$= 2\pi \mu_0 U_0 R^3/3 d^2 z .$$

The weight of the diapir is easily evaluated as

$$\int \rho_D \vec{g} \, dV = 4/3 \, \pi R^3 \rho_D \vec{g} .$$

By summing the weight of the diapir with the integral of the normal pressure, yields

$$F_n + W = 4/3 \, \pi R^3 (\rho_D - \rho) \vec{g} + 2/3 \, \pi R^3 \mu_0 U_0 / d^2 z .$$

Since the shear stress at the surface of the diapir is assumed to be zero,

$$F_t = 0 .$$

The total force acting on the diapir is

[2.14] $$F_{T.I} = 4/3 \, \pi R^3 ((\rho_D - \rho) \vec{g} + \mu_0 U_0 / 2 d^2 z .$$

If mechanical equilibrium is assumed, that is the velocity has achieved a terminal value for the conditions given, then the sum of the forces acting on the diapir is zero.

$$F_{T.I} = 0$$

Therefore,

$$U_0 = 2 (\rho - \rho_D) \vec{g} \, d^2 z / \mu_0 .$$

The ascent velocity is related to U_0 by

$$U_\infty = \epsilon U_0$$

where

$$\epsilon = d/R .$$

The ascent velocity of a rising diapir is

[2.15] $$U_\infty = 2 (\rho - \rho_D) \vec{g} \, d^3 z / \mu_0 R .$$

The relationship in equation 2.15 applies to the ascent of a hot spherical magma body at any particular instant in time, given the temperature distribution surrounding the body and an input parameter describing the increase in viscosity across the width of a narrow deformation layer.

2.2 Heat Transfer Processes

In the last section a quasi-equilibrium assumption (the snapshot approach) is used to derive a solution for the steady state ascent velocity of an igneous diapir. The result is strongly dependent upon the temperature distribution in the surrounding country rock. This section describes the methods used to solve the energy equation for the entire system. Together, these processes control the efficiency at which a diapir can transport itself through the continental crust.

2.2.1 Mechanisms of Heat Transfer

As the diapir rises through the continental crust the overall temperature distribution will become quite complex. This is due, in part, to the differing mechanisms of heat transfer and the varying diapir and ambient temperatures. The solution methods presented here, and in other works of a similar nature (Marsh, 1982; Morris, 1982), do not dwell on closely constraining the temperature at a distance from the diapir; rather, I have concentrated on the temperature within

the immediate vicinity of the diapir.

Three differing heat transfer processes are taken into account in this study; free convection within the diapir, conduction within the country rock and forced convection within the deformation layer. Each process is discussed separately.

Free Convection

The igneous diapirs modeled in this study are many orders of magnitude lower in viscosity than the country rock they intrude. Free convection is assumed to be absent in the country rock, but it is the principal process transferring heat within the diapir. On the time scales dealt with here, the magma in the diapir experiences rapid convective overturning, whereas the country rock remains stagnant. Within the model the temperature gradient inside the diapir is assumed to be zero during individual snapshots. This can be justified by noting that the distance a diapir will rise when it nears its solidus temperature, a temperature at which free convection is greatly limited, is negligible due in part to the diapir's lack of plasticity.

Heat Conduction

The temperature distribution that results from heat conduction within the country rock can be approximated by using equation 2.16 for radial conduction from a spherical

source.

[2.16] $$\partial T/\partial t = \kappa\left(\partial^2 T/\partial r^2 + \frac{2}{r}\,\partial T/\partial r\right)$$

where κ is the thermal diffusivity of the country rock. The boundary conditions for this study would normally be time dependent, but by using the snapshot approach (subsection 2.1.1) these conditions become constants within individual snapshots and the initial condition becomes the initial state of the system at the onset of the snapshot.

at $r = R$, $T = T_o$ (diapir - country rock interface)

$r = \infty$, $T = T_\infty$ (ambient temperature)

when $t_{ss} = \emptyset$, $T = T(r)$ (snapshot's initial temperature distribution)

This initial state cannot be generalized to any group of snapshots and cannot be accurately predicted prior to ascent. In order to find a reasonable approximation to the temperature distribution within the country rock, equation 2.16 must be solved numerically.

The first step in finding a numerical solution for equation 2.16 is to make the variables dimensionless. Table 2.4 lists these dimensionless variables and their scales. The caret is used to distinguish variables that are defined differently in section 2.2.

The heat conduction equation, boundary conditions, and initial condition in dimensionless form are

[2.17] $$\partial T'/\partial \hat{t} = \partial^2 T'/\partial \hat{r}^2 + \frac{2}{\hat{r}+1}\,\partial T'/\partial \hat{r}$$

	Dimensionless Variables	Scales
Temperature	$T' = \frac{T - T_\infty}{T_o - T_\infty}$	$T = T'(T_o - T_\infty) + T_\infty$
Time	$\hat{t} = \frac{t \alpha_o}{R^2}$	$t = \hat{t} R^2 / \alpha_o$
Radial distance	$\hat{r} = \frac{r - R}{R}$	$r = \hat{r} R + R$
Thermal diffusivity	$\alpha' = \alpha / \alpha_o \; (=1)$	$\alpha = \alpha' \alpha_o$

TABLE 2.4

at $\hat{r} = 0, \; T' = 1$

$\hat{r} = \infty, \; T' = 0$

when $\hat{t} = 0, \; T' = T'(r)$.

The numerical method used to solve equation 2.17 is a forward difference approximation. Breaking each term down into its equivalent difference formula, yields

$$\partial T'/\partial \hat{t} = T'_{i,j+1} - T'_{i,j} / \Delta \hat{t}$$

$$\partial T'/\partial \hat{r} = T'_{i+1,j} - T'_{i,j} / \Delta \hat{r}$$

and $$\partial^2 T'/\partial \hat{r}^2 = T'_{i+1,j} - 2T'_{i,j} + T'_{i-1,j} / (\Delta \hat{r})^2 .$$

Inserting these back into equation 2.17 and rearranging,

[2.18] $$T'_{i,j+1} = \frac{\Delta \hat{t}}{\Delta \hat{r}^2}\left(T'_{i+1,j} - 2T'_{i,j} + T'_{i-1,j}\right) + \frac{2}{\hat{r}+1}\frac{\Delta \hat{t}}{\Delta \hat{r}}\left(T'_{i+1,j} - T'_{i,j}\right) + T'_{i,j} .$$

Errors are introduced when numerical methods are used to approximate the solution to a partial differential equation. To lessen these errors, and insure a realistic level of conditional stability (i.e., the stability of a function with change in the independent variables), the step size for the time ($\Delta\hat{t}$) and radial distance ($\Delta\hat{r}$) intervals must be chosen with care. In Burden et al. (1981), the error in a similar parabolic partial differential equation is, $\sigma(\Delta\hat{t} + (\Delta\hat{r})^2)$. for the first set of terms on the right hand side of equation 2.18. The second set of terms has an error of $\sigma(\Delta\hat{t} + \Delta\hat{r})$. For the function to be conditionally stable, the following inequalities must be satisfied,

$$\Delta\hat{t}/(\Delta\hat{r})^2 \leqslant 0.5$$

and $$\Delta\hat{t}/\Delta\hat{r} \leqslant 0.5 .$$

I found an interval size of $\Delta\hat{r}$ = 5 m and $\Delta\hat{t}$ = 1.ØE+7 seconds to be both reasonable and accurate for a diapir with a radius of 2.5 km rising through country rock with a thermal diffusivity on the order of 1.ØE-6 m^2/sec. The following dimensionless step sizes result,

[2.19a] $\Delta\hat{t} = 1.6\,E-6$

[2.19b] $\Delta\hat{r} = 2.0\,E-3$.

The magnitude of the error that would result using these step sizes is $\mathcal{O}(1Ø^{-6})$ for the first set of terms on the right hand side of 2.18 and $\mathcal{O}(1Ø^{-3})$ for the second set of terms. In practice, the first error will dominate in the vicinity of the spherical source because the contribution to the temperature distribution in this region is far greater from the first set of terms in equation 2.18. These errors apply to the dimensionlesss temperature which varies between 1.Ø at the diapir - country rock interface and Ø.Ø in the country rock at a distance.

Figure 2.1 compares the dimensionless temperature distribution that results from equation 2.18, using the step sizes in 2.19, and the results from a popular analytical solution, given an initially flat temperature distribution in the surrounding medium (Carslaw and Jaeger, 1959). The two results diverge slightly at greater distances from the diapir. This can be attributed to the error that results from using a finite step size to approximate the actual asymptotic temperature distribution. Note that the error at

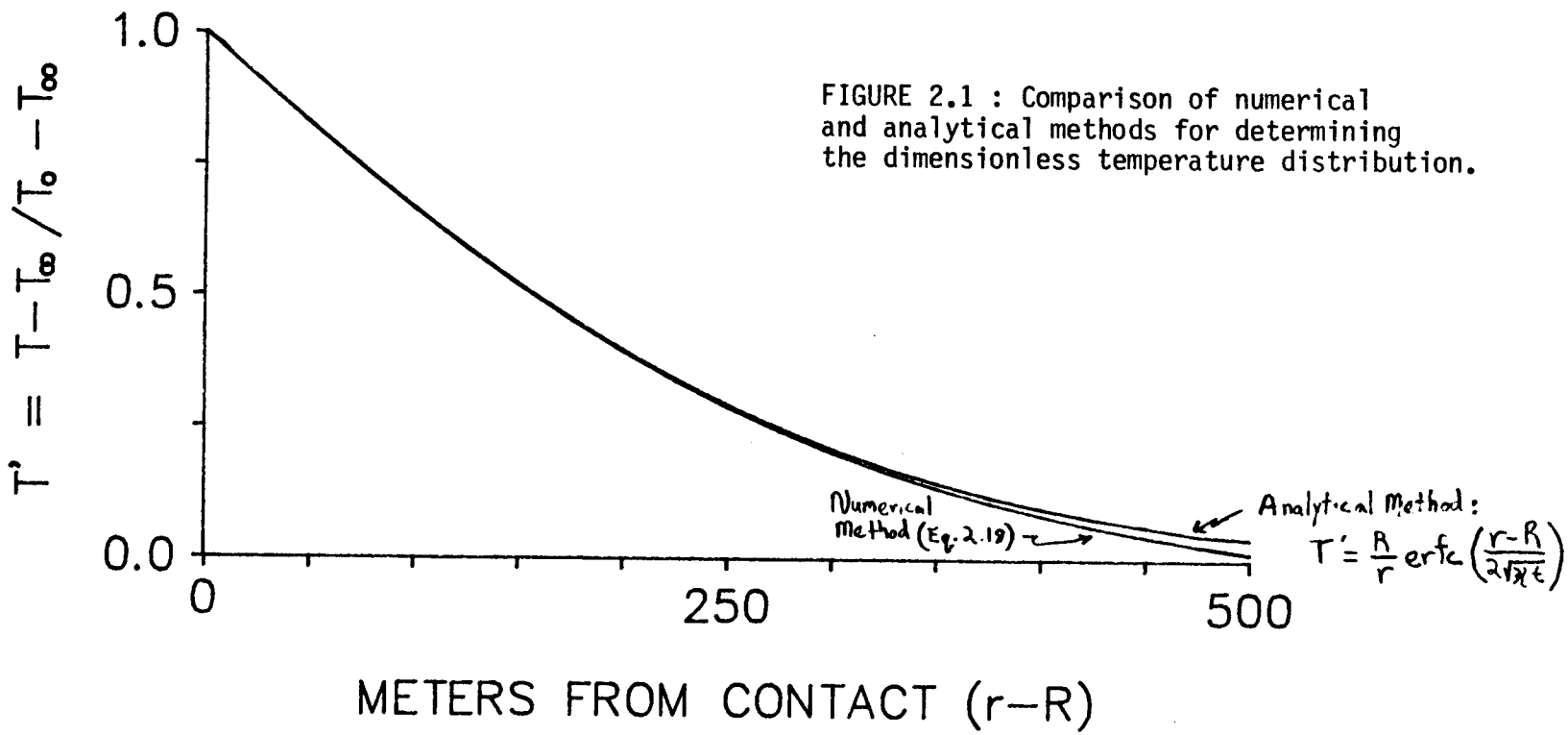

FIGURE 2.1 : Comparison of numerical and analytical methods for determining the dimensionless temperature distribution.

500 m away from the diapir is approximately 0.03 in dimensionless temperature. Due to the propagation of errors in successive runs, this error will be larger as time goes on. In the case of Figure 2.1 , equation 2.18 was solved 3200 times.

The test for conditional stability results in

$$\Delta\hat{t}/(\Delta\hat{r})^2 = 0.4 < 0.5$$

and

$$\Delta\hat{t}/\Delta\hat{r} = 0.8\,E\text{-}3 < 0.5 \ .$$

These signify that the step sizes chosen will not cause unrealistic perturbations in the resulting temperature distribution. This is illustrated by the the smoothness of the curve shown in Figure 2.1.

Forced Convection

Forced convection within the deformation layer is the most difficult process to model accurately. In previous works concerning igneous diapirism with a thin layer of deforming country rock (Marsh, 1982; Morris, 1982), forced convection was dealt with in relationships containing pure numbers (e.g., Peclet number, Nusselt number, etc.). The use of pure numbers has been avoided in this study because a single number can not describe the system entirely. For instance, the Peclet number ($Pe = U_\infty R/\chi$ for the diapir only) is a ratio of the velocity of the fluid to the thermal diffusivity. Although the thermal diffusivity is assumed to be constant within the country rock, the velocity of the

country rock within the deformation layer varies significantly across the entire width. Figures 2.2a and 2.2b are graphs of the dimensionless tangential velocity versus dimensionless distance within a deformation layer for two different deformation factors, F. For either case, a single Peclet number could not apply to the region as a whole.

The method I introduce here is totally independent of constraints imposed by pure numbers. This method, referred to as the "cyclic method", is an iterative approach to solving the problem of energy and material transfer within the deformation layer. The curves shown in Figures 2.2a and 2.2b are broken into 1Ø intervals of equal length. A number at the midpoint of each interval represents the relative magnitude of the velocity for that particular region (the sum of the numbers is 5Ø). The amount of energy transferred by forced convection at any point within the deformation layer is proportional to the velocity at that point. The cyclic method uses this concept and the fact that material and energy are transferred when the diapir replaces country rock within the deformation layer by ascending through it. The material lost should be taken over the entire width of the deformation layer. This method, together with the snapshot approach, allows material and energy to be transferred within a single interval for an individual snapshot, but over a series of snapshots it will occur across the entire deformation layer. Intervals with higher velocities (i.e.,

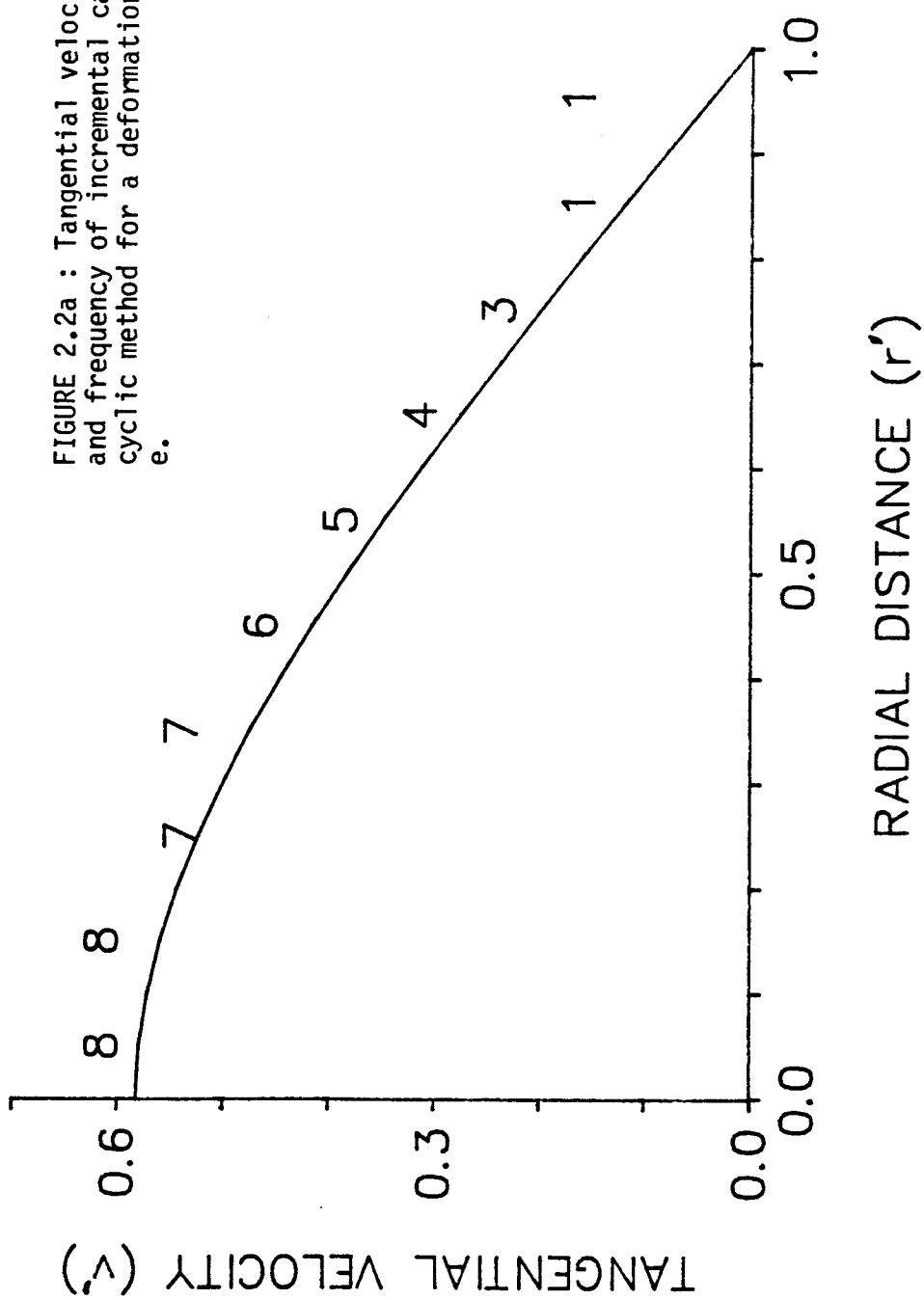

FIGURE 2.2a : Tangential velocity profile and frequency of incremental calls to the cyclic method for a deformation factor of e.

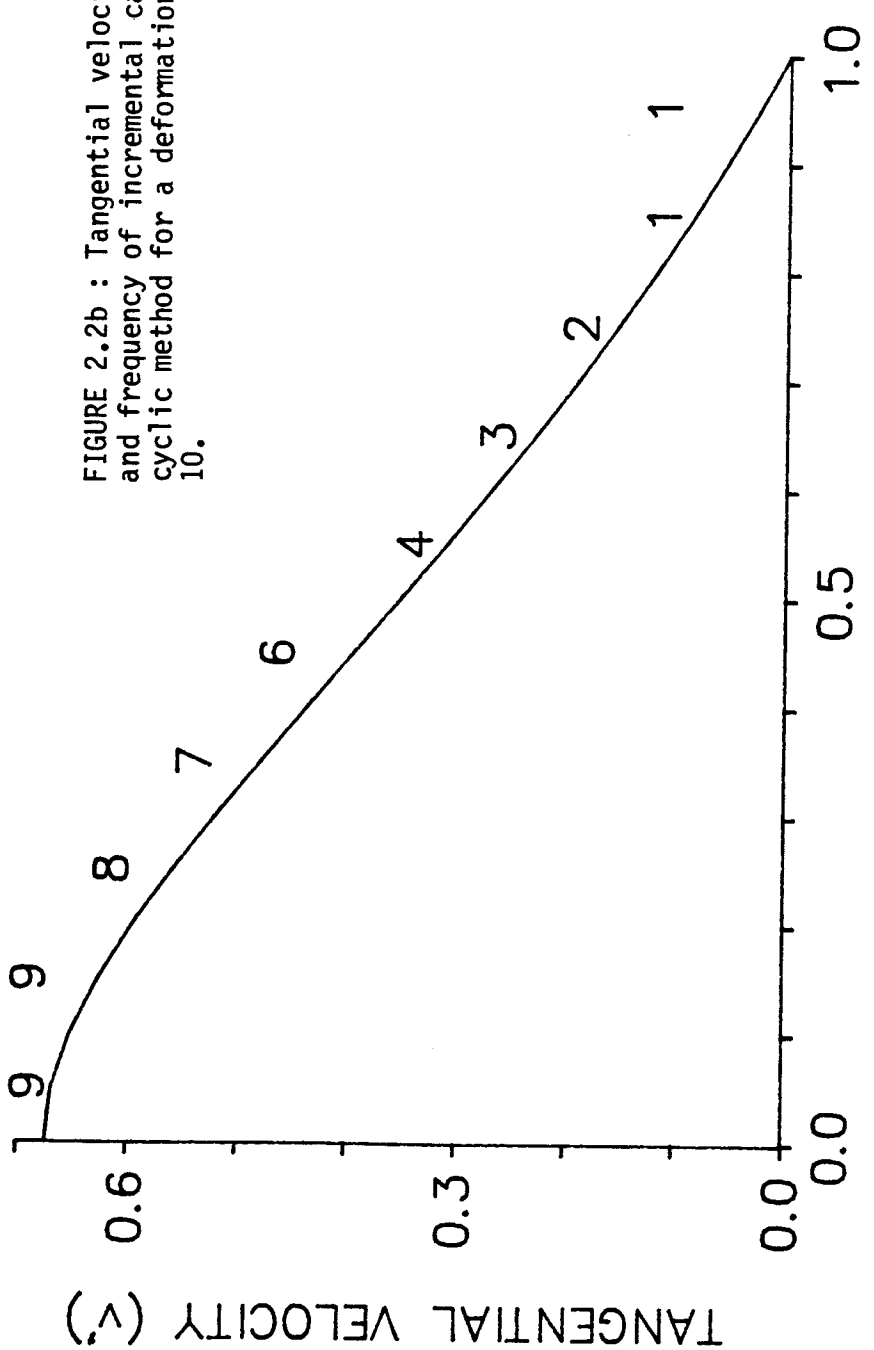

FIGURE 2.2b : Tangential velocity profile and frequency of incremental calls to the cyclic method for a deformation factor of 10.

intervals undergoing a larger amount of strain) will be called upon more often to take up the deformation than those with lower velocities. The numbers at the midpoints in Figures 2.2a and 2.2b are actually the number of times that a particular interval will take up the deformation within a series of 50 snapshots.

When the diapir rises relatively small distances, it essentially transfers material adjacent to its upper hemisphere, via forced convection within the deformation layer, to its lower hemisphere. The amount of material transferred over the upper hemisphere of the diapir is

$$\frac{2}{3}\pi\left(U_\infty \Delta t_{ss} h(\theta)\right)^3$$

where Δt_{ss} is the duration of a snapshot and $h(\theta)$ is some function of the polar angle.

Although the cyclic method is a rather crude approach, it is a useful first order approximation to the energy and material transported within the deformation layer. Other advantages of this method are its compatibility with the snapshot approach and cost effectiveness when run relative to more elaborate models.

2.2.2 Heat Generation

During ascent, heat will be generated within the diapir by latent heat of crystallization, decay of radioactive isotopes, and the conversion of potential energy to kinetic energy.

Over an extended period of time, heat released by the crystallization of the magma body will be significant. An extremely simple calculation involving the input of three parameters will control the heat added to the diapir linearly between the solidus and liquidus temperatures. These parameters are the temperature at which crystallization begins (liquidus), the temperature at which crystallization is complete (solidus), and the equivalent temperature added to the diapir due to latent heat of crystallization. The result will be "pretty much the same" (Marsh,1982) as incorporating the exact thermodynamic relationships into the model.

As the diapir rises through the crust, it is being transported to regions of lower potential energy. Within the deformation layer thermal energy will be released by viscous dissipation. This is directly related to the loss of potential energy. Spera (1980) points out that in order for viscous dissipation, or frictional heating, to be significant the Gruntfest number ($Gu = \gamma\sigma^2 d^2/K\mu$) must exceed 0.88. Due to the high average viscosities across the relatively narrow deformation layer, this would seldom occur. Therefore, viscous dissipation will be considered negligible and any conversion of potential energy will occur within the diapir.

The conversion of potential energy to kinetic energy and the heat added by the decay of radioactive isotopes are small compared to the latent heat of crystallization. But in order

to be complete, the amount of thermal energy produced by these processes will be added to the equivalent temperature term used primarily for latent heat of crystalization.

Calculations of the exact amount of equivalent temperature used in model runs is discussed in Chapter III.

2.3 The Computer Model

In the last two sections relationships for the ascent velocity and models for heat transfer processes are derived separately. In this section I apply the temperature distribution models to the ascent velocity relationship, resulting in a coherent model of time dependent ascent velocity.

The program "Socrates", used to generate time dependent velocity profiles, is in Appendix A. The following is a simple summary of what Socrates does:

1) A period of free flux of heat from the diapir yielding an initial temperature distribution.

2) Heat conduction from the diapir to the surrounding country rock for a period equal to the length of a "snapshot", yielding a new temperature distribution.

3) Energy gained by the surroundings from the last step is calculated.

4) Width of the deformation layer is calculated from the temperature distribution.

5) Diapir rises, generating forced convection within the deformation layer and a new 'initial' temperature distribution.

6) The new diapiric temperature is determined by calculating of the energy lost to the cooler surroundings and energy gained from the heat generating processes.

7) New depth and undisturbed ambient temperatures are calculated.

8) Go to (2).

From the above summary it is apparent that Socrates expends most of its effort on bookkeeping. Descriptions of methods used for some of the more tedious chores are left for documentation in the actual program (Appendix A). The more important points are discussed in this section. These include the free flux period, calculating the deformation layer's thickness, the effect of diapiric ascent on the size and shape of the deformation layer, and calculating the undisturbed ambient temperatures.

2.3.1 Visualization

A simple sketch illustrating the diapiric model is shown in Figure 2.3. The diapiric temperature (T_o), undisturbed ambient temperature (T_∞), ascent velocity (U_∞), deformation layer's thickness (d), and other parameters are illustrated.

The lower hemisphere of the diapir is considered an

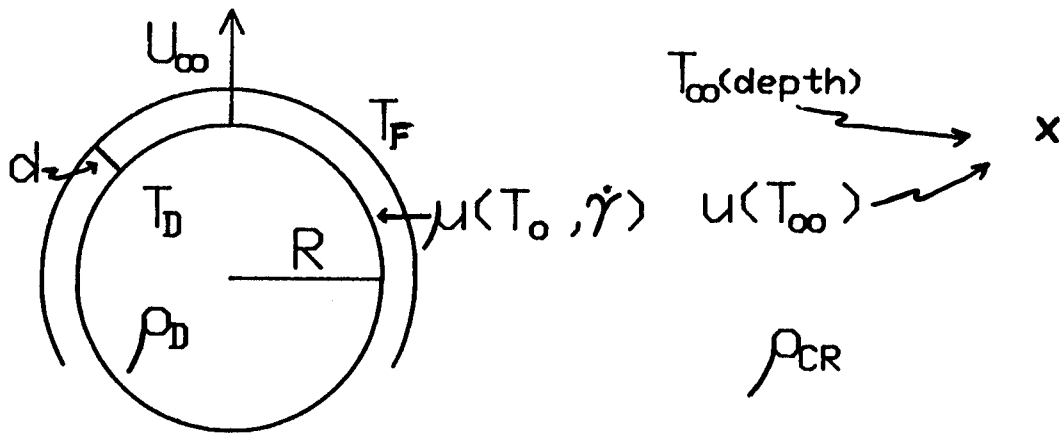

FIGURE 2.3 : A simple representation of the model at an instant in time.

insulated boundary between itself and the country rock. In other words, during ascent heat loss from the diapir only occurs through the upper hemisphere's surface. This is justified because heat flux is proportional to the temperature gradient, which is much larger adjacent to the upper portion of the diapir than the lower portion for two reasons. Firstly, the undisturbed ambient temperature is lower at higher regions in the crust (this is significant in large diapirs), and secondly, the country rock surrounding the lower portion of the diapir has been exposed to heat lost from the diapir for an extended period of time. Both contribute to a considerably steeper temperature gradient near the top of the diapir, and therefore a much higher heat flux.

As the diapir rises it will be surrounded by country rock with progressively cooler ambient temperatures. Over an extended period of time this could have a significant effect on the heat loss from the diapir. If a temperature gradient of 25°C/km is assigned to the country rock then a rise of 4 kilometers will drop the temperature of the country rock at a distance by 100°C.

In Figure 2.3 the ambient temperature is defined at the depth to the top of the diapir. Therefore, the undisturbed ambient temperature at a particular depth to the top of the diapir is

[2.20] $$T_\infty = dT_\infty/dX \ (\text{Depth}) + T_s$$

where dT_∞/dx is the linear temperature gradient within the continental crust and T_S is the surface temperature.

2.3.2 Deformation Layer

The relationship for the ascent velocity found in section 2.1 is

[2.15] $$U_\infty = 2(\rho - \rho_D)\vec{g}\, d^3 Z/\mu_o R$$

where Z is a constant, the value of which depends on the increase in viscosity across the deformation layer of thickness d. In order to find the ascent velocity at any given time, two parameters must be known; the increase in viscosity across the deformation layer, F, and the actual width of the deformation layer.

Marsh (1982) assumes the deformation layer to be some fraction of the diapir's radius, whereas Morris (1982) has allowed the deformation layer to implicitly rely on the surrounding temperature distribution. This is done by allowing F to be constant. Therefore, the edge of the deformation layer can be found at a temperature where the viscosity, $\mu(T_F)$, is a factor of F greater than at the diapir - country rock interface, $\mu(T_o)$. This temperature can be found from the viscosity - temperature relationship.

$$\mu_F/\mu_o = F = \exp(\gamma(T_o - T_F))$$

Therefore,

[2.21] $$T_F = T_o - \ln(F)/\gamma .$$

Knowing T_F, the deformation layer's thickness, d, can

easily be found from the surrounding temperature distribution.

Thus far it has been assumed, without mention, that the deformation layer's thickness does not vary with θ. Whether this would be the case in a continuum approach will not be debated here. If finite periods of heat flux , from the diapir, are allowed to elapse prior to instantaneous ascent, as is necessary by the snapshot approach, then potentially abnormal outlines of the deformation layer will result. To alleviate this problem, the volume of the material replaced within the deformation layer adjacent to the upper hemisphere, due to the diapir rising through it, is reshaped into a hollow hemisphere of equal thickness. A portion of this hemisphere is then deleted from the deformation layer at a distance from the diapir - country rock interface that is determined by the cyclic method discussed in section 2.2. Since the deformation layer is thin relative to the diapir's radius, the average thickness deleted following a snapshot is approximately half the actual ascent distance.

2.3.3 Initial and Final Stages

The model discussed thus far has not concerned itself with the initial stages of igneous diapirism, where magma separates from a source. Also, little has been added to the model to constrain the final stages, when the magma body ceases to rise by ductily deforming a thin region of country

rock adjacent to it. Both of these end members entail complex condtions that are not easily incorporated into the model. Rather than rederive the model to include these conditions, an estimation of the states of the system when the diapiric ascent model begins to apply and when it ceases to be valid, are made.

Free Flux

The thermal conditions present in the country rock when the magma body begins diapiric ascent are more complex than a simple flat temperature distribution at the initial depth. To assist in modeling a realistic initial temperature distribution within the surrounding country rock, I have chosen to enter a parameter that describes a period of 'free flux' from the diapir. That is, the diapir will heat the adjacent country rock at no cost to the diapir's energy reservoir. The length of this free flux period is generally on the order of 10 years.

Unlike the conduction of heat away from the diapir during ascent, the condition prior to free flux is a flat temperature distribution found at the diapir's initial depth (T_{∞_i}). From Carlslaw and Jaeger (1959, p.247) the following is used during this period,

[2.23] $$\frac{T-T_{\infty_i}}{T_{o_i}-T_{\infty_i}} = \frac{R}{r}\,erfc\left(\frac{r-R}{\sqrt{4\chi t_{ff}}}\right)$$

where t_{ff} is the length of the free flux period. This solution is more accurate, and cost efficient, than the

numerical solution for the same initial condition. Unfortunately, this sort of solution can not be used during the remainder of the ascent model due to the complexities in the snapshots' initial temperature distributions.

Cessation

The diapiric model has both physical and mathematical reasoning to account for cessation. The simplest physical limitation is the lack of thermal energy. When this occurs, the ascent velocity will be far too slow, causing the diapir to cool below its solidus without appreciable ascent. Mathematically, the equation for the ascent velocity (2.15) assumes that ϵ (=d/R) is much less than unity. When this is not the case, the ascent velocity equation is invalid.

Fortunately, both of the stated limitations of the modeled diapir are related. When the pluton rises too slowly, it will heat the country rock out to a greater distance than during rapid ascent periods. Eventually, this will cause the deformation layer to exceed the width where the ascent velocity equation is valid.

In order to stop the diapir due to physical and/or mathematical reasons, some constraints on the rate of ascent and width of the deformation layer must be stated. I have chosen ϵ to be no greater than 0.1 at any time during ascent. This allows an order of magnitude difference between the radius of the diapir and the width of the deformation layer.

"Too slow" an ascent velocity is defined as 1.ØE-1Ø cm/sec. Since the diapir may start up slowly in some circumstances, until sufficient energy is transferred to the adjacent country rock, the minimum ascent velocity will not apply for the first few hundred years.

The final consideration for cessation is when the diapiric temperature reaches the solidus. Theoretically ascent could continue, but realistically the diapir could not transfer heat efficiently enough to soften the adjacent country rock. Also, the stress-free boundary condition used to derive the ascent velocity relationship would no longer apply.

2.4 Summary

This chapter has described in detail the various stages in the development of a coherent and continuous mathematical model for diapiric ascent. Figure 2.4 is a network that illustrates the salient features of the derivation and the application of the snapshot approach presented in this chapter.

Both numerical and analytical techniques are used to solve the equations describing rheological and thermal conditions. Due to the temperature dependent rheology, these equations had to be solved simultaneously.

The principal analytical method used is scaling analysis. The method results in a rather simple set of equations and boundary conditions, which yield a closed

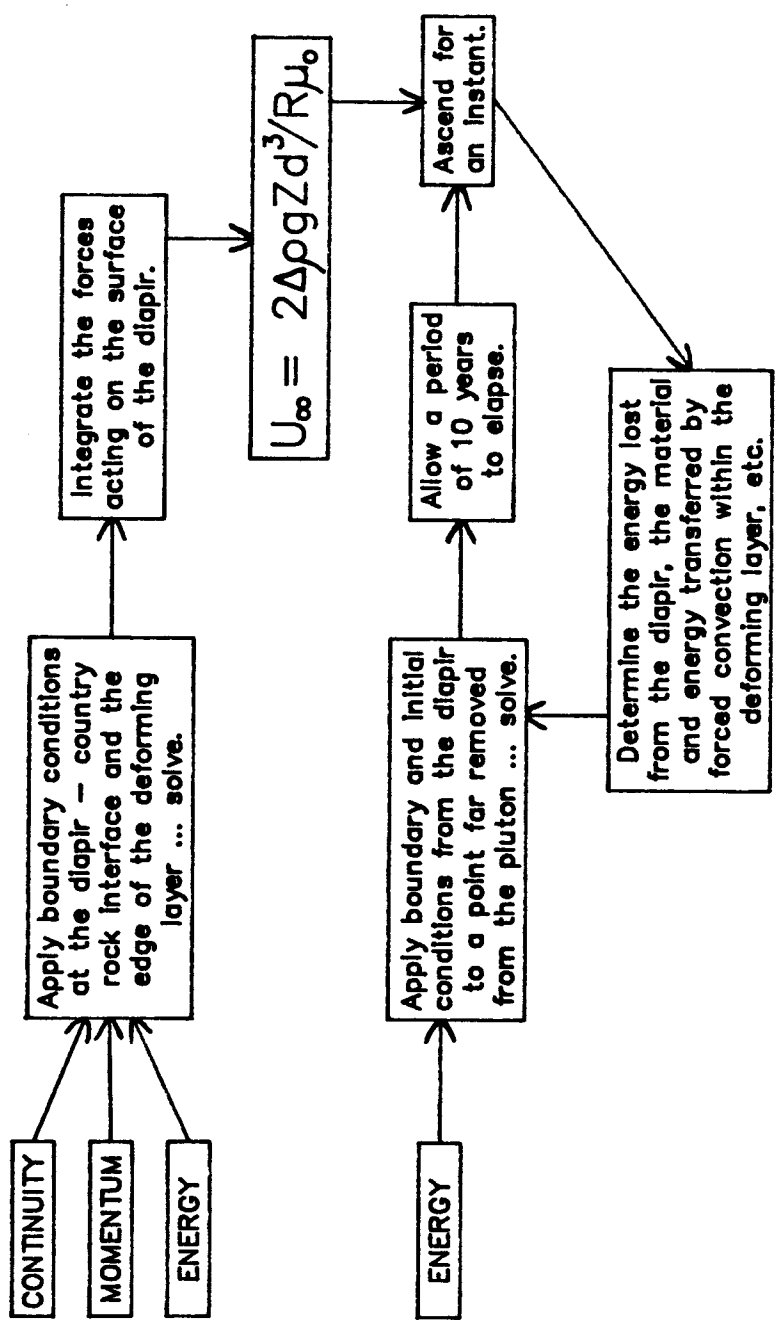
CONTINUITY
MOMENTUM
ENERGY
Apply boundary conditions at the diapir – country rock interface and the edge of the deforming layer ... solve.
Integrate the forces acting on the surface of the diapir.
$U_\infty = 2\Delta\rho g Z d^3/R\mu_o$
Ascend for an instant.
ENERGY
Apply boundary and initial conditions from the diapir to a point far removed from the pluton ... solve.
Allow a period of 10 years to elapse.
Determine the energy lost from the diapir, the material and energy transferred by forced convection within the deforming layer, etc.

FIGURE 2.4

solution for the ascent velocity equation. By use of a series of difference approximations, the heat flow for the entire system is solved. The snapshot approach is implemented in order to relate the entire system of solutions to a single temporal variable.

CHAPTER III

MODEL RUNS

3.0 Introduction

Ten computer simulations, using the FORTRAN program Socrates (see Appendix A), were performed on a UNIVAC 1100/82. Due to the multivariate character of rising granitoid diapirs, results of runs with contrasting input parameters varied considerably.

This chapter consists of two sections: the first is a discussion of the input files for model runs (the complete input files are listed in Appendix B), and the second portion presents graphic illustrations of the velocity profiles and one of the temperature profiles generated by these runs. A complete output file for a sample run of Socrates is given in Appendix C.

3.1 Input

3.1.1 Rheological Data

Two different temperature-dependent country rock rheologies are discussed here. The first material, CR1, involves a Newtonian relationship for obsidian containing 1/2 weight percent water (Shaw, 1963). The second material, CR2, is a non-Newtonian wet dunite that behaves like a power-law fluid, yielding an effective viscosity that is dependent upon temperature and shear strain rate (Carter and Ave'Lallemant,

1970; Carter, 1976).

Although the results of Carter and Ave'Lallemant (1970) are very similar to other studies concerning the rheology of dunite (Chopra and Paterson, 1981), some ambiguity still exists between experimental procedures and natural systems. For instance, Schmid (1982) points out that there is a problem with extrapolating from common laboratory shear strain rates of 10^{-2}/sec to 10^{-7}/sec and geologically reasonable strain rates of 10^{-10}/sec to 10^{-15}. This is a reasonable argument, but in order to perform experiments at lower strain rates would take an unacceptable length of time.

There is a possibility that the rheology found from experimental results yields an effective viscosity for a material that, when acted upon in nature, is much lower. Two mechanisms that could account for enhanced ductility during crustal processes are grain boundary sliding at low strain rates (Chopra and Paterson, 1981) and solid state reactions during metamorphism (White and Knipe, 1978). Chopra and Paterson noted that weakening effects caused by water along the grain boundaries may only be prominent at low strain rates. As of yet, this has not been conclusively proven by experiment. White and Knipe described a complex interaction of processes that may lower the effective viscosity of a rock during metamorphism. These processes include increased chemical diffusivity, expulsion of fluids, and the formation of unstrained minerals. Presently, these processes have not

been fully reproduced in the laboratory.

The flow laws used in this work were not chosen as ideal representations of the situation studied, but because they are the best descriptions of the rheological properties of the rocks available in the literature.

Another rheological constraint considered is the increase in viscosity across the deformation layer, F. This deformation factor is user-defined, and may have a significant effect on the ascent velocity mechanism. The auxiliary input files that define forced convection must be derived on the basis of this factor.

Newtonian Fluid

For the country rock modeled as an obsidian (Shaw, 1963), the Arrhenius relationship in equation 3.1 is used to determine the viscosity (μ) for a given temperature.

[3.1] $$\mu(T) = \mu_\infty \exp(E/RT)$$

where E = 293 kJ/mol and $\log_{10}\mu_\infty$ = -3.0 (poise).
The following viscosities are found at the corresponding temperature using equation 3.1:

u(1000°C) = 1.050E+9 poise

u(900°C) = 1.111E+10 poise

u(800°C) = 1.826E+11 poise

u(700°C) = 5.333E+12 poise

and u(600°C) = 3.374E+14 poise.

Figure 3.1 illustrates the variation of viscosity with

temperature for the data given above.

The mathematical model derived in Chapter II uses equation 3.2 to determine temperature dependent viscosity.

[3.2] $$\mu(T) = \mu_o \exp(\gamma(T_o - T))$$

Equating equations 3.1 and 3.2 shows that the variation parameter γ, is temperature dependent.

[3.3] $$\gamma = \left(E/RT + \ln(\mu_\infty/\mu_o)\right)/(T_o - T)$$

For a temperature equal to 1300 K (T_o), the viscosity found using equation 3.1 is 5.927E+8 poise. Using equation 3.3, γ is found to range from 0.021/deg at 1000°C to 0.031 at 600°C. Since the difference is significant, γ is calculated after each snapshot.

Power-Law Fluid

In the case of the wet dunite, the experimental data of Carter and Ave'Lallemant (1970) are described by the following relationship for a non-Newtonian fluid,

[3.4] $$\dot{\gamma} = A \exp(-E/RT)\sigma^n$$

where $\dot{\gamma}$ is a shear strain rate (not to be confused with a viscous variation parameter γ, of equation 3.3), A is the pre-exponential, and σ is the shear stress.

The effective viscosity for a power-law fluid, described by equation 3.4, is dependent on temperature and shear strain rate. This is shown by equation 3.5.

[3.5] $$\mu(T, \dot{\gamma}) = \dot{\gamma}/\sigma$$

Rearranging equation 3.4 into the form of 3.5, yields

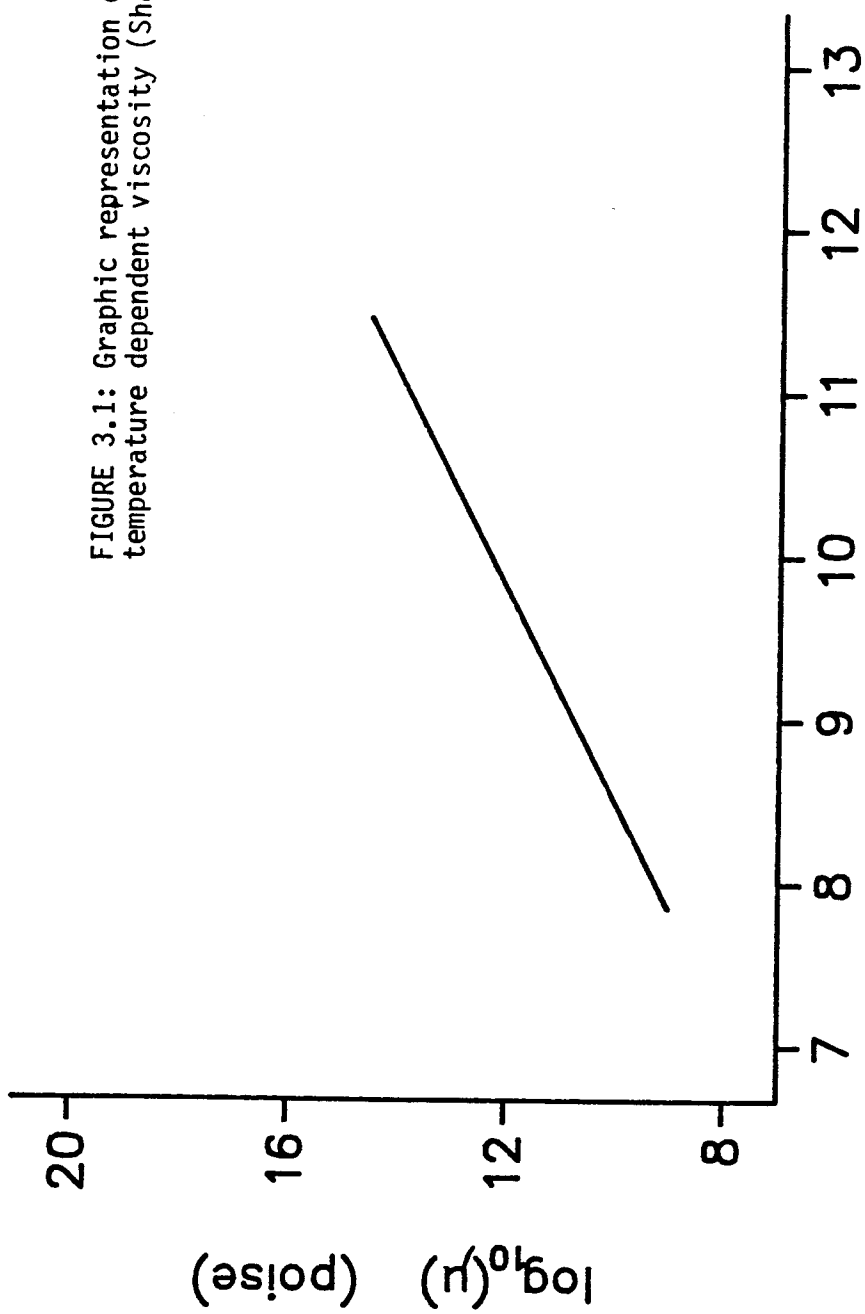

FIGURE 3.1: Graphic representation of CR1's temperature dependent viscosity (Shaw, 1963).

[3.6] $$\mu(T,\dot{\gamma}) = \left(1/A^{1/n}\left(\exp\left(E/RT\right)\right)^{1/n}\dot{\gamma}^{1/n-1}\right)$$

The shear strain rate in spherical coordinates is determined from equation 3.7.

[3.7] $$\dot{\gamma} = 1/r\,\partial u/\partial\theta + \partial v/\partial r - v/r$$

Using the dimensionless variables described in Chapter II, equation 3.7 becomes

[3.8] $$\dot{\gamma} = \frac{U_\infty}{r}\partial u'/\partial\theta + \frac{RU_\infty}{d^2}\partial v'/\partial r' - \frac{RU_\infty}{rd}v'.$$

By implementing the methods used in Chapter II for assessing the negligible terms to be dropped, equation 3.8 simplifies to

[3.9] $$\dot{\gamma} = \frac{RU_\infty}{d^2}\partial v'/\partial r'$$

where

$$\partial v'/\partial r' = \frac{\sin\theta}{2Z}\, r'\exp(r'\chi)$$

Given the factor increase in viscosity across the deformation layer, F, the maximum strain rate within the deformation layer can easily be found (a point where $\partial^2 v'/\partial r'^2 = 0$). For an F = e, $\left|\partial v'/\partial r'\right|_{max}$ is approximately 0.81. Modeling a diapir with a radius of 2.5 km, surrounded by a deformation layer 150 m wide, and ascending 15 km in 50,000 years (U_∞ = 9.5E-7 cm/sec), results in a shear strain rate of 8.6E-10/sec. This strain rate is used to determine relative values for the effective viscosities of a wet dunite at differing temperatures. The results will not effect the actual viscosities calculated during the computer simulation which may be larger or smaller, depending on the instantaneous ascent velocity and the deformation layer's width within a

particular snapshot.

Carter and Ave'Lallemant (1970) have made the following estimates for the other parameters needed to solve for the viscosity:

$A = 1.51E{-}16$ bayres^{-n}/sec

$E = 226$ KJ/mol

and $n = 2.1$.

Using a shear strain rate of 8.6E-10/sec and the corresponding temperatures, the following values for the effective viscosity result:

$u(1000^{\circ}C) = 4.999E{+}16$ poise

$u(900^{\circ}C) = 1.189E{+}17$ poise

$u(800^{\circ}C) = 3.305E{+}17$ poise

$u(700^{\circ}C) = 1.148E{+}18$ poise

and $u(600^{\circ}C) = 5.267E{+}18$ poise.

Figure 3.2 illustrates the variation of viscosity with temperature for the given shear strain rate.

In the case of the Newtonian fluid, the variation parameter γ, is found to be a function of temperature. For a power-law fluid γ depends on both temperature and shear strain rate.

$$\mu(T,\dot{\gamma}) = \mu_o \exp(\gamma(T_o - T))$$
$$= (1/A^{1/n}(\exp(E/RT))^{1/n}\dot{\gamma}^{1/n-1}$$

Rearranging,

[3.10] $$\gamma = \ln\left(\frac{\mu(T,\dot{\gamma})}{\mu_o}\right)/(T_o - T)$$

For the given shear strain rate and a μ(1300 K) of 4.052E+16

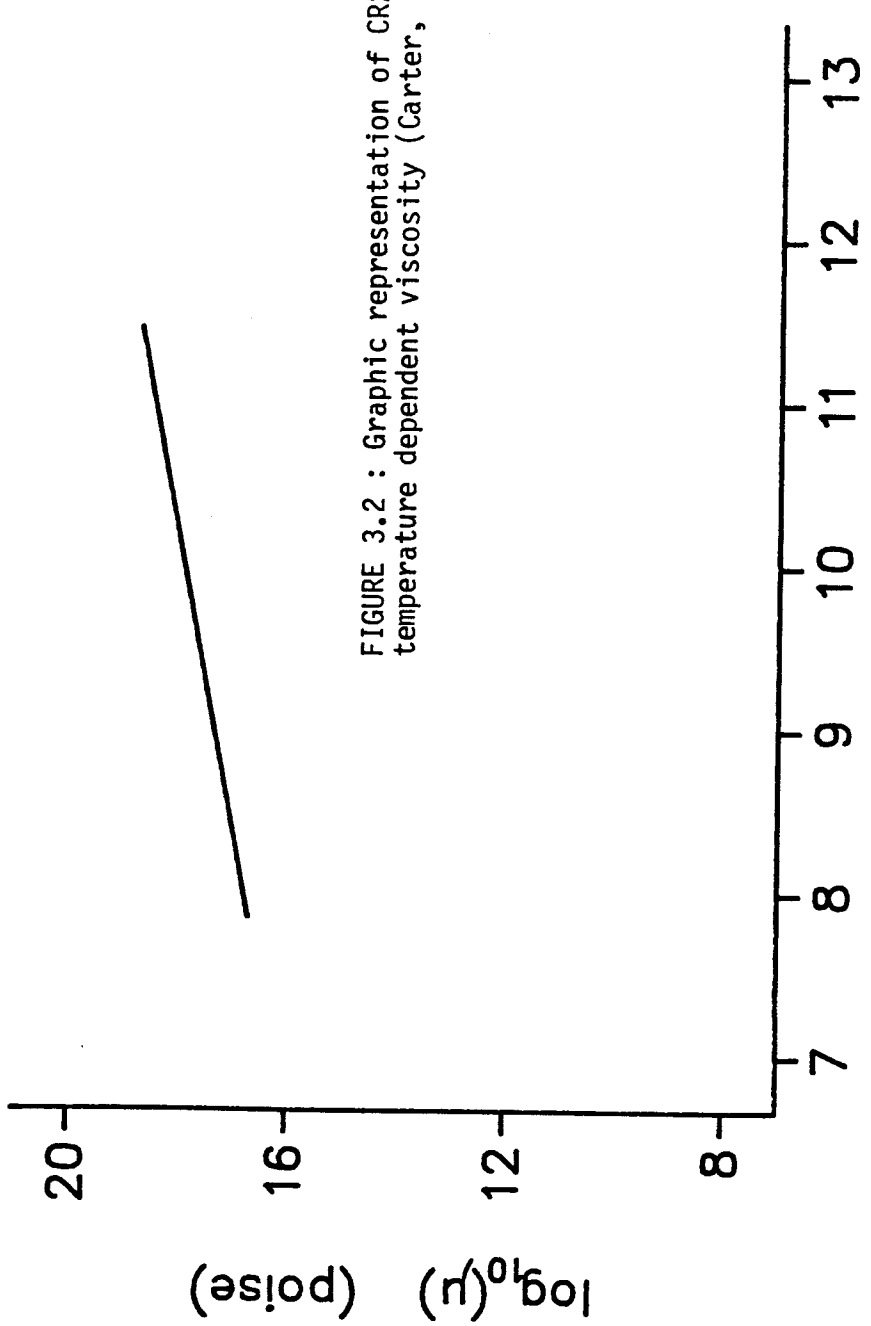

FIGURE 3.2 : Graphic representation of CR2's temperature dependent viscosity (Carter, 1976).

poise, γ varies from 0.0078 at 1000°C to 0.0114 at 600°C. As in the case of the Newtonian fluid, γ is calculated following each snapshot.

Deformation Factor

The deformation layer's width is proportional to the increase in viscosity across it. Since the ascent velocity relationship defined in Chapter II is dependent upon the cube of the deformation layer's width, the increase in viscosity becomes an important value when determining ascent velocity. In a similar study, Morris (1982) defined this deformation factor to be e (F = 2.72). With the exception of one run, a factor of e is also used in this study. In order to assess the sensitivity of the model on this parameter, one run using a factor of ten (F = 10) is performed.

3.1.2 Thermal Constraints

Since the rheology of country rocks modeled in this study are strongly dependent on temperature, the thermal properties of the system are very important. These properties include the initial diapiric temperature, the crustal geothermal gradient, the heat capacities and thermal diffusivity of the country rock, and generation of heat within the diapir.

Initial Diapir Temperature

As mentioned before, numerous runs of the model were made to assess relative contributions of various parameters. Initial diapir temperatures were varied from 850°C to 1200°C.

Five of the ten runs began with a diapir initially at 850°C, a value expected in many I-type and S-type granites (Wyllie et al., 1976; Wells, 1980; Huang and Wyllie, 1981; Stern and Wyllie, 1981; Clemens and Wall, 1984). In order to compare results at the same depth, several runs were initiated at 1000°C. At the suggestion of Gilbert Hanson (see Shirey and Hanson, 1984), a run was initiated within the upper lithosphere at 1200°C to simulate the transport of granitoids produced in the lithospheric mantle. A single run of 960°C was performed in order to provide a continuous thermal connection with the 1200°C run when it reached lower crustal levels, changing the encompassing country rock from CR2 (wet dunite) to CR1 (obsidian).

Geothermal Gradient

Realistic orogenic geothermal gradients, within the crust, of 25°C/km and 30°C/km (Clark, 1966) were used in eight of the models. In order to examine the variation of the ascent velocity profile with the gradient, two runs with a constant ambient temperature of 600°C were performed.

Heat Capacity and Thermal Diffusivity

To determine the thermal diffusivity, the density, specific heat and thermal conductivity of the country rock must be known. These properties are somewhat dependent upon temperature. For simplicity, and a good approximation, these values are determined at an estimated average temperature for the system (T_{ave}) or from other reliable sources of data.

For all of the models, the diapir's density is assumed to be 2.5 g/cm^3. This is a reasonable value for a partially crystalline magma body of granitoid composition (Clark, 1966). The country rock's density is assumed to be that of average crust, 2.85 g/cm^3 (Dziewonski et al., 1975). The two exceptions to this are the models rising through dunite, where density of the encompassing rock is assumed to be 3.3 g/cm^3 (Parsons and Sclater, 1977).

The specific heat and thermal conductivity for both diapir and country rock were determined from the equations used by Wells (1980).

[3.11] $c = 753 + 0.46T - 1.45\times10^{7}/T^{2}$ J/kg

[3.12] $K = (0.311 + 1.72\times10^{-4}T)^{-1} + 2.1\times10^{-3}(T-800)$ W/m deg

For a diapir between 850 and 650°C (T_{ave} = 1023.15 K),

c = 1.210E+7 erg/g deg.

For a diapir between 1000 and 650°C (T_{ave} = 1098.15 K),

c = 1.246E+7 erg/g deg.

For a diapir between 1200 and 850°C (T_{ave} = 1298.15 K),

c = 1.342E+7 erg/g deg.

For country rock at 600°C (T_{ave} = 873.15 K),

c = 1.136E+7 erg/g deg,

K = 2.322E+5 erg/sec cm deg

and $\kappa = K/\rho c = 0.007$ cm^2/sec

where c is the specific heat, K is the thermal conductivity, and κ is the thermal diffusivity.

One run was initiated at a significantly greater depth. In this run the encompassing rock was assigned the following values from Parsons and Sclater (1977):

ρ = 3.33 g/cm^3,

c = 1.172E+7 erg/g deg

and κ = 0.008 cm^2/sec.

Heat Generation

It was mentioned in Chapter II that latent heat of crystallization is the dominant source of heat generation within the diapirs modeled in this study. Other sources of significant heat production include the conversion of potential energy to thermal energy as the diapir rises and the decay of radioactive isotopes. For these models, the above sources of heat are converted to an equivalent temperature, which is added to the diapir over a specified range of temperature represented by the liquidus and solidus for the granitoid.

The heat production from latent heat of crystallization and radioactive decay for a granitoid are estimated to be

1.8E-4 W/m and 1.6E-6 W/m (Harrison and McDougall, 1980). Using a specific heat on the order of 1.2E+3 J/kg deg, a density of 2.5E+3 kg/m^3, and a period of time on the order of 1.0E+6 years, yields 189°C of equivalent temperature added to the system from latent heat of crystallization and approximately 2°C from the decay of radioactive isotopes.

The conversion of potential energy to equivalent temperature is estimated to be about 1.5°C/km of ascent for most magma bodies (Marsh, 1982). Assuming a total ascent of 10 km results in 15°C added to the system.

The total equivalent temperature added to the system over the specified range is 206°C. This value is used in all the runs regardless of the length of ascent or the amount of rise.

The liquidus and solidus temperatures for all of the bodies are determined to be 800°C and 650°C respectively (Wyllie et al., 1976). Although these values may vary considerably in nature, depending on the depth and composition, I have chosen to concentrate on the actual ascent mechanics rather than its petrological implications.

3.1.3 Auxiliary Input Files

The mechanics of Grout's diapirism involves the shouldering aside of country rock by the rising diapir. The model developed in this study assumes that the deformation of the encompassing country rock occurs within a thin layer

surrounding the magma body.

In Chapter II, the cyclic method for determining the exact surficial region where deformation occurs during an individual snapshot is described. In order to apply the cyclic method to the computer models, an array of 5Ø numbers is entered into the model, explicitly defining the velocity profile within the deformation layer using discrete intervals. This velocity profile depends on the increase in viscosity across the deformation layer, F.

Two auxiliary files, FCONE and FCON1Ø, have been created. FCONE represents a random distribution of numbers that points to one of the ten intervals within the deformation layer when the increase in viscosity across the layer is e. FCON1Ø is the analogous file for a 1Ø-fold increase in viscosity. Both of these are listed in Appendix B (Note that the differences in the arrays may become more apparent if referred back to Figures 2.2a and 2.2b).

3.1.4 Overview of Input Data

Table 3.1 illustrates the variation in the data used to generate profiles from Socrates. A complete listing of the data entered is presented in Appendix B. Note that some of the runs listed in Table 3.1 are for 2 and 1Ø km diapirs, and the remaining runs are for 5 km bodies. The version of Socrates found in Appendix A is for a 5 km diapir. In order to model larger and smaller diapirs, Socrates had to be

INPUT PARAMETERS

SIDATA#	Size	Initial Diapir Temp.	Initial Depth	Crustal Gradient	Surface Temp.	Country Rock	Deformation Factor
1	5 km	850°C	30 km	25°/km	10°C	CR1	e
2	5 km	1000°C	30 km	25°/km	10°C	CR1	e
3	5 km	1000°C	30 km	25°/km	10°C	CR1	10
4	5 km	850°C	25 km	30°/km	10°C	CR1	e
5	5 km	850°C	30 km	0°/km	600°C	CR1	e
6	10 km	1000°C	30 km	0°/km	600°C	CR2	e
7	10 km	850°C	30 km	25°/km	10°C	CR1	e
8	2 km	850°C	30 km	25°/km	10°C	CR1	e
9	10 km	1200°C	40 km	25°/km	10°C	CR2	e
10	10 km	960°C	32 km	25°/km	10°C	CR1	e

TABLE 3.1

edited to include the change in dimensions and the modification of the cessation routine, which determines whether the deformation layer has exceeded a width equal to one tenth of the body's radius. These particular variations in size do not add significant error, or conditional instability, to the numerical approaches used.

3.2 Results

A number of figures are presented in this section, representing the results obtained from the ten models run using Socrates. A thorough discussion of the results is presented in Chapter IV.

Figures 3.3 to 3.12 illustrate the ascent velocity profiles as a function of time. All of these are in thousands of years elapsed and meters of ascent per year, except for Figure 3.9 which is in millimeters per year.

Figures 3.13 represents the decrease in diapir temperature (T_D), temperature at the outer edge of the deforming layer (T_F), and undisturbed ambient temperature (T_∞) versus elapsed time for the first run (SODATA1). Figure 3.14 illustrates the decrease in the temperature distribution with time for SODATA1. The complete output file for this run is in Appendix C. In order to conserve space, the output files from the other runs are not published in this study.

SODATA9 and SODATA1Ø, found in Figures 3.11 and 3.12, represents a model of mantle granitoid production. SODATA9

is a 10 km diapir that rises from 40 km to 32 km within CR2 (wet dunite). SODATA10 is the same body initiated at 32 km and surrounded by CR1 (obsidian), with a diapir temperature equal to SODATA9's at its 32 km cutoff.

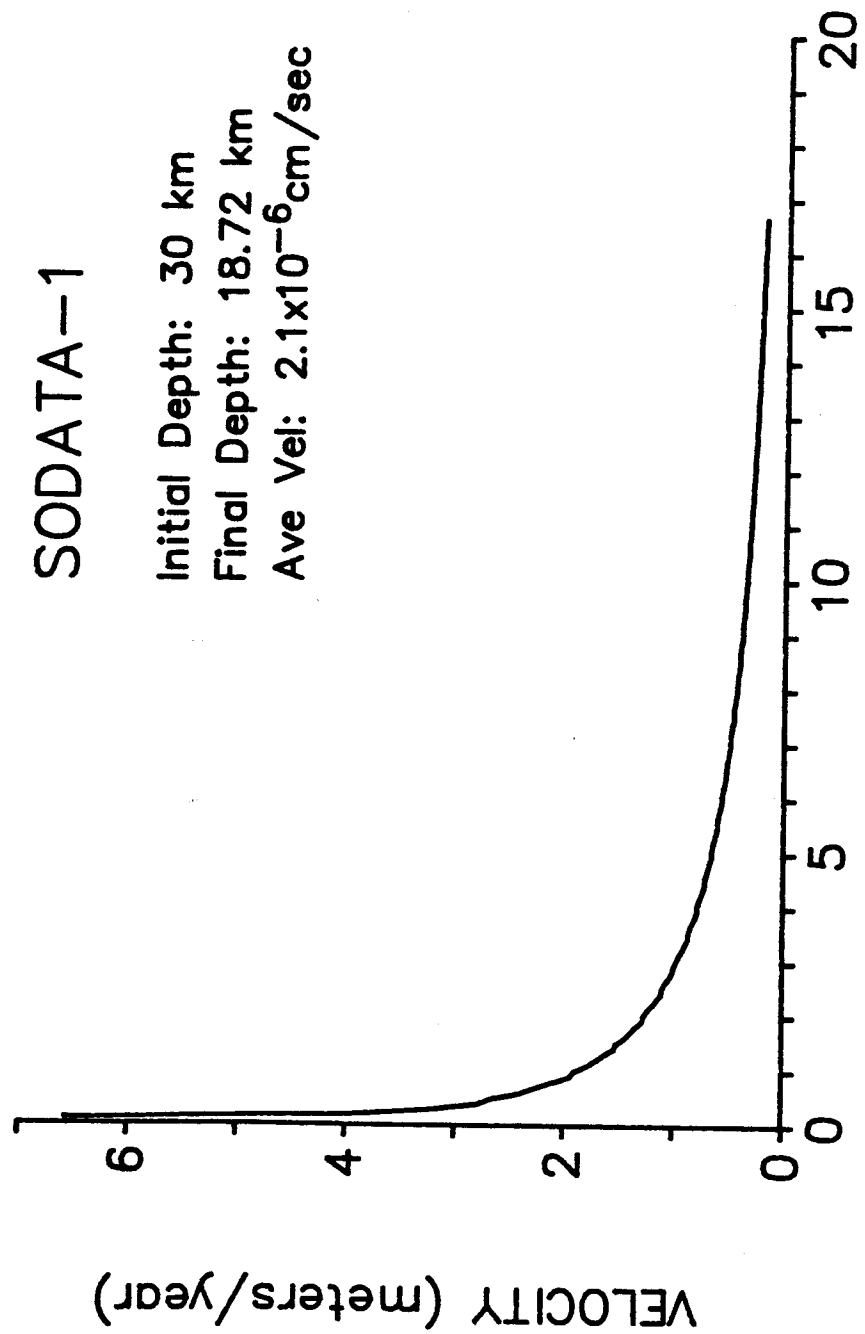
SODATA-1
Initial Depth: 30 km
Final Depth: 18.72 km
Ave Vel: 2.1x10^{-6}cm/sec
VELOCITY (meters/year)
TIME (10^3 years)
0
2
4
6
0
5
10
15
20

FIGURE 3.3

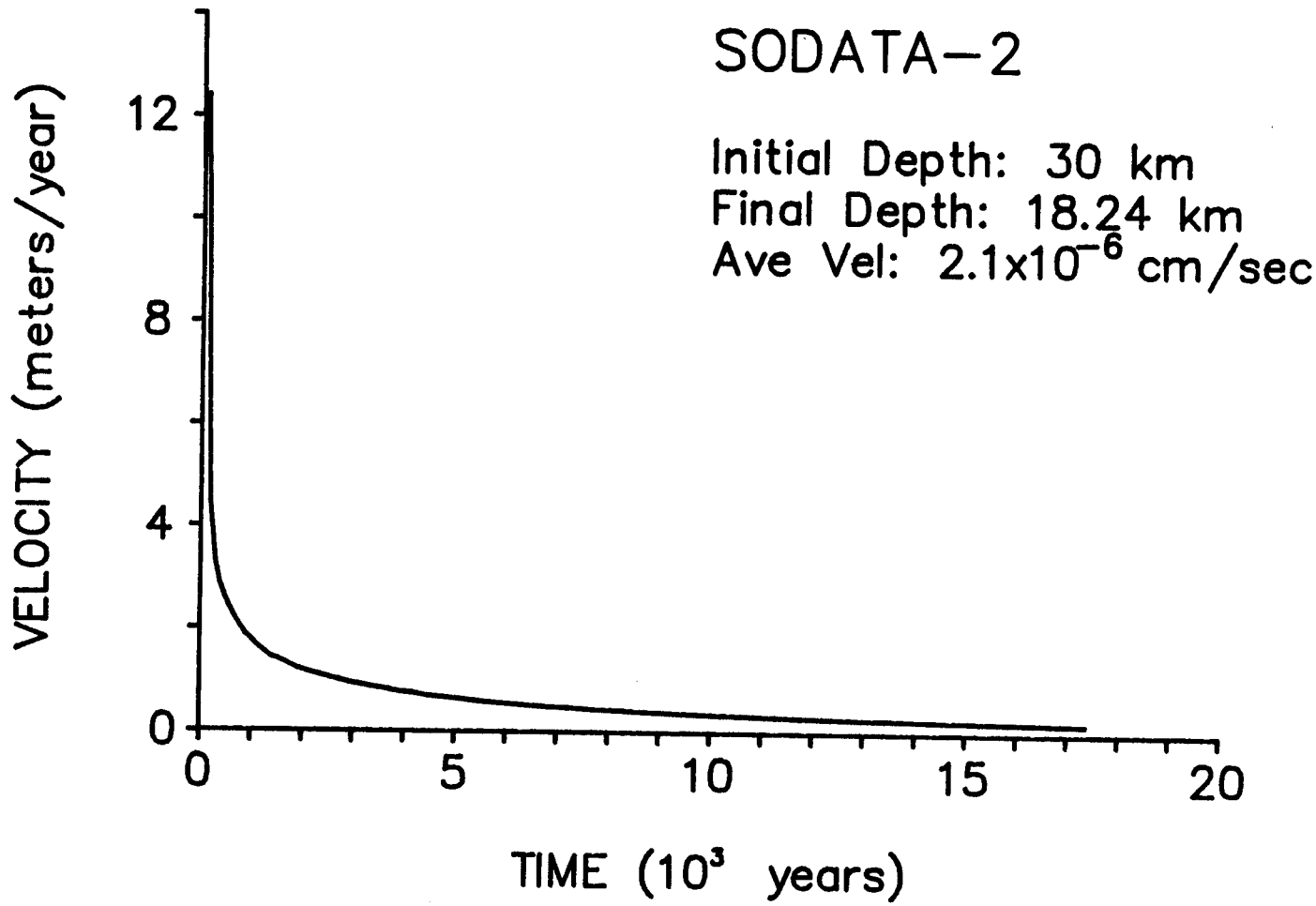
SODATA–2
Initial Depth: 30 km
Final Depth: 18.24 km
Ave Vel: 2.1x10⁻⁶ cm/sec
VELOCITY (meters/year)
12
8
4
0
0
5
10
15
20
TIME (10³ years)

FIGURE 3.4

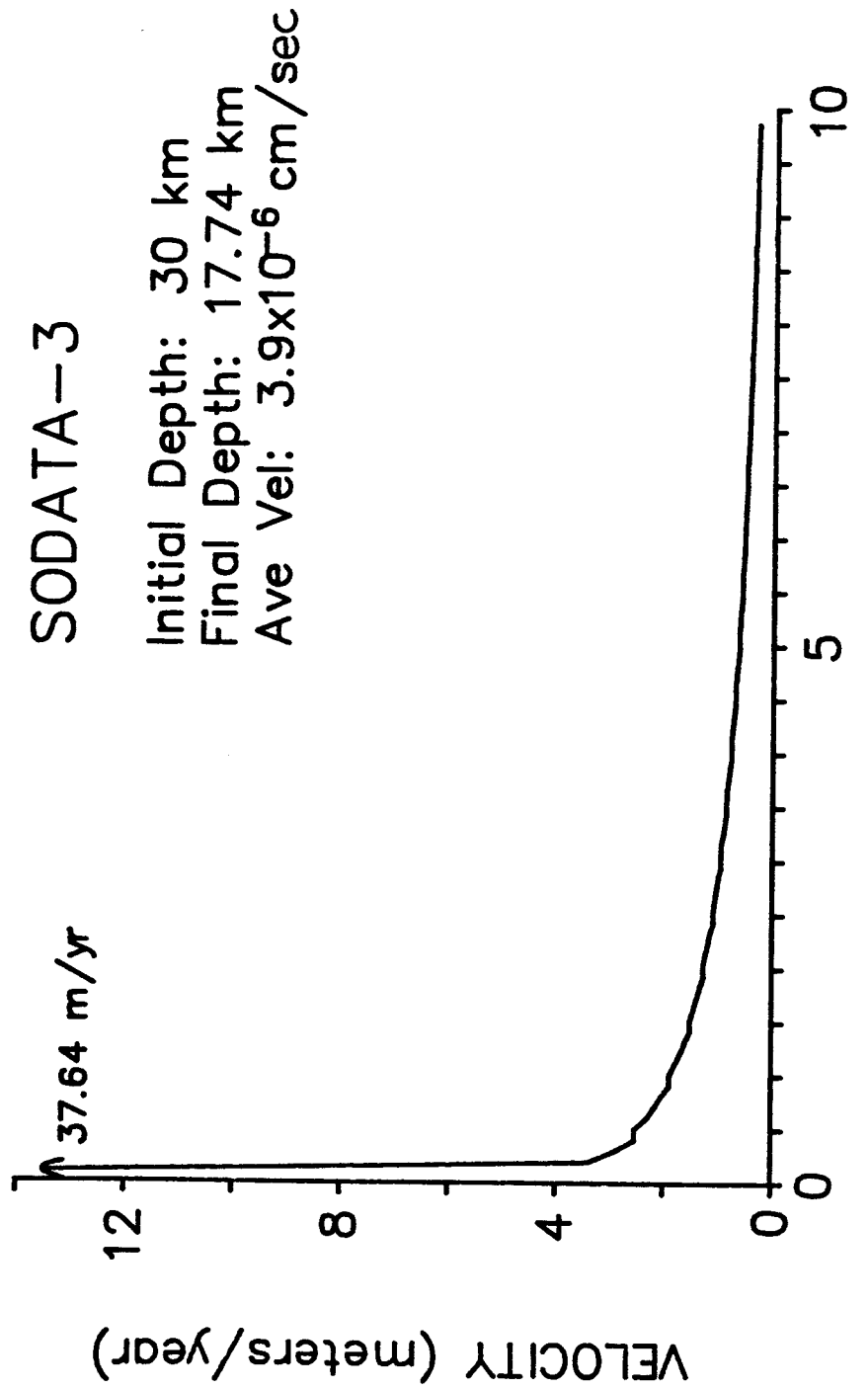
SODATA-3
Initial Depth: 30 km
Final Depth: 17.74 km
Ave Vel: 3.9x10⁻⁶ cm/sec
37.64 m/yr
VELOCITY (meters/year)
12
8
4
0
0
5
10
TIME (10³ years)

FIGURE 3.5

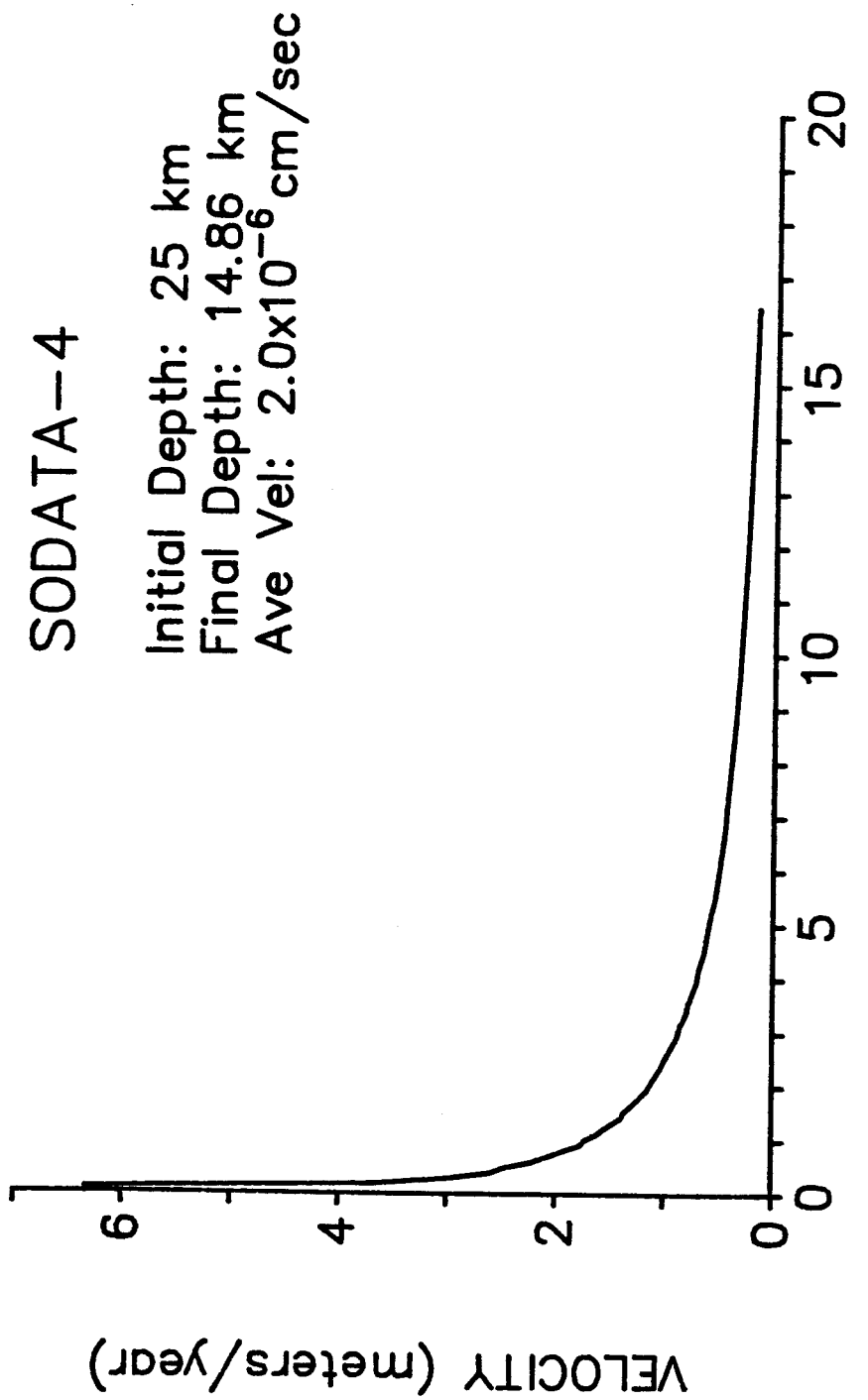
SODATA—4
Initial Depth: 25 km
Final Depth: 14.86 km
Ave Vel: 2.0x10^{-6}cm/sec
VELOCITY (meters/year)
6
4
2
0
0
5
10
15
20
TIME (10^3 years)

FIGURE 3.6

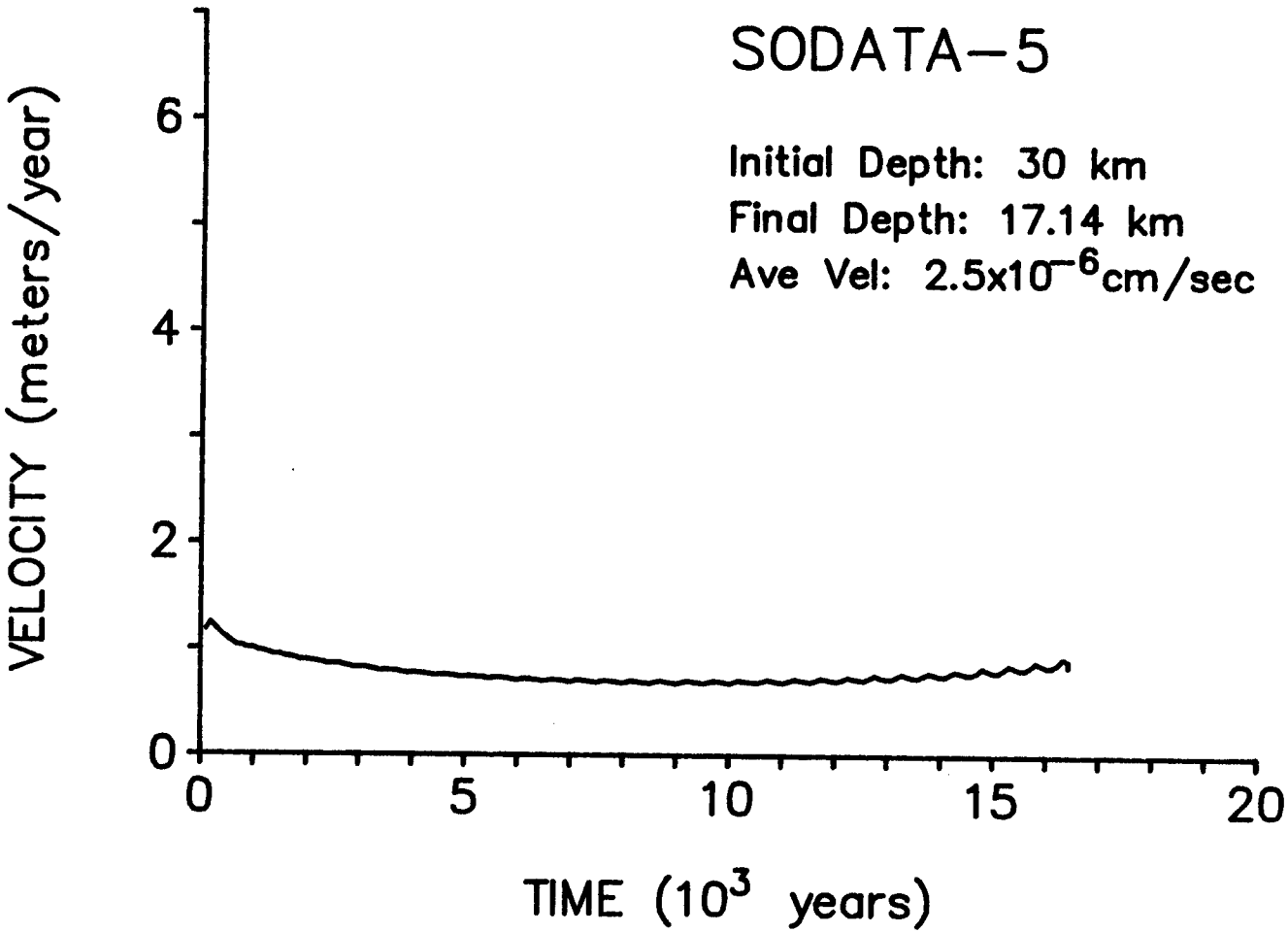
SODATA–5
Initial Depth: 30 km
Final Depth: 17.14 km
Ave Vel: 2.5x10⁻⁶cm/sec
VELOCITY (meters/year)
0
2
4
6
0
5
10
15
20
TIME (10³ years)

FIGURE 3.7

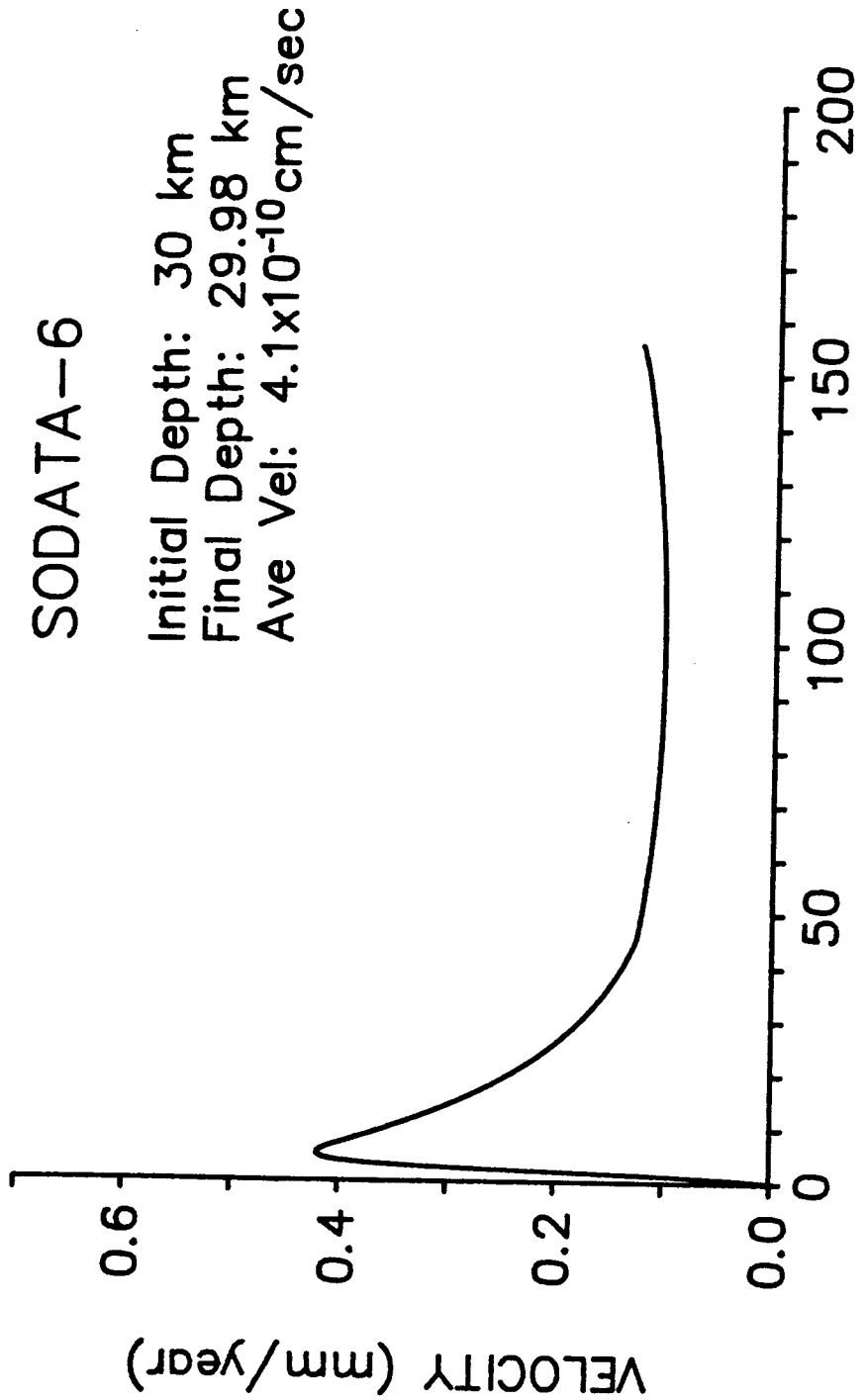
SODATA-6
Initial Depth: 30 km
Final Depth: 29.98 km
Ave Vel: 4.1x10-10cm/sec
VELOCITY (mm/year)
0.0
0.2
0.4
0.6
0
50
100
150
200
TIME (10³ years)

FIGURE 3.8

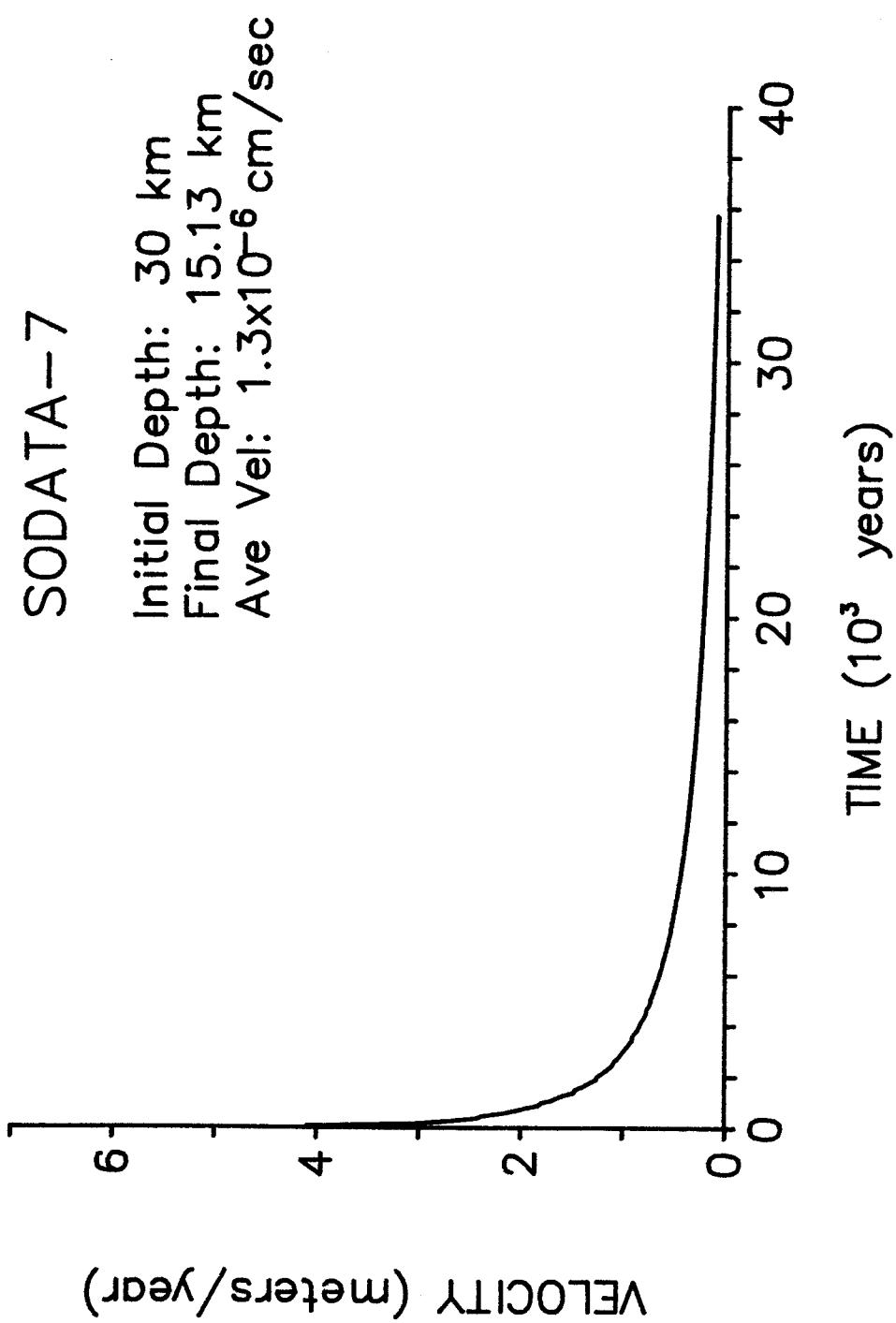
SODATA—7
Initial Depth: 30 km
Final Depth: 15.13 km
Ave Vel: 1.3x10⁻⁶ cm/sec
VELOCITY (meters/year)
6
4
2
0
0
10
20
30
40
TIME (10³ years)

FIGURE 3.9

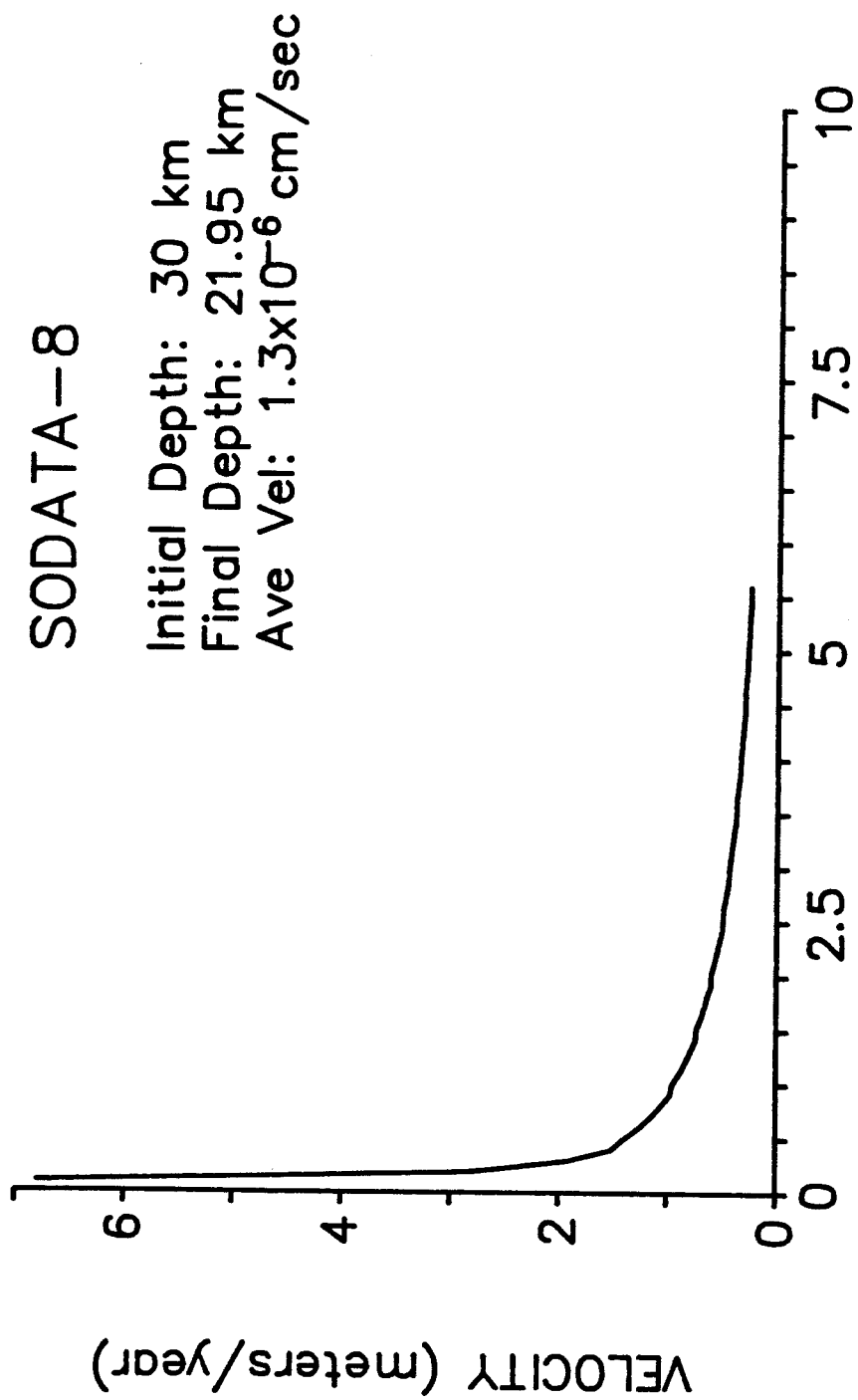
SODATA-8
Initial Depth: 30 km
Final Depth: 21.95 km
Ave Vel: 1.3x10⁻⁶ cm/sec
VELOCITY (meters/year)
6
4
2
0
0
2.5
5
7.5
10
TIME (10³ years)

FIGURE 3.10

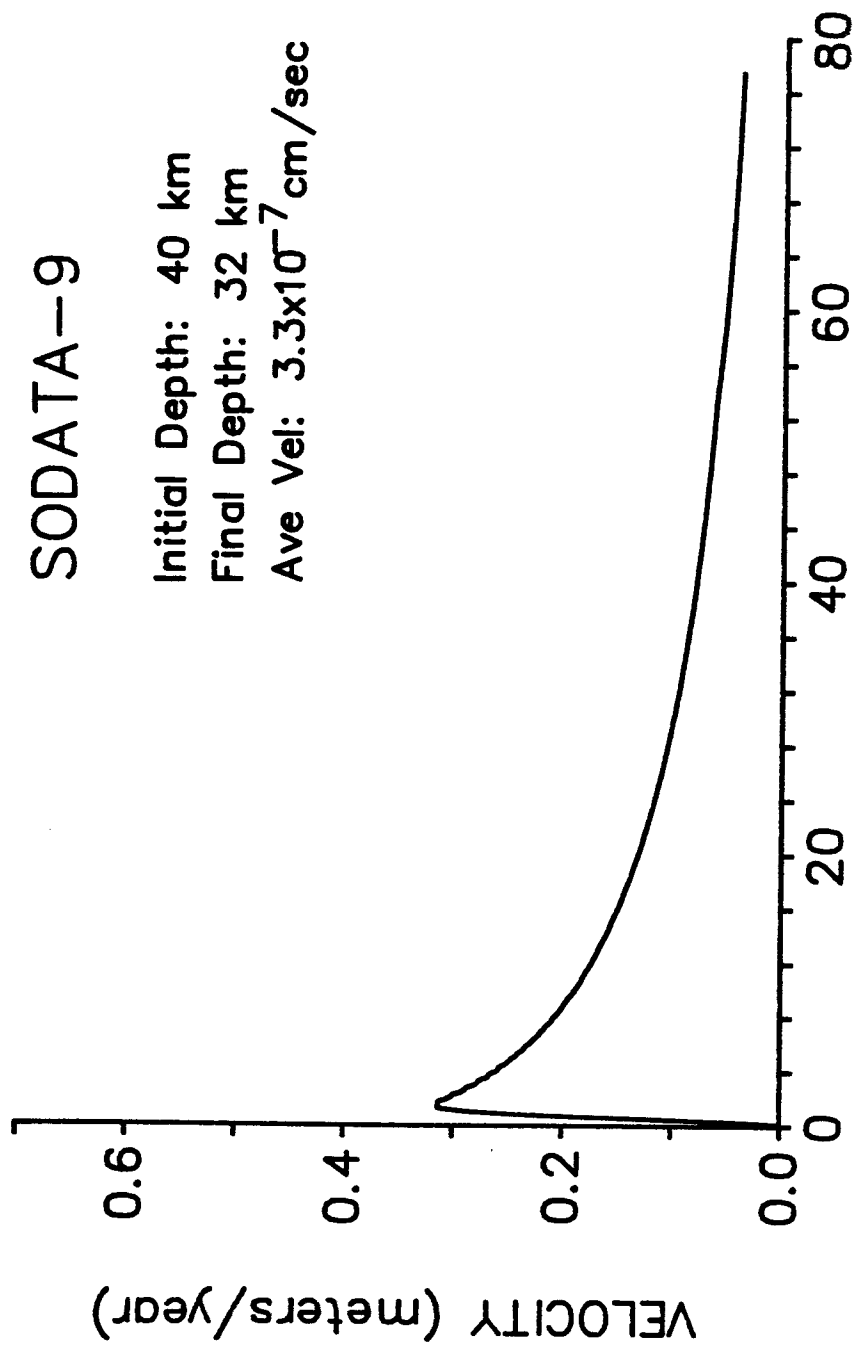
SODATA–9
Initial Depth: 40 km
Final Depth: 32 km
Ave Vel: 3.3x10⁻⁷cm/sec
VELOCITY (meters/year)
0.0
0.2
0.4
0.6
0
20
40
60
80
TIME (10³ years)

FIGURE 3.4

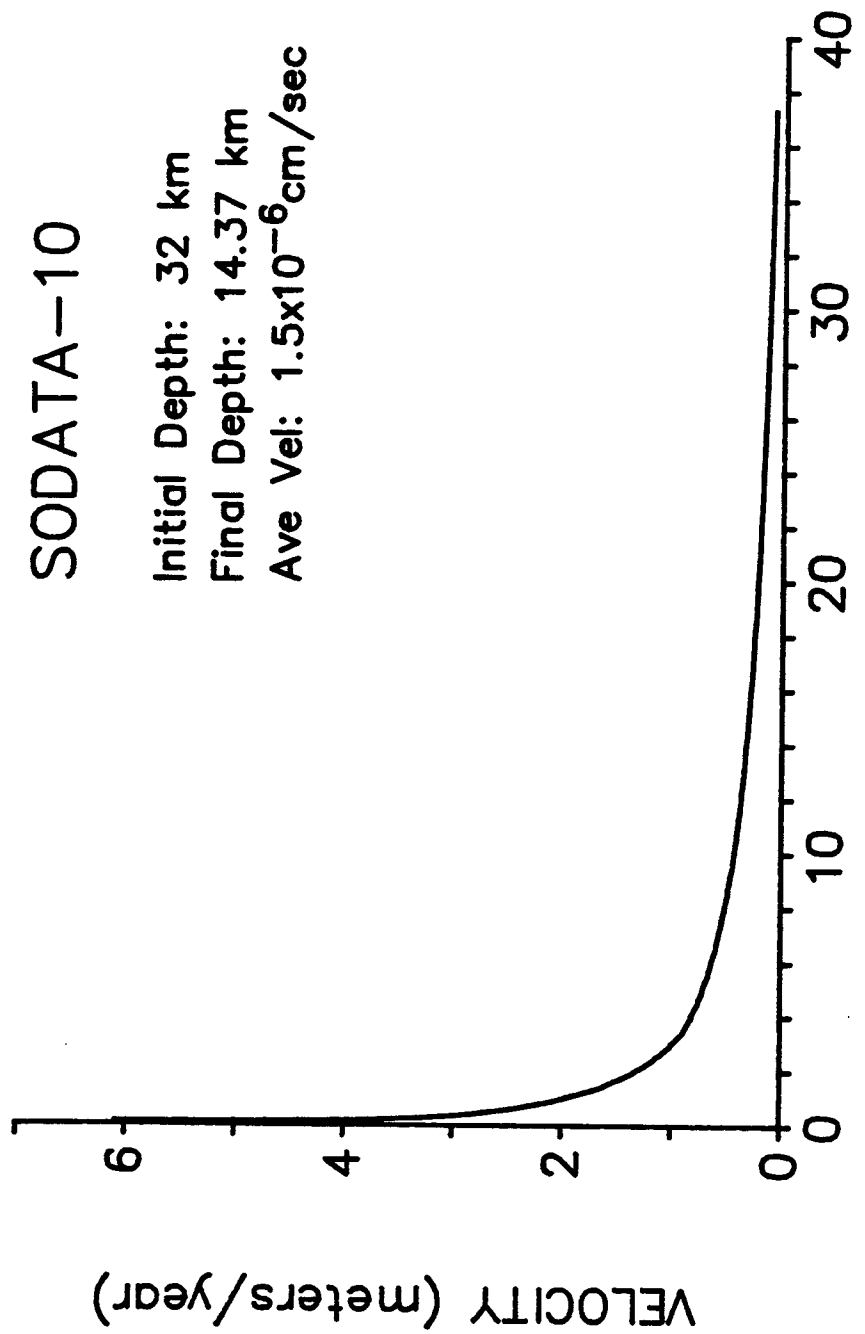
SODATA–10
Initial Depth: 32 km
Final Depth: 14.37 km
Ave Vel: 1.5x10^{-6}cm/sec
VELOCITY (meters/year)
6
4
2
0
0
10
20
30
40
TIME (10^3 years)

FIGURE 3.12

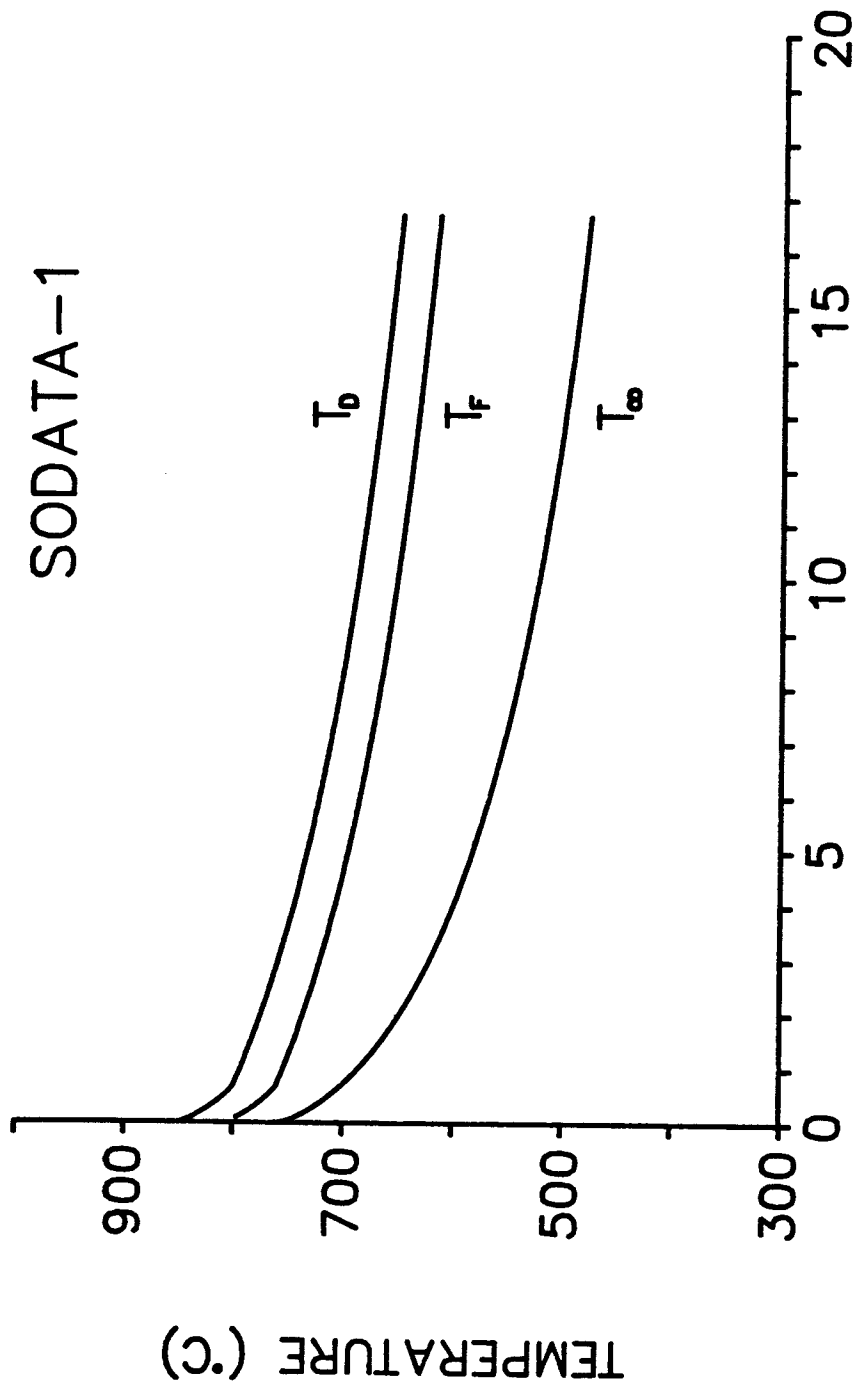
SODATA-1
T_b
T_F
T_∞
900
700
500
300
0
5
10
15
20
TIME (10^3 years)
TEMPERATURE (°C)

FIGURE 3.13

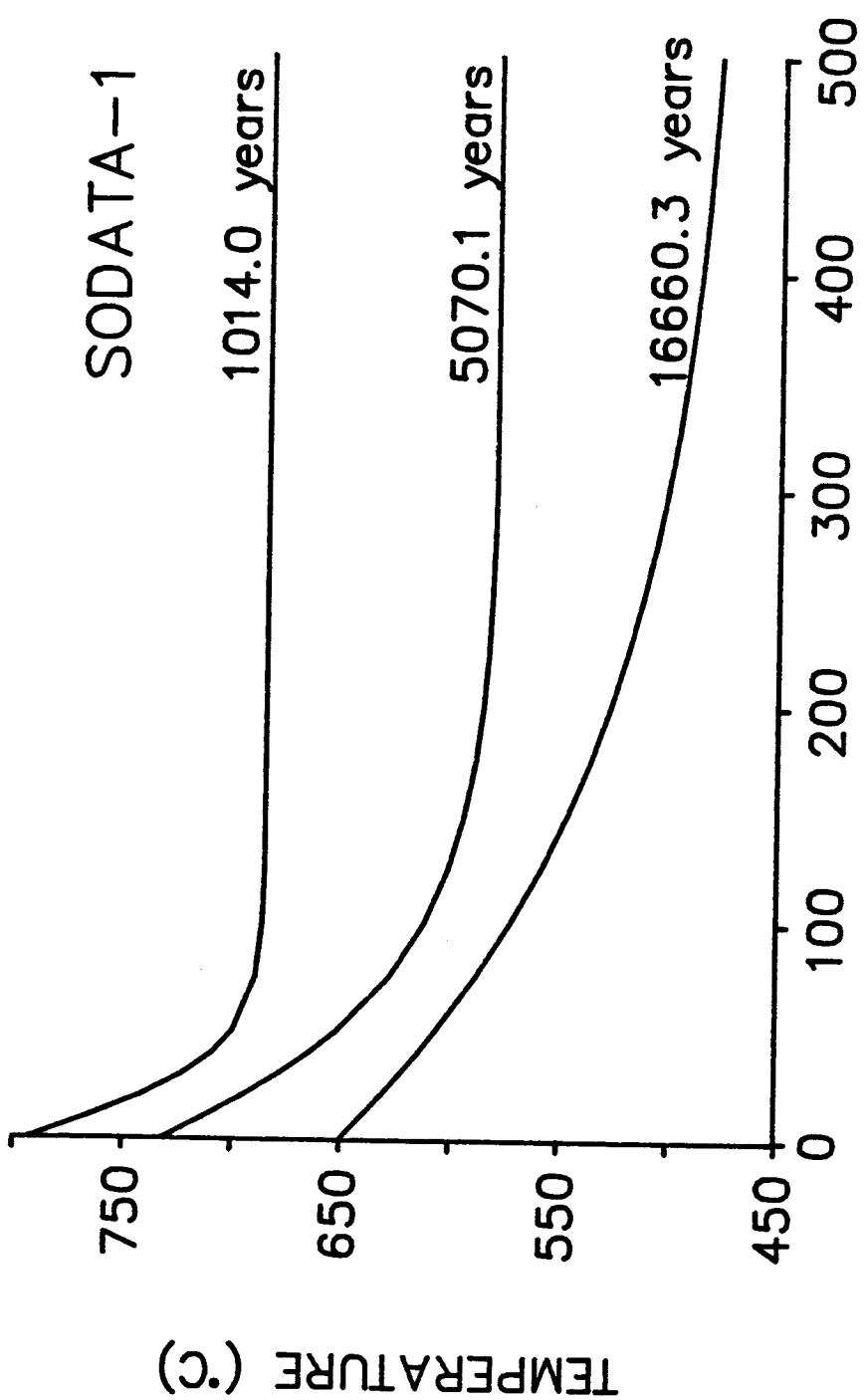
SODATA-1
1014.0 years
5070.1 years
16660.3 years
TEMPERATURE (°C)
750
650
550
450
0
100
200
300
400
500
Meters from Contact (r-R)

FIGURE 3.14

CHAPTER IV

DISCUSSION

4.Ø Introduction

Along with a thorough discussion of the results, presented in Figures 3.3-3.14 and 4.2, several miscellaneous aspects of granitoid diapirism are discussed in this chapter. Included is a comparison of the ascent velocity relationship derived in Chapter II, using the stress-free boundary condition, with a relationship involving the no-slip boundary condition. The no-slip condition is implied in many experimental studies. For example, the case of solid balls dropped through fluids (Ribe, 1983). Also worthy of mention, Stokes (1851) used the no-slip condition to derive his famous flow equation (see equation 1.1).

As in most any study, this work has room for improvement. Suggestions and proposals are made that point to future research in the field of igneous transport processes. Finally, a concluding section summarizes the salient observations made in this study.

4.1 Discussion of Results

Due to the multivariate nature of igneous diapirism, numerous runs were performed using Socrates, the computer program developed in this study (see Appendix A). In Chapter III, the ascent velocity profiles generated from these runs

are illustrated graphically. In this section, the results are interpreted relative to changes in specific input parameters (Note that "SODATA#" is simply the file element name where the output data can be found ... Socrates Output DATA).

Figure 4.1 is a link-node diagram that relates the input for most of the models to the standard model, SODATA1 (see Appendix C), by varying one or two parameters. A link explicitly represents a change in a particular parameter. SODATA6 is not connected to any nodes because numerous parameters were changed in an unsuccessful attempt to get the diapir through wet dunite at crustal temperatures. SODATA9 and SODATA1Ø are connected by an arrow that represents a continuous ascent through an encompassing power-law fluid (CR2) and into a Newtonian fluid (CR1).

The standard model (see Figures 3.3, 3.13. and 3.14) assigns the following values to the parameters used during the computer simulation:

Diameter of the diapir, $2R = 5$ km

Country rock's rheology is CR1 (Newtonian)

Deformation layer's viscosity factor, $F = e$

Initial depth, $X_o = 3Ø$ km

Geothermal gradient, $dT/dX = 25^oC/km$

Surface temperature, $T_s = 1Ø^oC$

Density of country rock, $\rho = 2.85 g/cm^3$

Thermal diffusivity, $\kappa = Ø.ØØ7 cm^2/sec$

and Initial diapir temperature, T_o = 850°C.

Figure 4.2 illustrates the initial and final depths of emplacement and the average ascent velocity for the nine models considered. Note that SODATA9 and SODATA1Ø are considered to be one model.

Comparing the first two runs in Figures 3.3, 3.4, and 4.2, it is apparent that the increase in initial diapir temperature did not change the average ascent velocity. By allowing the diapir an additional 15Ø°C, the body rose only half a kilometer higher in the crust.

The input data for SODATA3 is identical to that for the second run except for the increase in the deformation factor F, from e to 1Ø. This enabled the diapir to process more country rock within the deforming layer at any instant during ascent. This result yields an average ascent velocity that is nearly twice as fast. Two consequences of this increase in F point to unrealistic results. Firstly, ascent velocity (see Figure 3.5) exceeds 37 m/year in the first 1ØØ years, which seems to be extraordinarily fast. Secondly, all of the ascent profiles generated using a deformation factor of e define smooth curves, whereas the profile generated by this model contains many perturbations early in ascent (see Figures 3.3 to 3.12). This suggests that the snapshot approach, or the snapshot duration of ten years, was inappropriate for this ascent model.

The fourth run (see Figure 3.6) is initiated at a depth

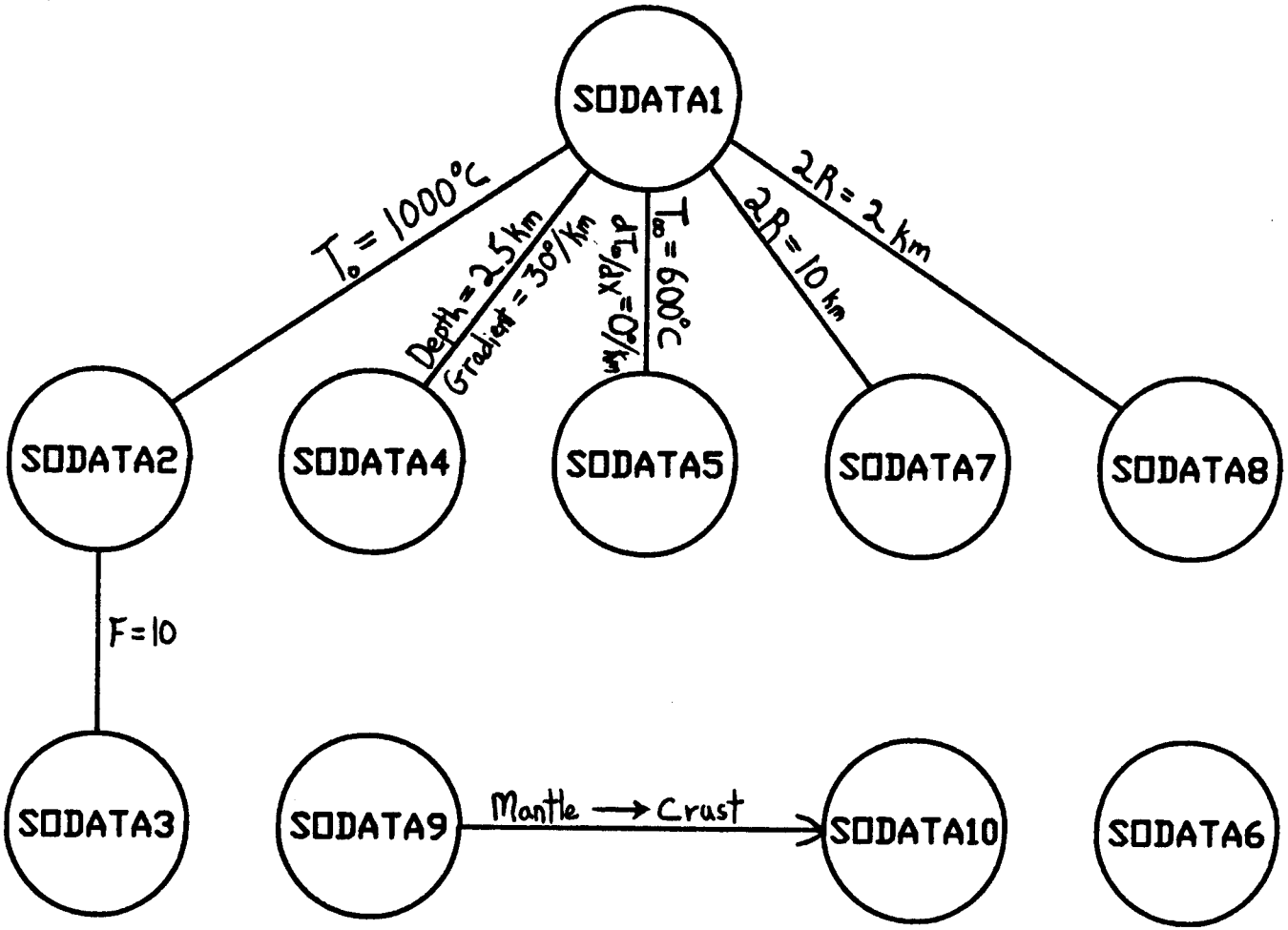
SODATA1
T_o = 1000°C
Depth = 2.5 km
Gradient = 30°/km
T_s = 600°C
$\partial T/\partial x = \partial P/\partial x$
2R = 10 km
2R = 2 km
SODATA2
SODATA4
SODATA5
SODATA7
SODATA8
F = 10
SODATA3
SODATA9
Mantle → Crust
SODATA10
SODATA6

FIGURE 4.1

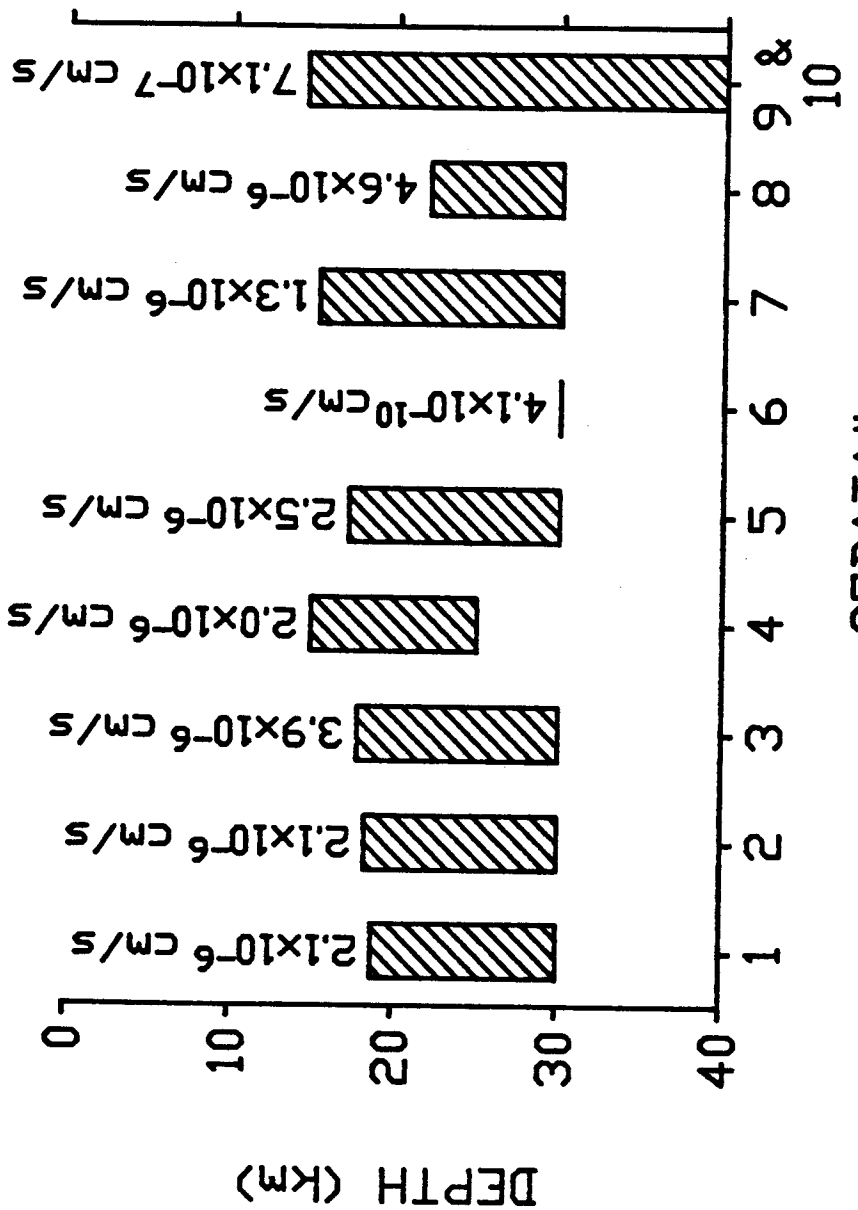
DEPTH (KM)
0
10
20
30
40
1
2
3
4
5
6
7
8
9
10
SODATA#
2.1x10-6 cm/s
2.1x10-6 cm/s
3.9x10-6 cm/s
2.0x10-6 cm/s
2.5x10-6 cm/s
4.1x10-10cm/s
1.3x10-6 cm/s
4.6x10-6 cm/s
7.1x10-7 cm/s

FIGURE 4.2

of 25 km with a crustal gradient of 30°C/km. Initially this model and the standard are surrounded by country rock with identical ambient temperatures. Because of this, it encountered cooler ambient temperatures for the same distance risen relative to the standard. The result illustrates that the two diapirs cooled in approximately the same time, but the standard model ascended a greater distance and at a faster rate. This suggests that the ambient temperature distribution is an important parameter in determining ascent velocity, whereas the loss of energy to the surroundings is not significantly affected by small changes in the crustal temperature gradient above a rising pluton. This is contrary to the opinion of Marsh (1982) and Morris (1982) who implement constant ambient temperatures in their models, on the premise that rather small variations in this parameter does not effect ascent considerably.

Following this lead, the ambient temperature distribution in the fifth run was held constant at 600°C. The body cooled in about the same period of time as the previous run and the standard, but average ascent velocity was significantly greater. This resulted in a larger total distance ascended by the body. Another interesting result of this run was the nearly constant ascent velocity of 0.8 m/year (see Figure 3.7) while other models exhibit exponential variations in their ascent profiles. The only possible reason for this behavior is the different ambient

temperature distributions. Although this suggests that the ambient temperature has an effect on the ascent velocity, the amount of additional ascent is only about 1 km more than the standard model. This indicates that preheating the country rock by repeated prior ascents, as advocated by Marsh (1982) and Morris (1982), is unneccessary for granitoid intrusion.

SODATA6 can not be compared directly to the standard model through the variation of a single parameter, the case in most of the other runs. The probable reason for the failure of this model to ascend an appreciable distance is that wet dunite, the encompassing country rock, is too sticky at crustal temperatures to allow appreciable flow. It can be concluded that a granitoid diapir will have an extremely difficult time shouldering aside dunite within the crust ... an intuitively acceptable result.

The velocity profile in SODATA6 does not translate into a significant ascent distance, but its shape is rather interesting (see Figure 3.8). Since the effective viscosity is dependent on shear strain rate, it must start very slowly and accelerate to a maximum velocity over a few thousand years. An exponential drop off in velocity following this is due mostly to a drop in diapir temperature, which is the case in most of the models run within the Newtonian country rock. Since the ascent velocity relationship used is dependent on d^3, the slight increase in velocity later in ascent is due to an increase in the width of the deformation layer, which is

growing larger near the stagnant body. This increase in ascent velocity is generally not illustrated by the other models because more mobile diapirs transfer material out of the deformation layer by ascending through it.

Another interesting result from the sixth run is the length of the cooling period relative to the other plutons. This stagnant body cooled at a rate of 2.0E-3 degrees per year, whereas the more mobile 10 km body in SODATA7 cooled at 5.6E-3 degrees per year. The variation is even greater when the additional 150°C within SODATA6, resulting in higher heat flux, is considered. This suggests that rising diapirs cool at a much faster rate than normally expected as a result of interaction with progressively cooler country rock.

Varying the size of the body significantly alters ascent velocity. In the seventh run a 10 km diapir was modeled using parameters identical to the standard. The result was a slow ascent velocity over a much longer period of cooling (see Figure 3.9). The pluton emplaced itself 2 1/2 km higher in the crust, relative to the standard, due to the additional energy available and the smaller surface to volume ratio.

In SODATA8 a 2 km diapir is modeled (see Figure 3.10). As expected the body ascended at a much faster rate than the standard model, but because the available energy needed to soften the country rock is much less, the pluton cooled to its solidus in a considerably shorter period of time. Therefore, the final emplacement depth of this pluton is

lower in the crust.

In comparing the effective energy available for a pluton to ascend a given distance, the total energy available and the energy lost in processing overlying country rock through the deformation layer must be considered. Since the total energy within a pluton is proportional to its volume, a 10 km diapir will have 8 times the available energy of a 5 km body.

$$\left(\tfrac{4}{3}\pi(5)^3\right) = 8\left(\tfrac{4}{3}\pi(2.5)^3\right)$$

For a diapir to ascend a specific distance, it must process a minimum volume equal to its cross-sectional area times the distance traveled. Comparing a 10 km and 5 km diapir rising 15 km in the crust, the larger body will have to process 4 times the amount of overlying material within its deformation layer.

$$\left(15\pi(5^2)\right) = 4\left(15\pi(2.5)^2\right)$$

The ratio of the total energy contrast (e.g., 8) and the contrast in processing energies (e.g., 4) is simply equal to the ratio of the bodys' radii. In other words, a 10 km diapir has twice the effective energy needed to ascend an equal distance relative to a 5 km body, and five times that of a 2 km body.

Comparing the ascent distances relative to their effective energy contrasts for 2 km (SODATA8), 5 km (SODATA1), and 10 km (SODATA7) diapirs, illustrates that a contrast in effective energy yields a much smaller contrast in ascent distances. The reason for this is that larger

diapirs will maintain a higher temperature over a given period, causing them to have a greater heat flux to the surroundings. Combining this with the fact that larger diapirs ascend at slower rates, suggests that a greater proportion of the energy lost to the surroundings is not used to propel the body upwards as compared to smaller diapirs. Hence, the 10 km pluton (SODATA7), only ascended an additional 30% as compared to the standard 5 km body (SODATA1), even though its effective energy was 200% greater.

SODATA9 and SODATA10 are merged into a single diapiric ascent model. For mantle derived granitoid plutons, the initial diapir temperatures are significantly higher (Shirey and Hanson, 1984). This enabled the body to shoulder aside the encompassing mantle rock, which was rheologically modeled as wet dunite. Because the dunite and the diapir were cooler, the sixth model did not rise a significant distance, but in this case the entire system was initially at an elevated temperature. Together, the ninth and tenth runs form a discontinuous ascent velocity profile (see Figures 3.11 and 3.12). However, it indicates that if a granitoid pluton has a sufficient amount of energy available, it can pierce the upper mantle and ascend through the lower crust. Note that the ascent velocity profile from SODATA9, as in SODATA6, achieves a maximum after a few thousand years have elapsed due to the shear strain rate-dependent effective viscosity.

4.2 Ascent Velocity With No-Slip Condition

Stokes' (1851) result for a sphere falling through a fluid and Ribe's (1983) experimental models were discussed in Chapter I. Both are inaccurate when applied to igneous diapirism because they do not emulate the essentially stress-free surface condition that is present during the rise of a hot fluid body within a medium that is also modeled as a fluid. In this section, the ascent velocity relationship is derived using the no-slip boundary condition. The physical appearance of the ascent velocity equation (equation 2.15) will remain the same, but the parameter Z will change.

To apply the no-slip boundary condition, the rederivation is initiated at "step 3" of sub-section 2.1.5. The θ-component of the momentum equation is

$$\partial P'/\partial\theta = \partial/\partial r' \left(\mu' \partial v'/\partial r'\right).$$

Integrating,

$$r'/\mu' \cdot \partial P'/\partial\theta + 1/\mu' \cdot K_1(\theta) = \partial v'/\partial r'.$$

Integrating again,

[4.1] $$v' = \partial P'/\partial\theta \int \frac{r'}{\mu'} dr' + K_1(\theta) \int \frac{1}{\mu'} dr' + K_2(\theta).$$

Applying the no-slip boundary condition of $v' = 0$ at $r' = 0$ and the outer condition of $v' = 0$ at $r' = 1$, yields

$$K_2(\theta) = 0$$

and $$K_1(\theta) = -\partial P'/\partial\theta \int_0^1 r'/\mu' \, dr' \Big/ \int_0^1 \frac{1}{\mu'} dr'.$$

By evaluating the definite integrals,

$$K_1(\theta) = -\partial P'/\partial\theta \, E$$

where

$$E = \left(\exp(\chi) - 1/\chi \exp(\chi) + 1/\chi\right) \Big/ \left(\exp(\chi) - 1\right).$$

Substituting this expression back in equation 4.1 and evaluating the indefinite integrals, yields

$$v' = \partial P'/\partial\theta \left(\left(K_4(\theta) - E K_3(\theta)\right) + \exp(r'\chi)\left(r'/\chi - 1/\chi^2 - E/\chi\right)\right).$$

Reapplying the no-slip condition ($v' = 0$ at $r' = 0$), results in

$$\left(K_4(\theta) - E K_3(\theta)\right) = 1/\chi^2 + E/\chi .$$

Therefore,

[4.2] $$v' = \partial P'/\partial\theta \left(1/\chi^2 + E/\chi + \exp(r'\chi)\left(r'/\chi - 1/\chi^2 - E/\chi\right)\right).$$

In step 4 of the solution process, the continuity equation is solved.

$$\partial u'/\partial r' + \partial v'/\partial\theta + v' \cot\theta = 0.$$

Integrating,

$$u' = -\left(\partial^2 P'/\partial\theta^2 + \partial P'/\partial\theta \cot\theta\right)\left(\int 1/\chi^2 + E/\chi + \exp(r'\chi)\left(r'/\chi - 1/\chi^2 - E/\chi\right) dr'\right).$$

Evaluating the definite integral, yields

$$u' = -\left(\partial^2 P'/\partial\theta^2 + \partial P'/\partial\theta \cot\theta\right)\left(r'/\chi^2 + E r'/\chi + \exp(r'\chi)\left(r'/\chi^2 - 2/\chi^3 - E/\chi^2\right) + K_5(\theta)\right).$$

Applying the no-slip condition, yields

$$K_5(\theta) = 2/\chi^3 + E/\chi^2.$$

Applying the boundary condition $u' = -\cos\theta$ at $r' = 1$, results in

$$\cos\theta = \left(\partial^2 P'/\partial\theta^2 + \partial P'/\partial\theta \cot\theta\right) Z$$

where Z, using the no-slip condition, is

[4.3] $$Z_{NS} = \left(1/\chi^2 + E/\chi + 2/\chi^3 + E/\chi^2 + \exp(\chi)\left(1/\chi^2 - 1/\chi^3 - E/\chi^2\right)\right).$$

Comparing this Z derived in Chapter II using the stress-free boundary condition,

[4.4] $$Z_{SF} = \left(2/\chi^3 + \exp(\chi)\left(2/\chi^2 - 2/\chi^3 - 1/\chi\right)\right).$$

The total force actng on the diapir's surface will be

slightly altered by the additional tangential force. Through the use of scaling analysis, this force can be shown to be a factor of ϵ (=d/R) less than the normal force and will therefore be neglected. The ascent velocity relationship derived in section 2.1 remains valid.

[4.5] $$U_\infty = 2(\rho - \rho_0)\vec{g}\, d^3 Z/\mu_0 R$$

Values for Z using the stress-free (SF) and the no-slip (NS) boundary conditions with a deformation factor of F = e, yields

$$Z_{NS}(e) = -0.0501 \quad \text{and} \quad Z_{SF}(e) = -0.1606 .$$

With a deformation factor of 10, yields

$$Z_{NS}(10) = -0.0255 \quad \text{and} \quad Z_{SF}(10) = -0.0663 .$$

These results show that by applying the no-slip boundary condition to igneous diapirism, about a factor of 3 drop in the corresponding ascent velocity occurs relative to the case when the stress-free boundary condition is applied.

4.3 Improvements and Future Work

The model derived in this study utilizes the natural character of the system as a basis to formulate a set of simplifying assumptions. The principal assumption is that the deformation of the surroundings is confined to a narrow region, referred to as the deformation layer. In order to calculate the width of the deformation layer, a parameter describing the amount viscosity increases across it, has to be given. The model bases its validity on the fact that the

calculated width of the deforming layer is much less than the diapir's radius. There are times during ascent when this is not the case. For instance, when the pluton is very near its source, a sufficient temperature difference between diapir and undisturbed country rock does not exist. This may result in a deformation layer that is too wide.

In order to alleviate the problem of small temperature contrasts, I propose a new model where the early stages of diapiric ascent will be modeled using an equation to describe isoviscous, or nearly isoviscous, flow. Note that Stokes' equation is not appropriate for this model because it was derived using the no-slip boundary condition. Later in ascent, when the temperature contrast between diapir and country rock is sufficiently large, the possibility of mechanical cracking or thermal spalling of the encompassing country rock should also be included in the model. In its entirety, this model would have the potential to accurately predict ascent velocity profiles of igneous diapirism, and related magma transport processes, over the entire course of ascent.

Another important assumption used to develop the model found in this study is the idea that the temperature distribution within the magma body is homogenous at a given instant. In other words, convection in the diapir occurs over such a short period that any sort of temperature gradient is erased. If this assumption is valid, the Nusselt

number, a pure number representing a ratio of the total heat transfer within the body to thermal conduction, must be sufficiantly large. For example, a Nusselt number of 2 would indicate that the assumption of a zero temperature gradient is grossly exaggerated. On the other hand, a Nusselt number of 1000 means that convective overturning is quite rapid within the body and the assumption is valid.

To determine the Nusselt number, the Rayleigh number must be evaluated first.

$$R_a = \alpha \vec{g} \Delta T R^3 \rho_D / \chi_D \mu$$

where α is the thermal expansion coefficient and ΔT is the temperature difference between the center and the margins of the convecting chamber. The viscosity of the diapir at about 750°C is on the order of 1.0E+7 poise (Shaw, 1963). Using an α of 5.0E-5/deg (Spera, 1982), a χ_D of 0.01 cm^2/sec, and assuming that temperature drops 50 degrees from the center of a 5 km diapir (R = 2.5 km) to its outer boundary, the Rayleigh number is found to be 9.58E+12. Spera states the following relationship between Nusselt and Rayleigh numbers:

$$Nu = R_a^{1/4}/2 .$$

From this, a Nusselt number of 495 results. This suggests that the assumption of a constant temperature within the diapir is valid.

Following the onset of crystallization, this relationship becomes progressively less reliable as the fluid movement becomes restricted by viscous interaction with the

crystals. This circumstance is better modeled as fluid motion in a porous media (Walker and Homsy, 1978; Chan et al., 1970). However, for even high states of crystallinity (i.e., relatively low permeability), the Nusselt number predicted by these models exceeds 10, a sufficient value for thermal equilibrium of the pluton within several hundred years.

In order to obey the conservation of energy principle and still have the model remain tractable, heat flux out of the spherical diapir was assumed to be distributed equally over the upper hemisphere, while the interface between the diapir and country rock over the lower hemisphere is an insulated boundary. In nature, the heat flux would be highest at the leading edge of the diapir and minimal below the body. This study may exaggerate the heat transfer over the upper hemisphere, as evident by the rather rapid cooling rates. Information on actual diapir cooling rates could be used in the computer simulation to control the heat flux from the surface. Another suggestion would be to segment the deformation layer into discrete intervals. Each segment would define a different crustal ambient temperature that is determined by the temperature gradient and the segment's depth during a particular snapshot. Energy and material would be transfered from upper segments and accumulate in lower segments. The biggest drawback for this proposal would be the large investment in computer time.

Experimental data for the rheology of geological materials, in particular common crustal rocks, is needed. One of the problems encountered in this study was the virtual absence of experimental data concerning the rheology of crustal rocks at reasonable temperatures and shear strain rates. As a result, obsidian had to be substituted for a more realistic crustal material. Considering that the experimental procedures used do not fully mimic the natural environment, the use of obsidian's rheological data is acceptable. The rheology of dunite was used because numerous sources of data exist. Unfortunately, crustal temperatures increase the experimentally determined effective viscosity of dunite to the point where the diapir modeled could not overcome the confining forces (SODATA6). A model run within dunite at higher temperatures did succeed in rising a significant distance (SODATA9).

4.4 Conclusion

In this study, an ascent velocity relationship for a granitoid diapir was derived and applied to a heat flow model within the crust. This relationship has a very strong dependence on the width of the variable viscosity deformation layer, formed by the loss of heat to the country rock and the buoyant force which propels the diapir through it.

The results of numerous computer simulations show that ascent velocity is strongly dependent on the rheology and

ambient temperature of the surrounding rock. Small variations in the crustal temperature gradient will significantly affect the average ascent velocity, but overall cooling rates remain unchanged.

Ascent velocity also varies with the size of the diapir. Larger bodies move more slowly and ascend for longer periods of time relative to smaller plutons. Due to greater amounts of effective energy available for ascent, larger bodies will rise greater distances. However, the additional amount of ascent is nominal compared to the contrasts in effective energy. The reason for this appears to be due to a greater loss of heat to the surroundings during slower ascent.

Mantle derived granitoid bodies can ascend diapirically through dunite if the temperatures are sufficiently high. At crustal temperatures, granitoids cannot overcome the confining forces imposed by the encompassing dunite during diapirism.

Modeling magma diapirs using a no-slip boundary condition decreases ascent velocity by a factor of 3 relative to the ascent velocity that results using the more realistic stress-free boundary condition. This should be considered when applying experimental models or Stokes' result to the movement of spherical magma bodies.

REFERENCES

Ahern, J.L., D.L. Turcotte, and E.R. Oxburgh, 1981. On the upward migration of an intrusion, Journal of Geology, Vol. 89, pp. 421-432.

Anderson, D.L., 1981. Rise of deep diapirs, Geology, Vol. 9, pp. 7-9.

Batchelor, G.K., 1967. An Introduction to Fluid Dynamics, Cambridge Univ. Press, 615 p.

Bateman, R., 1984. On the role of diapirism in the segregation, ascent and final emplacement of granitoid magmas, Tectonophysics, Vol. 110, pp. 211-231.

Berner, H., H. Ramberg, and O. Stephansson, 1972. Diapirism in theory and experiment, Tectonophysics, Vol. 15, pp. 197-218.

Bowen, N.L., 1948. The granite problem and the method of multiple prejudices, In: Gilluly, J. (Editor), Origin of Granite, Geol. Soc. Amer., Mem. 28, pp. 79-90.

Buddington, A.F., 1959. Granite emplacement with special reference to North America, Geol. Soc. Amer. Bull., Vol. 70, pp. 671-747.

Burden, R.L., J.D. Faires, and A.C. Reynolds, 1981. Numerical Analysis, Prindle, Weber and Schmidt: Boston, MA, 598 p.

Carslaw, H.S. and J.C. Jaeger, 1959. Conduction of Heat in Solids, Oxford University Press, 510 p.

Carter, N.L., 1976. Steady state flow of rocks, Rev. of Geophysics and Space Physics, Vol. 14, no. 3, pp. 301-360.

Carter, N.L. and H.G. Ave'Lallemant, 1970. High temperature flow of dunite and peridotite, Geol. Soc. Amer. Bull., Vol. 81, pp. 2181-2202.

Chappell, B.W. and A.J.R. White, 1974. Two contrasting granite types, Pacific Geology, Vol. 8, pp. 173-174.

Chan, B.K.C., C.M. Ivey, and J.M. Barry, 1970. Natural convection in enclosed porous media with rectangular boundaries, J. Heat Trans., Vol. 92, pp. 21-27.

Chopra, P.N. and M.S. Paterson, 1981. The experimental deformation of dunite, Tectonophysics, Vol. 78, pp. 453-473.

Clark, S.P. (Editor), 1966. Handbook of physical constants, Geol. Soc. Amer., Mem. 97, 587 p.

Clemens, J.D. and V.J. Wall, 1984. Origin and evolution of a peraluminous silicic ignimbrite suite: The Violet Town Volcanics, Contrib. Mineral. Petrol., Vol. 88, pp. 354-371.

Dziewonski, A.M., A.L. Hales, and E.R. Lapwood, 1975. Parametrically simple earth models consistent with geophysical data, Physics of the Earth and Planetary Interiors, Vol. 10, pp. 12-48.

Faure, G., 1977. Principles of Isotope Geology, Wiley, New York, N.Y., 464 pp.

Grout, F.F., 1932. Petrography and Petrology, McGraw-Hill, New York, N.Y., 522 p.

Harrison, T.M. and I. McDougall, 1980. Investigations of an intrusive contact, northwest Nelson, New Zealand - I. Thermal, chronological and isotopic constraints, Geochim. Cosmochim. Acta, Vol. 44, pp 1985-2003.

Huang, W.L. and P.J. Wyllie, 1981. Phase relationships of S-type granite with H_2O to 35 kbar: Muscovite Granite From Harney Peak, South Dakota, J.G.R., Vol. 86, no. B11, pp. 10515-10529.

Hughes, C.J., 1982. Igneous Petrology, Elsevier, New York, N.Y., 551 pp.

Marsh, B.D., 1982. On the mechanics of igneous diapirism, stoping, and zone melting, Am. Jour. Sci., Vol. 282, pp. 808-855.

Marsh, B.D. and L.H. Kantha, 1978. On the heat and mass transfer from an ascending magma, E.P.S.L., Vol. 39, pp. 435-443.

Marsh, B.D. and S. Morris, 1981. Comment and reply on 'Rise of deep diapirs', Geology, Vol. 9, pp. 559-562.

Morris, S., 1982. The effects of a strongly temperature-dependent viscosity on slow flow past a hot sphere, J. Fluid Mech., Vol. 124, pp. 1-26.

Parsons, B. and J.G. Sclater, 1977. An analysis of the variation of ocean floor bathymetry and heat flow with age, J.G.R., Vol. 82, no. 5, pp. 803-827.

Pitcher, W.S., 1979, The nature, ascent and emplacement of granitic magmas, J. Geol. Soc. London, Vol. 136, 1979, pp. 627-662.

Rainville, E.D. and P.E. Bedient, 1981. Elementary Differential Equations, MacMillan, New York, N.Y., 529 p.

Ramberg, H., 1963. Experimental study of gravity tectonics by means of centrifuged models, Bull. Geol. Inst. Univ. Upps., Vol. 42, pp. 1-97.

Read, H.H., 1948. Granites and granites, In: Gilluly, J. (Editor), Origin of Granite, Geol. Soc. Amer., Mem. 28, pp. 1-19.

Ribe, N.M., 1983. Diapirism in the earth's mantle: Experiments on the motion of a hot sphere in a fluid with temperature-dependent viscosity, Jour. of Volcanology and Geothermal Res., Vol. 16, pp. 221-245.

Schmid, S.M., 1982. Microfabric studies as indicators of deformation mechanisms and flow laws operative in mountain building, In: Hsu, K.J. (Editor), Mountain Building Processes, pp. 89-104.

Shaw, H.R., 1963. Obsidian-H_2O viscosities at 1000 and 2000 bars in the temperature range 700° to 900°C, J.G.R., Vol. 68, no. 23, pp. 6337-6343.

Shirey, S.B. and G. Hanson, 1984. Mantle-derived Archaen monozodiorites and trachyandesites, Nature, Vol. 310, pp. 222-224.

Spera, F.J., 1980. Aspects of magma transport, In: Hargraves, R.B. (Editor), Physics of Magmatic Processes, Princeton Univ. Press, pp. 265-323.

Spera, F.J., 1982. Thermal evolution of plutons: A parameterized approach, Science, Vol. 207, pp. 299-301.

Stern, C.R. and P.J. Wyllie, 1981. Phase relationships of I-type granite with H_2O to 35 kilobars: The Dinkey Lukes Biotite-Granite from the Sierra Nevada Batholith, J.G.R., Vol. 86, no. B11, pp. 10412-10422.

Stokes, G.G., 1851. On the effect of the internal friction of fluids on the motion of pendulums, Cambridge Philos. Soc. Trans., Vol. 9, p. 8.

Turcotte, D.L., 1982. Magma migration, Ann. Rev. Earth Planet. Sci., Vol. 10, pp. 397-408.

Walker, K.L. and G.M. Homsy, 1978. Convection in a pourous cavity, J. Fluid Mech., Vol. 87, pp. 449-474.

Wells, P.R.A., 1980. Thermal models for the magmatic accretion and subsequent metamorphism of continental crust, E.P.S.L., Vol. 46, pp. 253-265.

White, S.H. and R.J. Knipe, 1978. Transformation- and reaction-enhanced ductility in rocks, J. Geol. Soc. London, Vol. 135, pp. 513-516.

Whitehead, J.A. and D.S. Luther, 1975. Dynamics of laboratory diapir and plume models, J.G.R. Vol. 80, no. 5, pp.705-717.

Windley, B.F., 1977. The Evolving Continents, Wiley, New York, N.Y., 385 pp.

Wyllie, P.J., W-L. Huang, C.R. Stern, and S. Aaaloe, 1976. Granitic Magmas: possible and impossible sources, water contents and crystallization sequences, Can. J. Earth Sci., Vol. 13, no. 8, pp. 1007-1019.

APPENDIX A

SOCRATES

SOCRATES is an ASCII FORTRAN (similar to FORTRAN 77) program written for implementation on the UNIVAC 1100/82 at the State University of New York at Albany. The algorithm developed uses the basic laws of fluid dynamics and heat transfer to model the ascent velocity profile of a rising granitic diapir within the rheological and thermal framework of the earth's crust.

The following is a complete alphabetized listing of all arrays, constants, and variables used within SOCRATES and the subprogram QUILL. A brief explanation accompanies each term.

A = DELT/DELR**2 : finite difference parameter.
ARG = L/DEN
AVU = The average ascent velocity over ten snapshots.
AYR = The duration of a year in seconds.
B = (2/((L/R)+1))*DELRT : array of difference parameters.
CBRDL = RDL**3
CD = Specific heat of the diapir.
CHI = -LOG(F)
CT = Integer used to count the iterations of the major loop.
CW = Specific heat of the country rock.
CYCLE = Array of random numbers between 0.05 and 0.95 for determining forced convection within the deformation layer.
DELR = 500.0/R
DELRHO = $R_W - R_D$
DELRT = DELT/DELR
DELT = 1.0E+7*K/R**2
DEN = 2.0*SQRT(K*FFP*AYR)
DEP = The depth to the top of the diapir.
DEPD = Diapir's energy per degree.
DGK = 273.15 K
DI = Initial depth to the top of the diapir.
DZ = Width of the deforming layer surrounding the diapir.
E = Activation energy used to determine the viscosity.
EADD = Energy added to the surroundings.
EDGC = E/GC
EPD = Array describing energy per degree within incremental volumes of country rock.
F = Deformation factor (2.71828 or 10.0).
FFP = Duration of the free flux period in years.
G = Viscous variation factor.
GC = Universal gas constant.

```
GEN = TOLT/(LIQT-SOLT)
GLOG = LOG(MUA/MU13)
GP = Initial estimation of the power-law's viscous variation
        factor.
GR = Acceleration due to gravity.
GRD = Crustal geothermal gradient.
I = Integer used as a counter within numerous loops.
ICLOSE = Integer describing region where material is deleted
        from the deforming layer.
ITER = Integer used as a counter in the major program loop.
J = Integer used as a counter within numerous loops.
K = Thermal diffusivity of the country rock.
KEY = 1 for Newtonian surroundings;
      2 for power-law surroundings.
L = Integer used to add increments of distance from R to RDL.
LIQT = Liquidus temperature of the magma.
MUA = Viscosity at infinite temperature.
MUC = Viscosity at the diapir - country rock contact.
MU13 = Viscosity at 1300 K.
N = Integer used as a pointer within the difference matrix.
NUM = Integer used as a pointer within the difference matrix.
ODA = (1/PA)**PL2
OUT = 1 when it is time to complete run; 0 otherwise.
PA = Pre-exponential used in the power-law determination of
        viscosity.
PEADD = Energy added to the affected region outside RDL.
PEPD = Energy per degree in the affected region outside RDL.
PI = 3.14159...
PL1 = Exponent used in power-law determination of viscosity.
PL2 = 1/PL1
PL3 = PL2-1.0
POINT = Interpolated distance outside RDL where energy is
        gained (affected region).
PSLOPE = Slope of the interpolated temperature distribution
        within affected region outside RDL.
PTAVE = Average temperature of affected region outside RDL.
PVOL = Volume of the affected region outside RDL.
PXAVE = Half volume width of the affected region outside RDL.
P23 = PI*2.0/3.0
P34 = PI*3.0/4.0
P43 = PI*4.0/3.0
QAVU = QUILL equivalent of AVU.
QAYR = QUILL equivalent of AYR.
QCT = QUILL equivalent of CT.
QDEP = QUILL equivalent of DEP.
QDZ = QUILL equivalent of DZ.
QMUC = QUILL equivalent of MUC.
QOUT = QUILL equivalent of OUT.
QSST = QUILL equivalent of SST.
QTA = QUILL equivalent of TA.
```

QTD = QUILL equivalent of TD.
QTF = QUILL equivalent of TF.
QTI = QUILL equivalent of TI.
R = Radius of the diapir : 2.5 km in this version SOCRATES.
RCW = RW*CW
RD = Density of the diapir.
RDL = Radius of the diapir + 500 meters.
RTSR = R*SR
RW = Density of the country rock.
SECS = Number of seconds elapsed in the entire ascent period.
SOLT = Solidus temperature of the magma.
SR = Dimensionless strain rate.
SST = Duration of a snapshot : approximately 10 years.
SU = Sum of the ascent velocities : used in averaging.
T = Array of dimensionless temperature values between 0.0 and 1.0.
TA = Array of actual temperature values between TD and TI.
TD = Temperature of the diapir.
TDIF = Difference between the temperatures of the diapir and the outer edge of the deforming layer.
TDMI = Difference between diapir and undisturbed ambient temperatures.
TD1 = Parameter used to determine amount of heat generated within the diapir.
TD2 = Parameter used to determine amount of heat generated within the diapir.
TF = Temperature at the outer edge of the deforming layer.
TI = Undisturbed ambient temperature within surrounding country rock.
TOLT = Amount of equivalent temperature generated within the diapir.
TS = Undisturbed temperature at the earth's surface.
TO = Diapir's initial temperature.
UI = Ascent velocity within a particular snapshot.
V = Array storing 5 meter incremental volumes between R and RDL.
VCF = 2.0*DELRHO*GR*Z/R
VG = Counting integer between 1 and 50 that is used to determine the entry chosen from CYCLE.
VOL = Volume of the diapir.
X = Interpolated distance used to determine DZ.
YRS = Number of years elapsed during entire ascent period.
Z = EXP(CHI)*(2/CHI**2-2/CHI**3-1/CHI)+2/CHI**3
ZAP = Width of material to be deleted from the deforming layer.

```
C                          SOCRATES
C
C
C                   Written by  Keith I. Mahon
C                           Spring 1985
C
C                       S.U.N.Y. at Albany
C                  Department of Geological Sciences
C
C
C
C
C Declaration block for the main program SOCRATES.
C
C
      PROGRAM SOCRATES
C
      DIMENSION T(0:132,0:32),TA(0:100,2),B(132)
      DIMENSION EPD(100),V(100),CYCLE(50)
C
      REAL K,LIQT,MUA,MU13,MUC
      INTEGER CT,OUT,VG
C
      COMMON CT,OUT,SST,AVU,DEP,MUC,DZ,TD,TI,TF,TA,AYR
C
C
C
C
C Input block : all entries are in c.g.s. units and degrees
C Kelvin, except for FFP which is in years.
C
C
      READ(5,*)KEY
      IF (KEY .EQ. 1) THEN
        READ(5,*)E,MUA,MU13
      ELSE
        READ(5,*)E,PA,PL1
        READ(5,*)SR,GP
      END IF
C
      READ(5,*)RD,RW,F
      READ(5,*)CD,CW,K,FFP
      READ(5,*)TO,GRD,DI,TS
      READ(5,*)LIQT,SOLT,TOLT
C
      READ(5,*)CYCLE
C
C
C
C
```

```
C Constant value assignment block.
C
C
      R=2.5E+5
C
      PI=ACOS(-1.0)
      P23=PI*2.0/3.0
      P43=PI*4.0/3.0
      P34=PI*3.0/4.0
C
      GR=-981.0
      GC=8.31432E+7
      EDGC=E/GC
      DELRHO=RW-RD
      CHI=-LOG(F)
      Z=EXP(CHI)*(2/CHI**2-2/CHI**3-1/CHI)+2/CHI**3
      VCF=2.0*DELRHO*GR*Z/R
      AYR=3.15576E+7
      SST=3.2E+8
C
      VOL=P43*(R**3)
      GEN=TOLT/(LIQT-SOLT)
      DEPD=RD*CD*VOL
      RCW=RW*CW
      RDL=R+50000.0
      CBRDL=RDL**3
C
      DELT=1.0E+7*K/R**2
      DELR=500.0/R
      A=DELT/DELR**2
      DELRT=DELT/DELR
      L=0
C
      DO 10, I=1,132
        L=L+500
        B(I)=(2/((L/R)+1))*DELRT
   10 CONTINUE
C
      L=0
C
      DO 20, I=1,100
        L=L+500
        V(I)=P23*((R+L)**3-(R+L-500)**3)
        EPD(I)=V(I)*RCW
   20 CONTINUE
C
      IF (KEY .EQ. 1) THEN
        GLOG=LOG(MUA/MU13)
      ELSE
        PL2=1/PL1
```

```
          PL3=PL2-1.0
          ODA=(1/PA)**PL2
          RTSR=R*SR
        ENDIF
C
C
C
C
C Variable assignment block A : free flux determination and
C gradient calculation.
C
C
        DO 40, J=0,32
          T(0,J)=1.0
          DO 30, I=1,132
            T(I,J)=0.0
   30     CONTINUE
   40   CONTINUE
C
C
        DEN=2.0*SQRT(K*FFP*AYR)
        L=0
C
        DO 50, I=1,100
          L=L+500
          ARG=L/DEN
          T(I,0)=(R/(R+L))*ERFC(ARG)
   50   CONTINUE
C
        TI=GRD*DI+TS
        TDMI=TO-TI
C
        TA(0,1)=TO
        TA(0,2)=TA(0,1)
        DO 60, I=1,100
          TA(I,1)=T(I,0)*TDMI+TI
          TA(I,2)=TA(I,1)
   60   CONTINUE
C
C
C
C
C Variable assignment block B.
C
C
        TD=TO
        TD1=TD
        TD2=LIQT
C
        DZ=0.0
```

```
      SU=0.0
      AVU=0.0
C
      IF (KEY .EQ. 1) THEN
        G=(EDGC/TO+GLOG)/(1300.0-TO)
        UI=0.0
        DEP=DI
      ELSE
        G=GP
        UI=1.0E-8
        DEP=DI+UI*SST
      END IF
C
      OUT=0
      CT=0
      VG=0
C
C
C
C
C
C
C
C The snapshot loop : beginning of SOCRATES' major loop.
C
C
      DO 250, ITER=1,100000
C
      VG=MOD(CT,50)+1
      CT=CT+1
C
C
C
C
C Variable reassignment block.
C
C
      DEP=DEP-UI*SST
      TI=DEP*GRD+TS
      TDMI=TD-TI
      TDIF=LOG(F)/G
      TF=TD-TDIF
      EADD=0.0
      PEADD=0.0
C
C
C
C
C Temperature reassignment block : calculation of the dimen-
C sionless temperature gradient resulting from the flux of
```

```
C heat to the surroundings during a snapshot.
C
C
      NUM=101
      N=132
C
      DO 110, J=0,31
        N=N-1
        DO 100, I=1,N
          T(I,J+1) = A*(T(I+1,J)-2*T(I,J)+T(I-1,J))
     +       -B(J)*(T(I,J)-T(I+1,J))+T(I,J)
          IF ((T(I,J+1) .LT. 0.001) .AND. (J .EQ. 31)) THEN
            NUM=I
            GOTO 110
          ELSEIF (T(I,J+1) .LT. 0.001) THEN
            GOTO 110
          ENDIF
  100   CONTINUE
  110 CONTINUE
C
C
C
C
C Conversion block A : dimensionless temperature is converted
C to degrees Kelvin.
C
C
      TA(0,1)=TD
C
      DO 120, I=1,NUM-1
        TA(I,1)=T(I,32)*TDMI+TI
  120 CONTINUE
C
      DO 130, I=NUM,100
        TA(I,1)=TI
  130 CONTINUE
C
C
C
C
C Termination check block A.
C
C
      IF (TA(50,1) .GE. TF) THEN
        WRITE(8,*)
        WRITE(8,*)'THE PROGRAM HAS TERMINATED DUE TO'
        WRITE(8,*)' THE DEFORMATION LAYER EXCEEDING'
        WRITE(8,*)'      THE 250 METER LIMIT.'
        AVU=UI
        OUT=1
```

```
          CALL QUILL
          STOP
        ENDIF
C
C
C
C
C  Determination of the deforming layer's width.
C
C
        DO 140, I=1,NUM-1
          IF (TA(I,1) .LT. TF) THEN
            X=(TA(I,1)-TF)/(TA(I,1)-TA(I-1,1))
            DZ=I*500.0-X*500.0
            GOTO 150
          ENDIF
  140   CONTINUE
C
C
C
C
C  Determination of the contact viscosity and the value of
C  the viscous variation parameter.
C
C
  150   IF (KEY .EQ. 1) THEN
          MUC=MUA*EXP(EDGC/TA(0,1))
          G=(EDGC/TA(0,1)+GLOG)/(1300.0-TA(0,1))
        ELSE
          MU13=ODA*(EXP(EDGC/1300.0))**PL2*(RTSR*UI/DZ**2)**PL3
          MUC=ODA*(EXP(EDGC/TA(0,1)))**PL2*(RTSR*UI/DZ**2)**PL3
          G=LOG(MUC/MU13)/(1300.0-TA(0,1))
        ENDIF
C
C
C
C
C  Ascent velocity calculation.
C
C
        UI=VCF*(DZ**3)/MUC
C
C
C
C
C  Termination check block B and possible QUILL call.
C
C
        IF ((UI .LT. 1.0E-10) .AND. (CT .GT. 2000)) THEN
          WRITE(8,*)'THE PROGRAM HAS TERMINATED
```

```
          WRITE(8,*)'     DUE TO SLOW ASCENT.'
          AVU=UI
          OUT=1
          CALL QUILL
          STOP
        ELSE
          SU=SU+UI
          IF (MOD(CT,10) .EQ. 0) THEN
            AVU=SU/10.0
            CALL QUILL
            SU=0.0
            AVU=0.0
          ENDIF
        ENDIF
C
C
C
C
C Energy block : determines energy gained by the country
C rock since the last snapshot.
C
C
        IF (NUM .EQ. 101) THEN
          PSLOPE=(TA(100,1)-TA(99,1))/500.0
          POINT=(TI-TA(100,1))/PSLOPE
          PVOL=P23*((RDL+POINT)**3-CBRDL)
          PXAVE=CBRT(PVOL/P43+CBRDL)-RDL
          PTAVE=PSLOPE*PXAVE+TA(100,1)
          PEPD=RCW*PVOL
          PEADD=PEPD*(PTAVE-TI)
        ELSE
          PEADD=0.0
          PSLOPE=0.0
        ENDIF
C
        EADD=PEADD
C
        DO 160, I=1,NUM-1
          EADD=EADD+EPD(I)*(TA(I,1)-TA(I,2))
  160   CONTINUE
C
C
C
C
C Temperature determination and termination block C : as a
C result of energy loss and heat generation, the temperature
C of the diapir is recalculated.
C
C
        TD1=TD-EADD/DEPD
```

```
C
      IF (TD1 .LT. SOLT) THEN
        WRITE(8,*)
        WRITE(8,*)'THE PROGRAM HAS TERMINATED DUE TO'
        WRITE(8,*)'  SOLIDIFICATION OF THE DIAPIR.'
        AVU=UI
        OUT=1
        CALL QUILL
        STOP
      ENDIF
C
      IF ((TD1 .LT. LIQT) .AND. (TD1 .LT. TD2)) THEN
        TD=TD1+GEN*(TD2-TD1)
        TD2=TD1
      ELSE
        TD=TD1
      ENDIF
C
C
C
C
C Cyclic method block : readjusts the temperature within the
C deforming layer as a result of ascent.
C
C
      ZAP=UI*SST*0.5
      ICLOSE=INT(DZ*CYCLE(VG)/500.0)
C
      DO 170, I=ICLOSE+1,NUM-2
        TA(I,2)=ZAP*((TA(I+1,1)-TA(I,1))/500.0)+TA(I,1)
  170 CONTINUE
C
      IF (NUM .NE. 101) THEN
        DO 180, I=NUM-1,100
          TA(I,2)=TI
  180   CONTINUE
      ELSE
        DO 190, I=NUM-1,100
          TA(I,2)=ZAP*PSLOPE+TA(I-1,2)
          IF (TA(I,2) .LT. TI) TA(I,2)=TI
  190   CONTINUE
      ENDIF
C
      DO 200, I=1,ICLOSE
        TA(I,2)=TA(I,1)
  200 CONTINUE
C
C
C
C
```

```
C Conversion block B : conversion to dimensionless tempera-
C ture and preparation of matrix T for the next snapshot.
C
C
      DO 210, I=1,100
        T(I,0)=(TA(I,2)-TI)/TDMI
  210 CONTINUE
C
      DO 220, I=101,132
        T(I,0)=0.0
  220 CONTINUE
C
      DO 240, I=1,132
        DO 230, J=1,32
          T(I,J)=0.0
  230   CONTINUE
  240 CONTINUE
C
C
C
C
C Continuation point for the snapshot loop and termination
C point for SOCRATES.
C
C
 250 CONTINUE
C
C
      END
C
C
C
C
C
C
C
C Declaration block for the subprogram QUILL.
C
C
      SUBROUTINE QUILL
C
      DIMENSION QTA(0:100,2)
C
      INTEGER QCT,QOUT
C
      COMMON QCT,QOUT,QSST,QAVU,QDEP,QMUC,QDZ,QTD,QTI,
     +     QTF,QTA,QAYR
C
C
C
```

```
C
C Constant assignment block.
C
C
      SECS=QCT*QSST
      YRS=SECS/QAYR
      DGK=273.15
C
C
C
C
C Print block A : utilized on every call of QUILL.
C
C
      WRITE(8,*)
      WRITE(8,1100)YRS,QAVU*QAYR/100.0,QDEP/1.0E+5
      WRITE(8,1200)QDZ/100.0,QMUC
      WRITE(8,1300)QTD-DGK,QTF-DGK,QTI-DGK
      WRITE(8,*)
C
C
C
C
C Print block B : utilized on every tenth call of QUILL.
C
C
      IF ((MOD(QCT,100) .EQ. 0) .OR. (QOUT .EQ. 1)) THEN
        WRITE(8,*)'           THE TEMP OUT TO 500 METERS'
        J=-15
C
        DO 1000, I=1,100,4
          J=J+20
          WRITE(8,1400)J,QTA(I,1)-DGK,J+5,QTA(I+1,1)-DGK,
     +          J+10,QTA(I+2,1)-DGK,J+15,QTA(I+3,1)-DGK
 1000   CONTINUE
C
        WRITE(8,*)
      ENDIF
C
C
C
C
C Output format block.
C
C
 1100 FORMAT('YRS:',F8.1,'   VEL:',E10.4E2,'   DEP:',F9.5)
 1200 FORMAT(7X,'DL:',F7.2,'   VISC:',E10.4E2)
 1300 FORMAT(4X,'TD:',F6.1,'   TF:',F6.1,'   TI:',F6.1)
 1400 FORMAT(I3,':',F6.1,I5,':',F6.1,I5,':',F6.1,I5,':',F6.1)
C
```

```
C
C
C
C End of QUILL subprogram and return to main program.
C
C
      RETURN
C
C
      END
```

APPENDIX B

INPUT DATA FILES

Ten runs of the computer program SOCRATES were made on the UNIVAC 1100/82 at S.U.N.Y. at Albany. Within SOCRATES is an input block that enables the user to choose numerous thermal and rheological constraints to be placed on the model (see Appendix A). This section briefly discusses the input, and gives a complete listing of all the input files used to generate the models.

The principal file type used by SOCRATES is the SIDATA file. The following description applies to this file type.

Constraints on the country rock rheology:

line 1 - 1 for Newtonian rheology;
2 for power-law rheology.
line 2 (Nwtn) - Activation energy,
viscosity at infinite temperature,
and viscosity at 1300 K.
line 2a (P-L) - Activation energy,
pre-exponential,
and power-law exponent.
line 2b (P-L) - Dimensionless strain rate
and estimated viscous variation factor.

Miscellaneous thermal and physical constraints:

line 3 - Diapir's density,
country rock's density,
and deformation factor.
line 4 - Diapir's specific heat,
country rock's specific heat,
thermal diffusivity of the country rock,
and duration of the free flux period.
line 5 - Diapir's initial temperature,
crustal geothermal gradient,
initial depth to the top of the diapir,
and the earth's surface temperature.
line 6 - Magma's liquidus temperature,
magma's solidus temperature,
and equivalent temperature generated in the diapir.

The only dimensioned parameter used in SIDATA files that is not in c.g.s. units, or degrees Kelvin, is the duration of the free flux period (line 4) in years.

The other file type used by SOCRATES is the FCON file. This file is comprised of a list of 50 random numbers between 0.05 and 0.95 (increments of 0.1) that are used to determine the effects of forced convection on the temperature within the deforming layer. The random arrangement and frequency of the numbers in these files is the basis for the cyclic method described in Chapter II. Variation in the viscous variation factor results in a slight change in the velocity gradient across the deforming layer. The two files, FCONE and FCON10, correspond to viscous variation factors of 2.71828 and 10.0.

The following is a complete listing of the input data used during the ten model runs.

```
SIDATA1

1
2.93E+12 1.0E-3 5.927E+8
2.5 2.85 2.7183
1.210E+7 1.136E+7 0.007 10.0
1123.15 2.5E-4 3.0E+6 283.15
1073.15 923.15 206.0
```

```
SIDATA2

1
2.93E+12 1.0E-3 5.927E+8
2.5 2.85 2.7183
1.246E+7 1.136E+7 0.007 10.0
1273.15 2.5E-4 3.0E+6 283.15
1073.15 923.15 206.0
```

```
SIDATA3

1
2.93E+12 1.0E-3 5.927E+8
2.5 2.85 10.0
1.246E+7 1.136E+7 0.007 10.0
1273.15 2.5E-4 3.0E+6 283.15
1073.15 923.15 206.0
```

```
SIDATA4

1
2.93E+12 1.0E-3 5.927E+8
2.5 2.85 2.7183
1.210E+7 1.136E+7 0.007 10.0
1123.15 3.0E-4 2.5E+6 283.15
1073.15 923.15 206.0


SIDATA5

1
2.93E+12 1.0E-3 5.927E+8
2.5 2.85 2.7183
1.210E+7 1.136E+7 0.007 10.0
1123.15 0.0 3.0E+6 873.15
1073.15 923.15 206.0


SIDATA6

2
2.26E+12 1.51E-16 2.1
0.81 4.052E+16 0.01
2.5 3.33 2.7183
1.246E+7 1.172E+7 0.008 10.0
1273.15 0.0 3.0E+6 873.15
1073.15 923.15 206.0


SIDATA7

1
2.93E+12 1.0E-3 5.927E+8
2.5 2.85 2.7183
1.210E+7 1.136E+7 0.007 10.0
1123.15 2.5E-4 3.0E+6 283.15
1073.15 923.15 206.0
```

```
SIDATA8

1
2.93E+12 1.0E-3 5.927E+8
2.5 2.85 2.7183
1.210E+7 1.136E+7 0.007 10.0
1123.15 2.5E-4 3.0E+6 283.15
1073.15 923.15 206.0


SIDATA9

2
2.26E+12 1.51E-16 2.1
0.81 0.01
2.5 3.33 2.7183
1.342E+7 1.172E+7 0.008 10.0
1473.15 2.5E-4 4.0E+6 283.15
1073.15 923.15 206.0


SIDATA10

1
2.93E+12 1.0E-3 5.927E+8
2.5 2.85 2.7183
1.246E+7 1.136E+7 0.007 10.0
1233.15 2.5E-4 3.0E+6 283.15
1073.15 923.15 206.0


FCONE

0.45 0.35 0.65 0.75 0.25
0.35 0.25 0.65 0.15 0.65
0.75 0.05 0.85 0.25 0.05
0.45 0.05 0.15 0.05 0.25
0.35 0.45 0.15 0.15 0.75
0.05 0.45 0.25 0.55 0.35
0.15 0.35 0.15 0.05 0.55
0.15 0.25 0.25 0.15 0.05
0.45 0.05 0.35 0.55 0.55
0.45 0.55 0.35 0.95 0.65
```

FCON10

0.45	0.25	0.65	0.65	0.15
0.35	0.25	0.65	0.15	0.55
0.75	0.05	0.85	0.25	0.05
0.35	0.05	0.15	0.05	0.25
0.35	0.45	0.15	0.15	0.75
0.05	0.35	0.15	0.55	0.25
0.05	0.35	0.15	0.05	0.45
0.15	0.25	0.25	0.15	0.05
0.45	0.05	0.25	0.45	0.55
0.35	0.45	0.35	0.95	0.55

APPENDIX C

OUTPUT DATA FILE - SODATA1

```
YRS:   101.4   VEL: .6565E+01   DEP: 29.37786
       DL:  12.23   VISC: .5922E+11
    TD: 838.1   TF: 797.1   TI: 744.4

YRS:   202.8   VEL: .3985E+01   DEP: 28.96465
       DL:  12.34   VISC: .7705E+11
    TD: 829.0   TF: 788.3   TI: 734.1

YRS:   304.2   VEL: .3222E+01   DEP: 28.63631
       DL:  13.08   VISC: .9630E+11
    TD: 821.3   TF: 780.9   TI: 725.9

YRS:   405.6   VEL: .2779E+01   DEP: 28.34860
       DL:  13.11   VISC: .1181E+12
    TD: 814.4   TF: 774.3   TI: 718.7

YRS:   507.0   VEL: .2635E+01   DEP: 28.08406
       DL:  14.37   VISC: .1415E+12
    TD: 808.4   TF: 768.5   TI: 712.1

YRS:   608.4   VEL: .2384E+01   DEP: 27.83510
       DL:  13.83   VISC: .1669E+12
    TD: 802.9   TF: 763.2   TI: 705.9

YRS:   709.8   VEL: .2238E+01   DEP: 27.60718
       DL:  14.18   VISC: .1883E+12
    TD: 799.0   TF: 759.4   TI: 700.2

YRS:   811.2   VEL: .2086E+01   DEP: 27.39540
       DL:  14.42   VISC: .2002E+12
    TD: 797.0   TF: 757.5   TI: 694.9

YRS:   912.6   VEL: .1935E+01   DEP: 27.19709
       DL:  14.23   VISC: .2136E+12
    TD: 794.9   TF: 755.5   TI: 689.9
```

YRS: 1014.0 VEL: .1889E+01 DEP: 27.00683
DL: 14.86 VISC: .2281E+12
TD: 792.8 TF: 753.5 TI: 685.2

THE TEMP OUT TO 500 METERS

5: 779.0	10: 765.7	15: 753.1	20: 741.6
25: 731.3	30: 722.4	35: 714.8	40: 708.5
45: 703.4	50: 699.3	55: 696.1	60: 693.6
65: 691.6	70: 690.1	75: 688.9	80: 688.0
85: 687.3	90: 686.8	95: 686.4	100: 686.0
105: 685.8	110: 685.6	115: 685.4	120: 685.3
125: 685.2	130: 685.2	135: 685.2	140: 685.2
145: 685.2	150: 685.2	155: 685.2	160: 685.2
165: 685.2	170: 685.2	175: 685.2	180: 685.2
185: 685.2	190: 685.2	195: 685.2	200: 685.2
205: 685.2	210: 685.2	215: 685.2	220: 685.2
225: 685.2	230: 685.2	235: 685.2	240: 685.2
245: 685.2	250: 685.2	255: 685.2	260: 685.2
265: 685.2	270: 685.2	275: 685.2	280: 685.2
285: 685.2	290: 685.2	295: 685.2	300: 685.2
305: 685.2	310: 685.2	315: 685.2	320: 685.2
325: 685.2	330: 685.2	335: 685.2	340: 685.2
345: 685.2	350: 685.2	355: 685.2	360: 685.2
365: 685.2	370: 685.2	375: 685.2	380: 685.2
385: 685.2	390: 685.2	395: 685.2	400: 685.2
405: 685.2	410: 685.2	415: 685.2	420: 685.2
425: 685.2	430: 685.2	435: 685.2	440: 685.2
445: 685.2	450: 685.2	455: 685.2	460: 685.2
465: 685.2	470: 685.2	475: 685.2	480: 685.2
485: 685.2	490: 685.2	495: 685.2	500: 685.2

YRS: 1115.4 VEL: .1771E+01 DEP: 26.82395
DL: 14.31 VISC: .2431E+12
TD: 790.7 TF: 751.5 TI: 680.6

YRS: 1216.8 VEL: .1695E+01 DEP: 26.65152
DL: 14.42 VISC: .2579E+12
TD: 788.8 TF: 749.7 TI: 676.3

YRS: 1318.2 VEL: .1620E+01 DEP: 26.48723
DL: 14.71 VISC: .2748E+12
TD: 786.8 TF: 747.7 TI: 672.2

YRS: 1419.6 VEL: .1531E+01 DEP: 26.33074
DL: 14.64 VISC: .2928E+12

```
    TD: 784.8    TF: 745.8    TI: 668.3


YRS:  1521.0    VEL: .1509E+01    DEP: 26.17869
       DL:  15.24    VISC: .3108E+12
    TD: 782.9    TF: 743.9    TI: 664.5


YRS:  1622.4    VEL: .1436E+01    DEP: 26.03091
       DL:  14.80    VISC: .3290E+12
    TD: 781.1    TF: 742.2    TI: 660.8


YRS:  1723.8    VEL: .1384E+01    DEP: 25.89018
       DL:  14.95    VISC: .3490E+12
    TD: 779.2    TF: 740.4    TI: 657.3


YRS:  1825.2    VEL: .1337E+01    DEP: 25.75466
       DL:  15.25    VISC: .3703E+12
    TD: 777.4    TF: 738.6    TI: 653.9


YRS:  1926.6    VEL: .1277E+01    DEP: 25.62430
       DL:  15.21    VISC: .3915E+12
    TD: 775.6    TF: 737.0    TI: 650.6


YRS:  2028.0    VEL: .1265E+01    DEP: 25.49670
       DL:  15.79    VISC: .4154E+12
    TD: 773.8    TF: 735.2    TI: 647.4

          THE TEMP OUT TO 500 METERS
  5: 761.1   10: 748.7   15: 736.9   20: 725.8
 25: 715.7   30: 706.4   35: 698.2   40: 691.0
 45: 684.8   50: 679.4   55: 674.7   60: 670.7
 65: 667.3   70: 664.4   75: 661.9   80: 659.7
 85: 657.9   90: 656.3   95: 655.0  100: 653.8
105: 652.8  110: 651.9  115: 651.2  120: 650.6
125: 650.0  130: 649.6  135: 649.2  140: 648.8
145: 648.6  150: 648.3  155: 648.1  160: 647.9
165: 647.8  170: 647.6  175: 647.4  180: 647.4
185: 647.4  190: 647.4  195: 647.4  200: 647.4
205: 647.4  210: 647.4  215: 647.4  220: 647.4
225: 647.4  230: 647.4  235: 647.4  240: 647.4
245: 647.4  250: 647.4  255: 647.4  260: 647.4
265: 647.4  270: 647.4  275: 647.4  280: 647.4
285: 647.4  290: 647.4  295: 647.4  300: 647.4
305: 647.4  310: 647.4  315: 647.4  320: 647.4
325: 647.4  330: 647.4  335: 647.4  340: 647.4
```

```
345: 647.4   350: 647.4   355: 647.4   360: 647.4
365: 647.4   370: 647.4   375: 647.4   380: 647.4
385: 647.4   390: 647.4   395: 647.4   400: 647.4
405: 647.4   410: 647.4   415: 647.4   420: 647.4
425: 647.4   430: 647.4   435: 647.4   440: 647.4
445: 647.4   450: 647.4   455: 647.4   460: 647.4
465: 647.4   470: 647.4   475: 647.4   480: 647.4
485: 647.4   490: 647.4   495: 647.4   500: 647.4


YRS:  2129.4    VEL: .1233E+01    DEP: 25.37008
        DL:  15.40    VISC: .4378E+12
    TD: 772.2    TF: 733.6    TI: 644.3


YRS:  2230.8    VEL: .1181E+01    DEP: 25.25012
        DL:  15.57    VISC: .4613E+12
    TD: 770.5    TF: 732.0    TI: 641.3


YRS:  2332.2    VEL: .1143E+01    DEP: 25.13420
        DL:  15.87    VISC: .4881E+12
    TD: 768.8    TF: 730.4    TI: 638.4


YRS:  2433.6    VEL: .1101E+01    DEP: 25.02200
        DL:  15.87    VISC: .5143E+12
    TD: 767.2    TF: 728.8    TI: 635.5


YRS:  2535.0    VEL: .1099E+01    DEP: 24.91178
        DL:  16.75    VISC: .5431E+12
    TD: 765.5    TF: 727.2    TI: 632.8


YRS:  2636.4    VEL: .1068E+01    DEP: 24.80159
        DL:  16.10    VISC: .5712E+12
    TD: 764.0    TF: 725.7    TI: 630.0


YRS:  2737.9    VEL: .1029E+01    DEP: 24.69705
        DL:  16.26    VISC: .6010E+12
    TD: 762.4    TF: 724.2    TI: 627.4


YRS:  2839.3    VEL: .1000E+01    DEP: 24.59564
        DL:  16.55    VISC: .6337E+12
    TD: 760.8    TF: 722.7    TI: 624.9
```

YRS: 2940.7 VEL: .9676E+00 DEP: 24.49707
DL: 16.58 VISC: .6667E+12
TD: 759.3 TF: 721.2 TI: 622.4

YRS: 3042.1 VEL: .9664E+00 DEP: 24.40002
DL: 17.39 VISC: .7009E+12
TD: 757.8 TF: 719.7 TI: 620.0

THE TEMP OUT TO 500 METERS

5: 746.5	10: 735.4	15: 724.6	20: 714.4
25: 704.7	30: 695.8	35: 687.6	40: 680.1
45: 673.4	50: 667.4	55: 662.1	60: 657.3
65: 653.1	70: 649.4	75: 646.1	80: 643.1
85: 640.5	90: 638.1	95: 636.0	100: 634.2
105: 632.5	110: 631.0	115: 629.7	120: 628.5
125: 627.5	130: 626.6	135: 625.7	140: 625.0
145: 624.3	150: 623.8	155: 623.2	160: 622.8
165: 622.4	170: 622.0	175: 621.7	180: 621.4
185: 621.1	190: 620.9	195: 620.7	200: 620.5
205: 620.4	210: 620.2	215: 620.0	220: 620.0
225: 620.0	230: 620.0	235: 620.0	240: 620.0
245: 620.0	250: 620.0	255: 620.0	260: 620.0
265: 620.0	270: 620.0	275: 620.0	280: 620.0
285: 620.0	290: 620.0	295: 620.0	300: 620.0
305: 620.0	310: 620.0	315: 620.0	320: 620.0
325: 620.0	330: 620.0	335: 620.0	340: 620.0
345: 620.0	350: 620.0	355: 620.0	360: 620.0
365: 620.0	370: 620.0	375: 620.0	380: 620.0
385: 620.0	390: 620.0	395: 620.0	400: 620.0
405: 620.0	410: 620.0	415: 620.0	420: 620.0
425: 620.0	430: 620.0	435: 620.0	440: 620.0
445: 620.0	450: 620.0	455: 620.0	460: 620.0
465: 620.0	470: 620.0	475: 620.0	480: 620.0
485: 620.0	490: 620.0	495: 620.0	500: 620.0

YRS: 3143.5 VEL: .9437E+00 DEP: 24.30292
DL: 16.85 VISC: .7353E+12
TD: 756.3 TF: 718.4 TI: 617.6

YRS: 3244.9 VEL: .9119E+00 DEP: 24.21025
DL: 16.98 VISC: .7692E+12
TD: 755.0 TF: 717.1 TI: 615.3

YRS: 3346.3 VEL: .8890E+00 DEP: 24.12011
DL: 17.27 VISC: .8089E+12
TD: 753.5 TF: 715.6 TI: 613.0

```
YRS:  3447.7   VEL: .8631E+00   DEP: 24.03224
       DL:  17.31   VISC: .8483E+12
    TD: 752.0   TF: 714.2   TI: 610.8

YRS:  3549.1   VEL: .8619E+00   DEP: 23.94557
       DL:  18.07   VISC: .8903E+12
    TD: 750.6   TF: 712.8   TI: 608.6

YRS:  3650.5   VEL: .8450E+00   DEP: 23.85879
       DL:  17.61   VISC: .9323E+12
    TD: 749.2   TF: 711.5   TI: 606.5

YRS:  3751.9   VEL: .8221E+00   DEP: 23.77524
       DL:  17.73   VISC: .9736E+12
    TD: 748.0   TF: 710.3   TI: 604.4

YRS:  3853.3   VEL: .7991E+00   DEP: 23.69421
       DL:  18.01   VISC: .1022E+13
    TD: 746.5   TF: 708.9   TI: 602.4

YRS:  3954.7   VEL: .7784E+00   DEP: 23.61500
       DL:  18.07   VISC: .1068E+13
    TD: 745.2   TF: 707.7   TI: 600.4

YRS:  4056.1   VEL: .7852E+00   DEP: 23.53595
       DL:  18.77   VISC: .1117E+13
    TD: 743.9   TF: 706.4   TI: 598.4

          THE TEMP OUT TO 500 METERS
  5: 733.6    10: 723.4    15: 713.6    20: 704.1
 25: 695.0    30: 686.6    35: 678.7    40: 671.4
 45: 664.7    50: 658.6    55: 653.0    60: 648.0
 65: 643.4    70: 639.2    75: 635.4    80: 632.0
 85: 628.8    90: 626.0    95: 623.4   100: 621.0
105: 618.8   110: 616.9   115: 615.1   120: 613.5
125: 612.0   130: 610.6   135: 609.4   140: 608.3
145: 607.3   150: 606.3   155: 605.5   160: 604.7
165: 604.0   170: 603.4   175: 602.8   180: 602.3
185: 601.8   190: 601.4   195: 601.0   200: 600.7
205: 600.3   210: 600.0   215: 599.8   220: 599.5
225: 599.3   230: 599.1   235: 599.0   240: 598.8
245: 598.7   250: 598.4   255: 598.4   260: 598.4
265: 598.4   270: 598.4   275: 598.4   280: 598.4
```

```
285: 598.4   290: 598.4   295: 598.4   300: 598.4
305: 598.4   310: 598.4   315: 598.4   320: 598.4
325: 598.4   330: 598.4   335: 598.4   340: 598.4
345: 598.4   350: 598.4   355: 598.4   360: 598.4
365: 598.4   370: 598.4   375: 598.4   380: 598.4
385: 598.4   390: 598.4   395: 598.4   400: 598.4
405: 598.4   410: 598.4   415: 598.4   420: 598.4
425: 598.4   430: 598.4   435: 598.4   440: 598.4
445: 598.4   450: 598.4   455: 598.4   460: 598.4
465: 598.4   470: 598.4   475: 598.4   480: 598.4
485: 598.4   490: 598.4   495: 598.4   500: 598.4


YRS:  4157.5   VEL: .7629E+00   DEP: 23.45773
       DL:  18.37   VISC: .1168E+13
    TD: 742.6   TF: 705.1   TI: 596.4


YRS:  4258.9   VEL: .7445E+00   DEP: 23.38207
       DL:  18.49   VISC: .1218E+13
    TD: 741.4   TF: 703.9   TI: 594.6


YRS:  4360.3   VEL: .7274E+00   DEP: 23.30853
       DL:  18.95   VISC: .1272E+13
    TD: 740.1   TF: 702.7   TI: 592.7


YRS:  4461.7   VEL: .7104E+00   DEP: 23.23604
       DL:  18.83   VISC: .1329E+13
    TD: 738.8   TF: 701.5   TI: 590.9


YRS:  4563.1   VEL: .7132E+00   DEP: 23.16418
       DL:  19.51   VISC: .1388E+13
    TD: 737.6   TF: 700.3   TI: 589.1


YRS:  4664.5   VEL: .6956E+00   DEP: 23.09296
       DL:  19.15   VISC: .1446E+13
    TD: 736.4   TF: 699.1   TI: 587.3


YRS:  4765.9   VEL: .6798E+00   DEP: 23.02387
       DL:  19.26   VISC: .1503E+13
    TD: 735.7   TF: 698.1   TI: 585.6


YRS:  4867.3   VEL: .6651E+00   DEP: 22.95660
       DL:  19.71   VISC: .1570E+13
```

TD: 734.0 TF: 696.9 TI: 583.9

YRS: 4968.7 VEL: .6510E+00 DEP: 22.89021
DL: 19.61 VISC: .1636E+13
TD: 732.8 TF: 695.7 TI: 582.3

YRS: 5070.1 VEL: .6533E+00 DEP: 22.82437
DL: 20.26 VISC: .1701E+13
TD: 731.7 TF: 694.6 TI: 580.6

THE TEMP OUT TO 500 METERS

5: 722.3	10: 713.0	15: 703.9	20: 695.1
25: 686.7	30: 678.7	35: 671.2	40: 664.2
45: 657.7	50: 651.7	55: 646.1	60: 641.0
65: 636.2	70: 631.9	75: 627.8	80: 624.1
85: 620.6	90: 617.4	95: 614.5	100: 611.8
105: 609.2	110: 606.9	115: 604.8	120: 602.8
125: 600.9	130: 599.2	135: 597.7	140: 596.2
145: 594.9	150: 593.7	155: 592.5	160: 591.5
165: 590.5	170: 589.6	175: 588.8	180: 588.0
185: 587.3	190: 586.7	195: 586.1	200: 585.5
205: 585.0	210: 584.5	215: 584.1	220: 583.7
225: 583.3	230: 583.0	235: 582.7	240: 582.4
245: 582.1	250: 581.9	255: 581.6	260: 581.4
265: 581.2	270: 581.1	275: 580.9	280: 580.6
285: 580.6	290: 580.6	295: 580.6	300: 580.6
305: 580.6	310: 580.6	315: 580.6	320: 580.6
325: 580.6	330: 580.6	335: 580.6	340: 580.6
345: 580.6	350: 580.6	355: 580.6	360: 580.6
365: 580.6	370: 580.6	375: 580.6	380: 580.6
385: 580.6	390: 580.6	395: 580.6	400: 580.6
405: 580.6	410: 580.6	415: 580.6	420: 580.6
425: 580.6	430: 580.6	435: 580.6	440: 580.6
445: 580.6	450: 580.6	455: 580.6	460: 580.6
465: 580.6	470: 580.6	475: 580.6	480: 580.6
485: 580.6	490: 580.6	495: 580.6	500: 580.6

YRS: 5171.5 VEL: .6423E+00 DEP: 22.75863
DL: 19.93 VISC: .1771E+13
TD: 730.5 TF: 693.5 TI: 579.0

YRS: 5272.9 VEL: .6281E+00 DEP: 22.69481
DL: 20.03 VISC: .1839E+13
TD: 729.5 TF: 692.5 TI: 577.4

```
YRS:  5374.3   VEL: .6164E+00   DEP: 22.63247
       DL:  20.49   VISC: .1916E+13
    TD: 728.3   TF: 691.4   TI: 575.8


YRS:  5475.7   VEL: .6021E+00   DEP: 22.57111
       DL:  20.40   VISC: .1990E+13
    TD: 727.2   TF: 690.3   TI: 574.3


YRS:  5577.1   VEL: .6025E+00   DEP: 22.51033
       DL:  21.03   VISC: .2072E+13
    TD: 726.1   TF: 689.2   TI: 572.8


YRS:  5678.5   VEL: .5947E+00   DEP: 22.44954
       DL:  20.72   VISC: .2149E+13
    TD: 725.1   TF: 688.2   TI: 571.2


YRS:  5779.9   VEL: .5813E+00   DEP: 22.39046
       DL:  20.83   VISC: .2229E+13
    TD: 724.0   TF: 687.2   TI: 569.8


YRS:  5881.3   VEL: .5709E+00   DEP: 22.33271
       DL:  21.26   VISC: .2314E+13
    TD: 723.0   TF: 686.2   TI: 568.3


YRS:  5982.7   VEL: .5587E+00   DEP: 22.27579
       DL:  21.19   VISC: .2403E+13
    TD: 721.9   TF: 685.2   TI: 566.9


YRS:  6084.1   VEL: .5605E+00   DEP: 22.21940
       DL:  22.01   VISC: .2491E+13
    TD: 720.9   TF: 684.2   TI: 565.5

          THE TEMP OUT TO 500 METERS
  5: 712.3   10: 703.8   15: 695.5   20: 687.4
 25: 679.5   30: 672.0   35: 664.9   40: 658.2
 45: 651.8   50: 645.9   55: 640.4   60: 635.2
 65: 630.4   70: 626.0   75: 621.8   80: 617.9
 85: 614.3   90: 610.9   95: 607.7  100: 604.7
105: 602.0  110: 599.4  115: 597.0  120: 594.7
125: 592.6  130: 590.7  135: 588.8  140: 587.1
145: 585.5  150: 584.0  155: 582.6  160: 581.3
165: 580.1  170: 579.0  175: 577.9  180: 577.0
185: 576.0  190: 575.2  195: 574.4  200: 573.6
```

```
205: 572.9  210: 572.3  215: 571.7  220: 571.1
225: 570.6  230: 570.1  235: 569.7  240: 569.3
245: 568.9  250: 568.5  255: 568.2  260: 567.8
265: 567.5  270: 567.3  275: 567.0  280: 566.8
285: 566.5  290: 566.3  295: 566.1  300: 566.0
305: 565.8  310: 565.5  315: 565.5  320: 565.5
325: 565.5  330: 565.5  335: 565.5  340: 565.5
345: 565.5  350: 565.5  355: 565.5  360: 565.5
365: 565.5  370: 565.5  375: 565.5  380: 565.5
385: 565.5  390: 565.5  395: 565.5  400: 565.5
405: 565.5  410: 565.5  415: 565.5  420: 565.5
425: 565.5  430: 565.5  435: 565.5  440: 565.5
445: 565.5  450: 565.5  455: 565.5  460: 565.5
465: 565.5  470: 565.5  475: 565.5  480: 565.5
485: 565.5  490: 565.5  495: 565.5  500: 565.5


YRS:  6185.5   VEL: .5528E+00   DEP: 22.16275
       DL:  21.52   VISC: .2583E+13
    TD: 719.9   TF: 683.3   TI: 564.1


YRS:  6286.9   VEL: .5404E+00   DEP: 22.10784
       DL:  21.62   VISC: .2674E+13
    TD: 718.9   TF: 682.3   TI: 562.7


YRS:  6388.3   VEL: .5311E+00   DEP: 22.05410
       DL:  22.04   VISC: .2774E+13
    TD: 717.9   TF: 681.3   TI: 561.4


YRS:  6489.7   VEL: .5206E+00   DEP: 22.00108
       DL:  21.99   VISC: .2877E+13
    TD: 716.9   TF: 680.4   TI: 560.0


YRS:  6591.1   VEL: .5232E+00   DEP: 21.94841
       DL:  22.77   VISC: .2977E+13
    TD: 715.9   TF: 679.4   TI: 558.7


YRS:  6692.5   VEL: .5166E+00   DEP: 21.89552
       DL:  22.31   VISC: .3082E+13
    TD: 715.0   TF: 678.5   TI: 557.4


YRS:  6793.9   VEL: .5055E+00   DEP: 21.84417
       DL:  22.41   VISC: .3187E+13
    TD: 714.0   TF: 677.6   TI: 556.1
```

```
YRS:  6895.3   VEL: .4981E+00   DEP: 21.79376
       DL:  22.83   VISC: .3304E+13
    TD: 713.0   TF: 676.7   TI: 554.8


YRS:  6996.7   VEL: .4866E+00   DEP: 21.74421
       DL:  22.78   VISC: .3417E+13
    TD: 712.1   TF: 675.8   TI: 553.6


YRS:  7098.1   VEL: .4897E+00   DEP: 21.69487
       DL:  23.53   VISC: .3537E+13
    TD: 711.2   TF: 674.9   TI: 552.4

          THE TEMP OUT TO 500 METERS
  5: 703.2   10: 695.3   15: 687.6   20: 680.0
 25: 672.7   30: 665.6   35: 658.9   40: 652.5
 45: 646.4   50: 640.7   55: 635.3   60: 630.3
 65: 625.5   70: 621.0   75: 616.8   80: 612.9
 85: 609.1   90: 605.6   95: 602.3  100: 599.2
105: 596.3  110: 593.5  115: 590.9  120: 588.5
125: 586.2  130: 584.0  135: 582.0  140: 580.1
145: 578.3  150: 576.6  155: 575.0  160: 573.5
165: 572.0  170: 570.7  175: 569.5  180: 568.3
185: 567.2  190: 566.1  195: 565.2  200: 564.2
205: 563.4  210: 562.6  215: 561.8  220: 561.1
225: 560.4  230: 559.8  235: 559.2  240: 558.6
245: 558.1  250: 557.6  255: 557.2  260: 556.7
265: 556.3  270: 555.9  275: 555.6  280: 555.2
285: 554.9  290: 554.6  295: 554.4  300: 554.1
305: 553.8  310: 553.6  315: 553.4  320: 553.2
325: 553.0  330: 552.8  335: 552.7  340: 552.4
345: 552.4  350: 552.4  355: 552.4  360: 552.4
365: 552.4  370: 552.4  375: 552.4  380: 552.4
385: 552.4  390: 552.4  395: 552.4  400: 552.4
405: 552.4  410: 552.4  415: 552.4  420: 552.4
425: 552.4  430: 552.4  435: 552.4  440: 552.4
445: 552.4  450: 552.4  455: 552.4  460: 552.4
465: 552.4  470: 552.4  475: 552.4  480: 552.4
485: 552.4  490: 552.4  495: 552.4  500: 552.4


YRS:  7199.5   VEL: .4876E+00   DEP: 21.64502
       DL:  23.15   VISC: .3650E+13
    TD: 710.3   TF: 674.0   TI: 551.1


YRS:  7300.9   VEL: .4745E+00   DEP: 21.59679
       DL:  23.20   VISC: .3770E+13
```

```
     TD: 709.4    TF: 673.2    TI: 549.9


YRS:  7402.3    VEL: .4663E+00    DEP: 21.54959
       DL:  23.60    VISC: .3899E+13
     TD: 708.5    TF: 672.3    TI: 548.7


YRS:  7503.7    VEL: .4564E+00    DEP: 21.50314
       DL:  23.57    VISC: .4035E+13
     TD: 707.6    TF: 671.4    TI: 547.6


YRS:  7605.1    VEL: .4590E+00    DEP: 21.45687
       DL:  24.29    VISC: .4169E+13
     TD: 706.7    TF: 670.5    TI: 546.4


YRS:  7706.5    VEL: .4575E+00    DEP: 21.41014
       DL:  23.95    VISC: .4301E+13
     TD: 705.8    TF: 669.7    TI: 545.3


YRS:  7807.9    VEL: .4473E+00    DEP: 21.36467
       DL:  23.99    VISC: .4435E+13
     TD: 705.0    TF: 668.9    TI: 544.1


YRS:  7909.3    VEL: .4381E+00    DEP: 21.32032
       DL:  24.38    VISC: .4580E+13
     TD: 704.1    TF: 668.1    TI: 543.0


YRS:  8010.7    VEL: .4295E+00    DEP: 21.27661
       DL:  24.36    VISC: .4729E+13
     TD: 703.2    TF: 667.2    TI: 541.9


YRS:  8112.2    VEL: .4315E+00    DEP: 21.23309
       DL:  25.05    VISC: .4879E+13
     TD: 702.4    TF: 666.4    TI: 540.8

          THE TEMP OUT TO 500 METERS
  5: 695.0    10: 687.6    15: 680.4    20: 673.3
 25: 666.5    30: 659.8    35: 653.5    40: 647.4
 45: 641.6    50: 636.1    55: 630.9    60: 625.9
 65: 621.3    70: 616.8    75: 612.6    80: 608.7
 85: 604.9    90: 601.4    95: 598.0   100: 594.8
105: 591.8   110: 588.9   115: 586.2   120: 583.6
125: 581.1   130: 578.8   135: 576.6   140: 574.6
```

```
145: 572.6   150: 570.7   155: 569.0   160: 567.3
165: 565.7   170: 564.2   175: 562.8   180: 561.4
185: 560.2   190: 559.0   195: 557.8   200: 556.7
205: 555.7   210: 554.8   215: 553.9   220: 553.0
225: 552.2   230: 551.4   235: 550.7   240: 550.0
245: 549.3   250: 548.7   255: 548.1   260: 547.6
265: 547.1   270: 546.6   275: 546.1   280: 545.7
285: 545.3   290: 544.9   295: 544.5   300: 544.1
305: 543.8   310: 543.5   315: 543.2   320: 542.9
325: 542.7   330: 542.4   335: 542.2   340: 542.0
345: 541.8   350: 541.6   355: 541.4   360: 541.3
365: 541.1   370: 540.8   375: 540.8   380: 540.8
385: 540.8   390: 540.8   395: 540.8   400: 540.8
405: 540.8   410: 540.8   415: 540.8   420: 540.8
425: 540.8   430: 540.8   435: 540.8   440: 540.8
445: 540.8   450: 540.8   455: 540.8   460: 540.8
465: 540.8   470: 540.8   475: 540.8   480: 540.8
485: 540.8   490: 540.8   495: 540.8   500: 540.8


YRS:  8213.6   VEL: .4305E+00   DEP: 21.18914
       DL:  24.75   VISC: .5033E+13
    TD: 701.6   TF: 665.6   TI: 539.7


YRS:  8315.0   VEL: .4215E+00   DEP: 21.14630
       DL:  24.79   VISC: .5182E+13
    TD: 700.8   TF: 664.8   TI: 538.7


YRS:  8416.4   VEL: .4131E+00   DEP: 21.10448
       DL:  25.18   VISC: .5348E+13
    TD: 699.9   TF: 664.0   TI: 537.6


YRS:  8517.8   VEL: .4055E+00   DEP: 21.06323
       DL:  25.16   VISC: .5519E+13
    TD: 699.1   TF: 663.2   TI: 536.6


YRS:  8619.2   VEL: .4074E+00   DEP: 21.02213
       DL:  25.84   VISC: .5684E+13
    TD: 698.3   TF: 662.5   TI: 535.6


YRS:  8720.6   VEL: .4067E+00   DEP: 20.98063
       DL:  25.56   VISC: .5856E+13
    TD: 697.5   TF: 661.7   TI: 534.5
```

YRS: 8822.0 VEL: .3986E+00 DEP: 20.94011
DL: 25.60 VISC: .6030E+13
TD: 696.7 TF: 660.9 TI: 533.5

YRS: 8923.4 VEL: .3909E+00 DEP: 20.90053
DL: 25.97 VISC: .6208E+13
TD: 695.9 TF: 660.2 TI: 532.5

YRS: 9024.8 VEL: .3841E+00 DEP: 20.86146
DL: 25.97 VISC: .6396E+13
TD: 695.1 TF: 659.4 TI: 531.5

YRS: 9126.2 VEL: .3855E+00 DEP: 20.82254
DL: 26.62 VISC: .6594E+13
TD: 694.3 TF: 658.6 TI: 530.6

THE TEMP OUT TO 500 METERS

5: 687.4	10: 680.5	15: 673.8	20: 667.1
25: 660.7	30: 654.4	35: 648.4	40: 642.6
45: 637.0	50: 631.8	55: 626.7	60: 621.9
65: 617.4	70: 613.1	75: 608.9	80: 605.0
85: 601.3	90: 597.7	95: 594.3	100: 591.0
105: 588.0	110: 585.0	115: 582.2	120: 579.6
125: 577.0	130: 574.6	135: 572.3	140: 570.1
145: 568.0	150: 566.0	155: 564.1	160: 562.3
165: 560.6	170: 559.0	175: 557.4	180: 555.9
185: 554.5	190: 553.2	195: 551.9	200: 550.7
205: 549.6	210: 548.5	215: 547.4	220: 546.4
225: 545.5	230: 544.6	235: 543.7	240: 542.9
245: 542.1	250: 541.4	255: 540.7	260: 540.1
265: 539.4	270: 538.8	275: 538.3	280: 537.7
285: 537.2	290: 536.7	295: 536.3	300: 535.8
305: 535.4	310: 535.0	315: 534.7	320: 534.3
325: 534.0	330: 533.6	335: 533.3	340: 533.0
345: 532.8	350: 532.5	355: 532.3	360: 532.0
365: 531.8	370: 531.6	375: 531.4	380: 531.2
385: 531.0	390: 530.9	395: 530.6	400: 530.6
405: 530.6	410: 530.6	415: 530.6	420: 530.6
425: 530.6	430: 530.6	435: 530.6	440: 530.6
445: 530.6	450: 530.6	455: 530.6	460: 530.6
465: 530.6	470: 530.6	475: 530.6	480: 530.6
485: 530.6	490: 530.6	495: 530.6	500: 530.6

YRS: 9227.6 VEL: .3850E+00 DEP: 20.78328
DL: 26.37 VISC: .6777E+13
TD: 693.6 TF: 657.9 TI: 529.6

```
YRS:  9329.0   VEL: .3777E+00   DEP: 20.74489
       DL:  26.41   VISC: .6971E+13
    TD: 692.9   TF: 657.2   TI: 528.6

YRS:  9430.4   VEL: .3706E+00   DEP: 20.70735
       DL:  26.77   VISC: .7175E+13
    TD: 692.1   TF: 656.5   TI: 527.7

YRS:  9531.8   VEL: .3646E+00   DEP: 20.67028
       DL:  26.78   VISC: .7385E+13
    TD: 691.3   TF: 655.8   TI: 526.8

YRS:  9633.2   VEL: .3662E+00   DEP: 20.63336
       DL:  27.56   VISC: .7600E+13
    TD: 690.6   TF: 655.0   TI: 525.8

YRS:  9734.6   VEL: .3668E+00   DEP: 20.59591
       DL:  27.18   VISC: .7808E+13
    TD: 689.9   TF: 654.3   TI: 524.9

YRS:  9836.0   VEL: .3595E+00   DEP: 20.55937
       DL:  27.21   VISC: .8025E+13
    TD: 689.1   TF: 653.6   TI: 524.0

YRS:  9937.4   VEL: .3533E+00   DEP: 20.52363
       DL:  27.69   VISC: .8252E+13
    TD: 688.4   TF: 652.9   TI: 523.1

YRS: 10038.8   VEL: .3475E+00   DEP: 20.48825
       DL:  27.57   VISC: .8482E+13
    TD: 687.7   TF: 652.2   TI: 522.2

YRS: 10140.2   VEL: .3499E+00   DEP: 20.45297
       DL:  28.35   VISC: .8726E+13
    TD: 686.9   TF: 651.5   TI: 521.3

          THE TEMP OUT TO 500 METERS
  5: 680.5   10: 674.1   15: 667.8   20: 661.6
 25: 655.5   30: 649.6   35: 643.8   40: 638.3
 45: 633.0   50: 627.9   55: 623.0   60: 618.3
 65: 613.9   70: 609.6   75: 605.5   80: 601.7
```

```
 85: 597.9   90: 594.4   95: 591.0  100: 587.7
105: 584.6  110: 581.6  115: 578.8  120: 576.1
125: 573.5  130: 571.0  135: 568.6  140: 566.3
145: 564.1  150: 562.1  155: 560.1  160: 558.2
165: 556.3  170: 554.6  175: 552.9  180: 551.4
185: 549.8  190: 548.4  195: 547.0  200: 545.7
205: 544.4  210: 543.2  215: 542.0  220: 540.9
225: 539.9  230: 538.9  235: 537.9  240: 537.0
245: 536.1  250: 535.3  255: 534.5  260: 533.7
265: 533.0  270: 532.3  275: 531.7  280: 531.0
285: 530.4  290: 529.8  295: 529.3  300: 528.8
305: 528.3  310: 527.8  315: 527.3  320: 526.9
325: 526.5  330: 526.1  335: 525.7  340: 525.4
345: 525.0  350: 524.7  355: 524.4  360: 524.1
365: 523.8  370: 523.5  375: 523.3  380: 523.0
385: 522.8  390: 522.6  395: 522.4  400: 522.2
405: 522.0  410: 521.8  415: 521.6  420: 521.3
425: 521.3  430: 521.3  435: 521.3  440: 521.3
445: 521.3  450: 521.3  455: 521.3  460: 521.3
465: 521.3  470: 521.3  475: 521.3  480: 521.3
485: 521.3  490: 521.3  495: 521.3  500: 521.3


YRS: 10241.6   VEL: .3483E+00   DEP: 20.41742
      DL:  27.97   VISC: .8950E+13
    TD: 686.3   TF: 650.9   TI: 520.4


YRS: 10343.0   VEL: .3416E+00   DEP: 20.38270
      DL:  28.01   VISC: .9195E+13
    TD: 685.6   TF: 650.2   TI: 519.6


YRS: 10444.4   VEL: .3359E+00   DEP: 20.34871
      DL:  28.47   VISC: .9446E+13
    TD: 684.9   TF: 649.5   TI: 518.7


YRS: 10545.8   VEL: .3308E+00   DEP: 20.31504
      DL:  28.38   VISC: .9709E+13
    TD: 684.2   TF: 648.8   TI: 517.9


YRS: 10647.2   VEL: .3332E+00   DEP: 20.28145
      DL:  29.16   VISC: .9960E+13
    TD: 683.5   TF: 648.2   TI: 517.0


YRS: 10748.6   VEL: .3326E+00   DEP: 20.24750
      DL:  28.78   VISC: .1022E+14
```

TD: 682.8 TF: 647.6 TI: 516.2

YRS: 10850.0 VEL: .3253E+00 DEP: 20.21444
DL: 28.81 VISC: .1048E+14
TD: 682.2 TF: 646.9 TI: 515.4

YRS: 10951.4 VEL: .3205E+00 DEP: 20.18201
DL: 29.25 VISC: .1076E+14
TD: 681.5 TF: 646.3 TI: 514.6

YRS: 11052.8 VEL: .3163E+00 DEP: 20.14982
DL: 29.16 VISC: .1104E+14
TD: 680.8 TF: 645.6 TI: 513.7

YRS: 11154.2 VEL: .3178E+00 DEP: 20.11776
DL: 29.92 VISC: .1133E+14
TD: 680.2 TF: 645.0 TI: 512.9

THE TEMP OUT TO 500 METERS

5: 674.1	10: 668.1	15: 662.1	20: 656.3
25: 650.5	30: 644.9	35: 639.4	40: 634.2
45: 629.1	50: 624.2	55: 619.4	60: 614.9
65: 610.6	70: 606.4	75: 602.5	80: 598.6
85: 595.0	90: 591.5	95: 588.1	100: 584.8
105: 581.7	110: 578.7	115: 575.9	120: 573.1
125: 570.5	130: 567.9	135: 565.5	140: 563.2
145: 560.9	150: 558.8	155: 556.7	160: 554.7
165: 552.8	170: 551.0	175: 549.3	180: 547.6
185: 546.0	190: 544.4	195: 542.9	200: 541.5
205: 540.2	210: 538.9	215: 537.6	220: 536.4
225: 535.3	230: 534.2	235: 533.1	240: 532.1
245: 531.1	250: 530.2	255: 529.3	260: 528.4
265: 527.6	270: 526.8	275: 526.1	280: 525.4
285: 524.7	290: 524.0	295: 523.4	300: 522.8
305: 522.2	310: 521.7	315: 521.1	320: 520.6
325: 520.1	330: 519.7	335: 519.2	340: 518.8
345: 518.4	350: 518.0	355: 517.6	360: 517.3
365: 516.9	370: 516.6	375: 516.3	380: 516.0
385: 515.7	390: 515.4	395: 515.2	400: 514.9
405: 514.7	410: 514.4	415: 514.2	420: 514.0
425: 513.8	430: 513.6	435: 513.4	440: 513.3
445: 512.9	450: 512.9	455: 512.9	460: 512.9
465: 512.9	470: 512.9	475: 512.9	480: 512.9
485: 512.9	490: 512.9	495: 512.9	500: 512.9

```
YRS: 11255.6   VEL: .3169E+00   DEP: 20.08543
       DL:  29.57   VISC: .1162E+14
    TD: 679.5   TF: 644.4   TI: 512.1


YRS: 11357.0   VEL: .3112E+00   DEP: 20.05381
       DL:  29.61   VISC: .1191E+14
    TD: 678.9   TF: 643.8   TI: 511.3


YRS: 11458.4   VEL: .3058E+00   DEP: 20.02285
       DL:  30.03   VISC: .1221E+14
    TD: 678.2   TF: 643.1   TI: 510.6


YRS: 11559.8   VEL: .3021E+00   DEP: 19.99212
       DL:  29.95   VISC: .1252E+14
    TD: 677.6   TF: 642.5   TI: 509.8


YRS: 11661.2   VEL: .3034E+00   DEP: 19.96151
       DL:  30.70   VISC: .1284E+14
    TD: 676.9   TF: 641.9   TI: 509.0


YRS: 11762.6   VEL: .3028E+00   DEP: 19.93063
       DL:  30.36   VISC: .1315E+14
    TD: 676.3   TF: 641.3   TI: 508.3


YRS: 11864.0   VEL: .2976E+00   DEP: 19.90039
       DL:  30.40   VISC: .1347E+14
    TD: 675.7   TF: 640.7   TI: 507.5


YRS: 11965.4   VEL: .2926E+00   DEP: 19.87076
       DL:  30.82   VISC: .1381E+14
    TD: 675.1   TF: 640.1   TI: 506.8


YRS: 12066.8   VEL: .2892E+00   DEP: 19.84134
       DL:  30.75   VISC: .1415E+14
    TD: 674.5   TF: 639.5   TI: 506.0


YRS: 12168.2   VEL: .2903E+00   DEP: 19.81204
       DL:  31.47   VISC: .1449E+14
    TD: 673.9   TF: 638.9   TI: 505.3

          THE TEMP OUT TO 500 METERS
```

```
  5: 668.1    10: 662.4    15: 656.8    20: 651.2
 25: 645.8    30: 640.4    35: 635.3    40: 630.2
 45: 625.3    50: 620.6    55: 616.1    60: 611.7
 65: 607.5    70: 603.5    75: 599.6    80: 595.9
 85: 592.3    90: 588.8    95: 585.5   100: 582.3
105: 579.2   110: 576.2   115: 573.3   120: 570.6
125: 567.9   130: 565.3   135: 562.9   140: 560.5
145: 558.2   150: 556.0   155: 553.9   160: 551.9
165: 549.9   170: 548.0   175: 546.2   180: 544.4
185: 542.8   190: 541.1   195: 539.6   200: 538.1
205: 536.6   210: 535.2   215: 533.9   220: 532.6
225: 531.4   230: 530.2   235: 529.1   240: 528.0
245: 526.9   250: 525.9   255: 524.9   260: 524.0
265: 523.1   270: 522.2   275: 521.4   280: 520.6
285: 519.8   290: 519.1   295: 518.4   300: 517.7
305: 517.0   310: 516.4   315: 515.8   320: 515.2
325: 514.7   330: 514.1   335: 513.6   340: 513.1
345: 512.7   350: 512.2   355: 511.8   360: 511.4
365: 510.9   370: 510.6   375: 510.2   380: 509.8
385: 509.5   390: 509.2   395: 508.9   400: 508.6
405: 508.3   410: 508.0   415: 507.7   420: 507.5
425: 507.2   430: 507.0   435: 506.8   440: 506.6
445: 506.3   450: 506.2   455: 506.0   460: 505.8
465: 505.6   470: 505.3   475: 505.3   480: 505.3
485: 505.3   490: 505.3   495: 505.3   500: 505.3

YRS: 12269.6   VEL: .2916E+00   DEP: 19.78233
       DL:  31.22   VISC: .1484E+14
    TD: 673.3   TF: 638.3   TI: 504.6

YRS: 12371.0   VEL: .2858E+00   DEP: 19.75328
       DL:  31.20   VISC: .1518E+14
    TD: 672.7   TF: 637.8   TI: 503.8

YRS: 12472.4   VEL: .2802E+00   DEP: 19.72491
       DL:  31.60   VISC: .1556E+14
    TD: 672.1   TF: 637.2   TI: 503.1

YRS: 12573.8   VEL: .2771E+00   DEP: 19.69673
       DL:  31.55   VISC: .1593E+14
    TD: 671.5   TF: 636.6   TI: 502.4

YRS: 12675.2   VEL: .2782E+00   DEP: 19.66867
       DL:  32.36   VISC: .1630E+14
    TD: 670.9   TF: 636.0   TI: 501.7
```

YRS: 12776.6 VEL: .2797E+00 DEP: 19.64015
DL: 32.02 VISC: .1668E+14
TD: 670.3 TF: 635.5 TI: 501.0

YRS: 12878.0 VEL: .2739E+00 DEP: 19.61231
DL: 32.00 VISC: .1707E+14
TD: 669.7 TF: 634.9 TI: 500.3

YRS: 12979.4 VEL: .2687E+00 DEP: 19.58510
DL: 32.38 VISC: .1747E+14
TD: 669.1 TF: 634.4 TI: 499.6

YRS: 13080.8 VEL: .2659E+00 DEP: 19.55807
DL: 32.34 VISC: .1788E+14
TD: 668.5 TF: 633.8 TI: 499.0

YRS: 13182.2 VEL: .2667E+00 DEP: 19.53115
DL: 33.12 VISC: .1828E+14
TD: 668.0 TF: 633.3 TI: 498.3

THE TEMP OUT TO 500 METERS

5: 662.6	10: 657.2	15: 651.9	20: 646.6
25: 641.4	30: 636.4	35: 631.4	40: 626.6
45: 621.9	50: 617.3	55: 613.0	60: 608.7
65: 604.6	70: 600.7	75: 596.9	80: 593.3
85: 589.7	90: 586.3	95: 583.0	100: 579.9
105: 576.8	110: 573.8	115: 571.0	120: 568.2
125: 565.6	130: 563.0	135: 560.5	140: 558.1
145: 555.8	150: 553.6	155: 551.4	160: 549.3
165: 547.3	170: 545.4	175: 543.5	180: 541.7
185: 540.0	190: 538.3	195: 536.7	200: 535.1
205: 533.6	210: 532.2	215: 530.8	220: 529.4
225: 528.1	230: 526.8	235: 525.6	240: 524.5
245: 523.3	250: 522.2	255: 521.2	260: 520.2
265: 519.2	270: 518.3	275: 517.4	280: 516.5
285: 515.7	290: 514.9	295: 514.1	300: 513.3
305: 512.6	310: 511.9	315: 511.2	320: 510.6
325: 510.0	330: 509.4	335: 508.8	340: 508.2
345: 507.7	350: 507.2	355: 506.7	360: 506.2
365: 505.8	370: 505.3	375: 504.9	380: 504.5
385: 504.1	390: 503.7	395: 503.3	400: 503.0
405: 502.6	410: 502.3	415: 502.0	420: 501.7
425: 501.4	430: 501.1	435: 500.8	440: 500.6
445: 500.3	450: 500.1	455: 499.8	460: 499.6
465: 499.4	470: 499.2	475: 499.0	480: 498.8

```
485: 498.7  490: 498.5  495: 498.3  500: 498.3


YRS: 13293.6   VEL: .2681E+00   DEP: 19.50383
       DL:  32.81   VISC: .1870E+14
    TD: 667.4   TF: 632.7   TI: 497.6


YRS: 13385.0   VEL: .2629E+00   DEP: 19.47711
       DL:  32.79   VISC: .1911E+14
    TD: 666.9   TF: 632.2   TI: 496.9


YRS: 13486.5   VEL: .2580E+00   DEP: 19.45098
       DL:  33.16   VISC: .1956E+14
    TD: 666.3   TF: 631.6   TI: 496.3


YRS: 13597.9   VEL: .2554E+00   DEP: 19.42502
       DL:  33.13   VISC: .1999E+14
    TD: 665.7   TF: 631.1   TI: 495.6


YRS: 13689.3   VEL: .2564E+00   DEP: 19.39914
       DL:  33.90   VISC: .2045E+14
    TD: 665.2   TF: 630.6   TI: 495.0


YRS: 13790.7   VEL: .2585E+00   DEP: 19.37282
       DL:  33.64   VISC: .2089E+14
    TD: 664.6   TF: 630.0   TI: 494.3


YRS: 13892.1   VEL: .2536E+00   DEP: 19.34704
       DL:  33.61   VISC: .2135E+14
    TD: 664.1   TF: 629.5   TI: 493.7


YRS: 13993.5   VEL: .2494E+00   DEP: 19.32178
       DL:  33.97   VISC: .2183E+14
    TD: 663.6   TF: 629.0   TI: 493.0


YRS: 14094.9   VEL: .2460E+00   DEP: 19.29677
       DL:  33.95   VISC: .2232E+14
    TD: 663.0   TF: 628.5   TI: 492.4


YRS: 14196.3   VEL: .2466E+00   DEP: 19.27187
       DL:  34.65   VISC: .2280E+14
```

TD: 662.5 TF: 627.9 TI: 491.8

THE TEMP OUT TO 500 METERS

5: 657.3	10: 652.2	15: 647.1	20: 642.1
25: 637.2	30: 632.4	35: 627.6	40: 623.0
45: 618.5	50: 614.1	55: 609.9	60: 605.8
65: 601.9	70: 598.0	75: 594.3	80: 590.8
85: 587.3	90: 584.0	95: 580.8	100: 577.6
105: 574.6	110: 571.7	115: 568.8	120: 566.1
125: 563.4	130: 560.9	135: 558.4	140: 556.0
145: 553.6	150: 551.4	155: 549.2	160: 547.1
165: 545.1	170: 543.1	175: 541.2	180: 539.4
185: 537.6	190: 535.8	195: 534.2	200: 532.6
205: 531.0	210: 529.5	215: 528.0	220: 526.6
225: 525.3	230: 524.0	235: 522.7	240: 521.5
245: 520.3	250: 519.1	255: 518.0	260: 516.9
265: 515.9	270: 514.9	275: 513.9	280: 513.0
285: 512.1	290: 511.2	295: 510.4	300: 509.6
305: 508.8	310: 508.0	315: 507.3	320: 506.6
325: 505.9	330: 505.3	335: 504.6	340: 504.0
345: 503.4	350: 502.9	355: 502.3	360: 501.8
365: 501.3	370: 500.8	375: 500.3	380: 499.8
385: 499.4	390: 498.9	395: 498.5	400: 498.1
405: 497.7	410: 497.4	415: 497.0	420: 496.6
425: 496.3	430: 496.0	435: 495.7	440: 495.4
445: 495.1	450: 494.8	455: 494.5	460: 494.2
465: 494.0	470: 493.7	475: 493.5	480: 493.3
485: 493.0	490: 492.8	495: 492.6	500: 492.4

YRS: 14297.7 VEL: .2481E+00 DEP: 19.24662
DL: 34.42 VISC: .2330E+14
TD: 661.9 TF: 627.4 TI: 491.2

YRS: 14399.1 VEL: .2437E+00 DEP: 19.22185
DL: 34.41 VISC: .2379E+14
TD: 661.4 TF: 626.9 TI: 490.5

YRS: 14500.5 VEL: .2397E+00 DEP: 19.19756
DL: 34.74 VISC: .2433E+14
TD: 660.9 TF: 626.4 TI: 489.9

YRS: 14601.9 VEL: .2366E+00 DEP: 19.17352
DL: 34.74 VISC: .2486E+14
TD: 660.3 TF: 625.9 TI: 489.3

```
YRS: 14703.3   VEL: .2371E+00   DEP: 19.14957
       DL:  35.43   VISC: .2539E+14
    TD: 659.8   TF: 625.4   TI: 488.7


YRS: 14804.7   VEL: .2385E+00   DEP: 19.12530
       DL:  35.22   VISC: .2593E+14
    TD: 659.3   TF: 624.9   TI: 488.1


YRS: 14906.1   VEL: .2350E+00   DEP: 19.10142
       DL:  35.21   VISC: .2647E+14
    TD: 658.8   TF: 624.4   TI: 487.5


YRS: 15007.5   VEL: .2308E+00   DEP: 19.07803
       DL:  35.55   VISC: .2705E+14
    TD: 658.2   TF: 623.9   TI: 487.0


YRS: 15108.9   VEL: .2278E+00   DEP: 19.05489
       DL:  35.54   VISC: .2763E+14
    TD: 657.7   TF: 623.4   TI: 486.4


YRS: 15210.3   VEL: .2281E+00   DEP: 19.03184
       DL:  36.20   VISC: .2821E+14
    TD: 657.2   TF: 622.9   TI: 485.8

          THE TEMP OUT TO 500 METERS
  5: 652.3   10: 647.4   15: 642.6   20: 637.8
 25: 633.1   30: 628.5   35: 624.0   40: 619.5
 45: 615.2   50: 611.0   55: 606.9   60: 603.0
 65: 599.2   70: 595.4   75: 591.9   80: 588.4
 85: 585.0   90: 581.7   95: 578.6  100: 575.5
105: 572.5  110: 569.6  115: 566.8  120: 564.1
125: 561.4  130: 558.9  135: 556.4  140: 554.0
145: 551.7  150: 549.4  155: 547.2  160: 545.1
165: 543.0  170: 541.0  175: 539.1  180: 537.2
185: 535.4  190: 533.6  195: 531.9  200: 530.3
205: 528.6  210: 527.1  215: 525.6  220: 524.1
225: 522.7  230: 521.3  235: 520.0  240: 518.7
245: 517.5  250: 516.3  255: 515.1  260: 514.0
265: 512.9  270: 511.8  275: 510.8  280: 509.8
285: 508.8  290: 507.9  295: 507.0  300: 506.1
305: 505.2  310: 504.4  315: 503.6  320: 502.8
325: 502.1  330: 501.4  335: 500.7  340: 500.0
345: 499.3  350: 498.7  355: 498.1  360: 497.5
365: 496.9  370: 496.3  375: 495.8  380: 495.3
385: 494.8  390: 494.3  395: 493.8  400: 493.3
```

```
405: 492.9   410: 492.4   415: 492.0   420: 491.6
425: 491.2   430: 490.8   435: 490.5   440: 490.1
445: 489.8   450: 489.4   455: 489.1   460: 488.8
465: 488.5   470: 488.2   475: 487.9   480: 487.6
485: 487.3   490: 487.1   495: 486.8   500: 486.6


YRS: 15311.7   VEL: .2294E+00   DEP: 19.00850
       DL:  36.02   VISC: .2880E+14
    TD: 656.7   TF: 622.4   TI: 485.2


YRS: 15413.1   VEL: .2261E+00   DEP: 18.98552
       DL:  36.02   VISC: .2940E+14
    TD: 656.2   TF: 621.9   TI: 484.6


YRS: 15514.5   VEL: .2221E+00   DEP: 18.96301
       DL:  36.33   VISC: .3002E+14
    TD: 655.7   TF: 621.4   TI: 484.1


YRS: 15615.9   VEL: .2193E+00   DEP: 18.94073
       DL:  36.33   VISC: .3065E+14
    TD: 655.2   TF: 620.9   TI: 483.5


YRS: 15717.3   VEL: .2204E+00   DEP: 18.91846
       DL:  37.01   VISC: .3128E+14
    TD: 654.7   TF: 620.4   TI: 483.0


YRS: 15818.7   VEL: .2207E+00   DEP: 18.89600
       DL:  36.80   VISC: .3193E+14
    TD: 654.2   TF: 620.0   TI: 482.4


YRS: 15920.1   VEL: .2175E+00   DEP: 18.87390
       DL:  36.80   VISC: .3257E+14
    TD: 653.7   TF: 619.5   TI: 481.8


YRS: 16021.5   VEL: .2138E+00   DEP: 18.85224
       DL:  37.18   VISC: .3324E+14
    TD: 653.2   TF: 619.0   TI: 481.3


YRS: 16122.9   VEL: .2116E+00   DEP: 18.83072
       DL:  37.12   VISC: .3393E+14
    TD: 652.7   TF: 618.5   TI: 480.8
```

YRS: 16224.3 VEL: .2121E+00 DEP: 18.80930
DL: 37.86 VISC: .3462E+14
TD: 652.2 TF: 618.1 TI: 480.2

THE TEMP OUT TO 500 METERS

5: 647.5	10: 642.9	15: 638.3	20: 633.8
25: 629.3	30: 624.9	35: 620.5	40: 616.3
45: 612.1	50: 608.0	55: 604.1	60: 600.2
65: 596.5	70: 592.9	75: 589.4	80: 586.0
85: 582.7	90: 579.5	95: 576.4	100: 573.3
105: 570.4	110: 567.5	115: 564.7	120: 562.0
125: 559.4	130: 556.9	135: 554.4	140: 552.0
145: 549.7	150: 547.4	155: 545.2	160: 543.0
165: 541.0	170: 538.9	175: 537.0	180: 535.1
185: 533.2	190: 531.4	195: 529.7	200: 528.0
205: 526.3	210: 524.7	215: 523.2	220: 521.7
225: 520.2	230: 518.8	235: 517.4	240: 516.1
245: 514.8	250: 513.5	255: 512.3	260: 511.1
265: 509.9	270: 508.8	275: 507.7	280: 506.7
285: 505.6	290: 504.6	295: 503.7	300: 502.7
305: 501.8	310: 500.9	315: 500.1	320: 499.3
325: 498.5	330: 497.7	335: 496.9	340: 496.2
345: 495.5	350: 494.8	355: 494.1	360: 493.4
365: 492.8	370: 492.2	375: 491.6	380: 491.0
385: 490.4	390: 489.9	395: 489.4	400: 488.8
405: 488.3	410: 487.9	415: 487.4	420: 486.9
425: 486.5	430: 486.0	435: 485.6	440: 485.2
445: 484.8	450: 484.4	455: 484.1	460: 483.7
465: 483.3	470: 483.0	475: 482.7	480: 482.3
485: 482.0	490: 481.7	495: 481.5	500: 481.2

YRS: 16325.7 VEL: .2126E+00 DEP: 18.78765
DL: 37.58 VISC: .3532E+14
TD: 651.7 TF: 617.6 TI: 479.7

YRS: 16427.1 VEL: .2093E+00 DEP: 18.76639
DL: 37.59 VISC: .3602E+14
TD: 651.2 TF: 617.1 TI: 479.2

YRS: 16528.5 VEL: .2058E+00 DEP: 18.74554
DL: 37.95 VISC: .3674E+14
TD: 650.8 TF: 616.7 TI: 478.6

YRS: 16629.9 VEL: .2037E+00 DEP: 18.72483
DL: 37.90 VISC: .3750E+14

TD: 650.3 TF: 616.2 TI: 478.1

THE PROGRAM HAS TERMINATED DUE TO
SOLIDIFICATION OF THE DIAPIR.

YRS: 16660.3 VEL: .2016E+00 DEP: 18.71869
DL: 37.98 VISC: .3783E+14
TD: 650.1 TF: 616.0 TI: 478.0

THE TEMP OUT TO 500 METERS

5: 645.3	10: 640.7	15: 636.0	20: 631.5
25: 627.1	30: 622.7	35: 618.5	40: 614.3
45: 610.3	50: 606.4	55: 602.5	60: 598.8
65: 595.2	70: 591.6	75: 588.2	80: 584.9
85: 581.6	90: 578.5	95: 575.4	100: 572.4
105: 569.5	110: 566.6	115: 563.9	120: 561.2
125: 558.6	130: 556.0	135: 553.6	140: 551.2
145: 548.8	150: 546.6	155: 544.3	160: 542.2
165: 540.1	170: 538.1	175: 536.1	180: 534.2
185: 532.3	190: 530.5	195: 528.8	200: 527.1
205: 525.4	210: 523.8	215: 522.2	220: 520.7
225: 519.2	230: 517.8	235: 516.4	240: 515.0
245: 513.7	250: 512.4	255: 511.1	260: 509.9
265: 508.7	270: 507.6	275: 506.5	280: 505.4
285: 504.4	290: 503.3	295: 502.4	300: 501.4
305: 500.5	310: 499.6	315: 498.7	320: 497.8
325: 497.0	330: 496.2	335: 495.4	340: 494.6
345: 493.9	350: 493.2	355: 492.5	360: 491.8
365: 491.1	370: 490.5	375: 489.9	380: 489.3
385: 488.7	390: 488.1	395: 487.6	400: 487.0
405: 486.5	410: 486.0	415: 485.5	420: 485.0
425: 484.6	430: 484.1	435: 483.7	440: 483.2
445: 482.8	450: 482.4	455: 482.0	460: 481.6
465: 481.3	470: 480.9	475: 480.6	480: 480.2
485: 479.9	490: 479.6	495: 479.3	500: 479.0